THE APPLICATION OF RECURRENT PULSE TECHNIQUES TO THE DETECTION OF FAULTS IN RELAY COILS

A Thesis

Presented to

the Faculty of Graduate Studies and Research

of the University of Manitoba

In Partial Fulfillment

of the Requirements for the Degree

Master of Science in

Electrical Engineering

by

Theodore Arnold Ewashko

May 1962

ABSTRACT

This thesis contains a report of an experimental study of the application of an Impulse Generator Simulator to the detection of permanent winding failures in relay coils. The sensitivity of a number of failure detection techniques was examined on coils specially tapped for controlled failures and on coils faulted by high voltage impulses. Methods based on an examination of the induced coil oscillation were found most suitable for detecting permanent failures in coil windings.

The internal impulse voltage distribution along the coil winding was examined for a $1\frac{1}{2}$ by 40 impulse; the largest voltage gradient was found to occur between the outer layers of the coil during the first few microseconds of the applied impulse.

PREFACE

Failure of relay coils in Electrical Distribution Systems, from excessive voltages induced by lightning and switching transients, has stimulated the desire to incorporate high voltage impulse tests in the specifications for selecting coils. Before these tests can be of any value, a method is required for detecting and evaluating damage incurred within the coils during the high voltage impulse tests. This thesis examines in particular the possibility of using low voltage impulses from the Impulse Generator Simulator to detect permanent winding failures.

The thesis is divided into four sections: Introduction; Study of Failure Detection Methods; Impulse Voltage Distribution within Coil Winding; Conclusions.

The first section is made up of four chapters. The first chapter outlines the problem, while the remaining three chapters describe the techniques and equipment used for the study. The second section, Chapter V to IX, describes the results for the failure detection methods and constitutes the body of the thesis. The third section, Chapter X, describes the internal voltage distribution within the coil. The fourth section, Chapter XI, summarizes the conclusions of this study.

The author wishes to acknowledge the assistance of Professor J.P.C. McMath in performing these experimental studies. Appreciation is also extended to the National Research Council for the financial assistance, to Pioneer Electric Limited for donating a supply of coils to this project, and to Mr. R.L. Baglow, M.Sc., for his assistance in proofreading this thesis.

TABLE OF CONTENTS

CHAPTER PAGE

LIST OF FIGURES

FIGURE PAGE

FIGURE PAGE

LIST OF TABLES

LIST OF GRAPHS

CHAPTER I

DEVELOPMENT AND STATEMENT OF THE PROBLEM

The advance in the electrical industry, after William Stanley demonstrated the practical use of power distribution by alternating current in 1886, was not accomplished without the growing pains which normally accompany new developments. The transformer especially, the key to this technique, plagued scientists for years by its resistance to conventional analysis. The frequent failures of transformers in distribution systems, resulting from excessive voltages induced by lightning and switching transients, stimulated an intense study of the transient behaviour of single-layer windings. Blume and Boyajian in 1917 reviewed these earlier studies which predicted that the initial voltage distribution within the winding would assume an exponential form controlled by the distributed capacitance, and experimentally verified this predicted initial voltage distribution (reference 11). With the advent of sensitive instruments and the high voltage impulse generator, transformer design improved to the point that transformers could withstand the stresses imposed by the environment. High voltage impulse tests were commonly specified as a condition for the purchase of transformers in order to demonstrate the ability of their winding to withstand high transient voltages. Inspection of the windings after such tests, on dismantling the coil, disclosed that failure had occurred during many of the tests. Since individual inspection of the transformers was very costly, methods were developed to detect these winding failures without dismantling the transformers. At the present time, the methods of failure detection are

capable of detecting failures occurring between adjacent turns in single-layer windings. However, theory and experimental techniques were directed towards testing single-layer windings, with only a few extensions to multi-layer windings.

As distribution systems have increased in size and complexity, relays have been incorporated as switches to protect and control the various sections of the system. These relays utilize compact multi-layer coils for efficient low power operation, and the use of the coils in new environments has presented problems similar to those faced by transformer designers. The analysis of the behaviour of the coils has been simulated by means of network theory, and digital and analogue computers have been necessary to solve the resulting equations (references 1, 2, 10, 11). An outline of the multi-layer coil theory and its associated analysis is given in Appendix "A". There has resulted in industry a considerable interest in extending the application of high voltage techniques to relay coils, since, if the impulse generator could be used to test the ability of the coil winding to withstand high transient voltages, the cost of developing new equipment and techniques would be greatly reduced. The demonstration of the ability of electric apparatus to withstand the impulse tests is of little value in itself unless adequate methods of detecting failures are available in conjunction with the tests. Therefore, before high voltage impulse techniques can be extended to relay coils, existing failure detection methods must be examined to determine if improvement or revision in the technique is necessary. If the required detection sensitivity cannot be satisfied by these techniques, new methods must be developed.

The main purpose of this study was to show the extent to which the Impulse Generator Simulator could be used for detection of faults incurred by high voltage impulse testing of multi-layer coils. To realize this objective, existing failure detection methods were modified to suit the generator, and new methods were developed to increase the detection sensitivity. In addition, the impulse voltage distribution along the winding was predicted from measurements taken at the end of layers randomly selected within the winding.

CHAPTER II

IMPULSE - FAILURE - DETECTION METHODS

High voltage impulse testing has long been recognized as a means of testing the durability of transformers to abnormal stresses; and the desire to use this test stimulated experimental and theoretical investigations to develop methods for detecting insulation failure that may occur during these tests. Present methods for detection of failures in transformers, as stated in A.S.A. Standard C-57, include "noise within the transformer; presence of smoke; excessive current or drop in voltage in the excitation circuit as indicated by magnetic oscillograms; failure of a gap or bushing to flashover although the oscillograms indicate a chopped wave; and presence of oscillations or other variations from the expected waveshape as indicated by cathode ray oscillograms". Most of these methods readily revealed a major breakdown of the winding, but failed to detect with certainty any small inter-turn fault (references 20, 31). However, techniques involving the cathode ray oscilloscope have been successful in detecting failures between adjacent turns in the transformer winding. Articles describing the techniques used during the high voltage impulse test are included in the bibliography, but will not be discussed as their material is irrelevant to the present subject (references 28, 16). The oscillographic methods of fault detection utilizing low voltage techniques were modified for the Impulse Generator Simulator and their capabilities and limitations examined during this investigation.

The Impulse Generator Simulator consists primarily of a large condenser which is charged through a rectifier and a high voltage transformer from a 110-volt alternating current source, and discharged through a pulse forming network. The parameters of this network can be controlled at will to yield a range of low voltage impulses which are limited to a maximum peak value of 600-800 volts depending on the desired output waveshape.

The low voltage impulse, used to energize the coils for the tests, will be defined before proceeding with the discussion on the fault detection methods.

II - I DESCRIPTION OF A LOW VOLTAGE IMPULSE

The impulse voltage is defined by the International Electrotechnical Commission as a "unidirectional transient voltage which, without appreciable oscillations, rises rapidly to a maximum value and falls, usually less rapidly, to zero". Refer to figures 2-1 and 2-2 for the following characteristics of the coil.

(a) Polarity. All experimental work performed for this thesis used a positive pulse to ground.

(b) Peak value or virtual peak value if oscillations exist. Refer directly to figure 2-2 for an illustration of the virtual peak of an impulse.

(c) Virtual front time, T_1. This is defined as "1.67 times the time interval T between the instants where the impulse amplitude is 30%, point A, and 90%, point B, of (virtual) peak value". The virtual zero is point C_1, the extrapolation of the line through points A and B to the zero line.

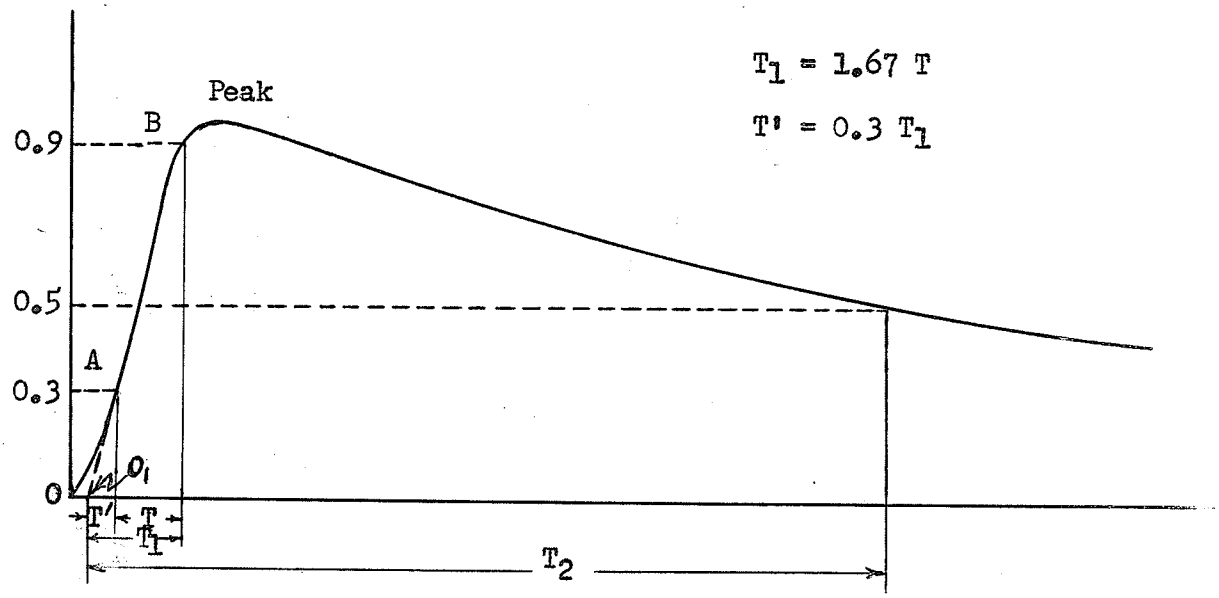

FIGURE 2-1

IMPULSE WAVEFORM PROPERLY DAMPED

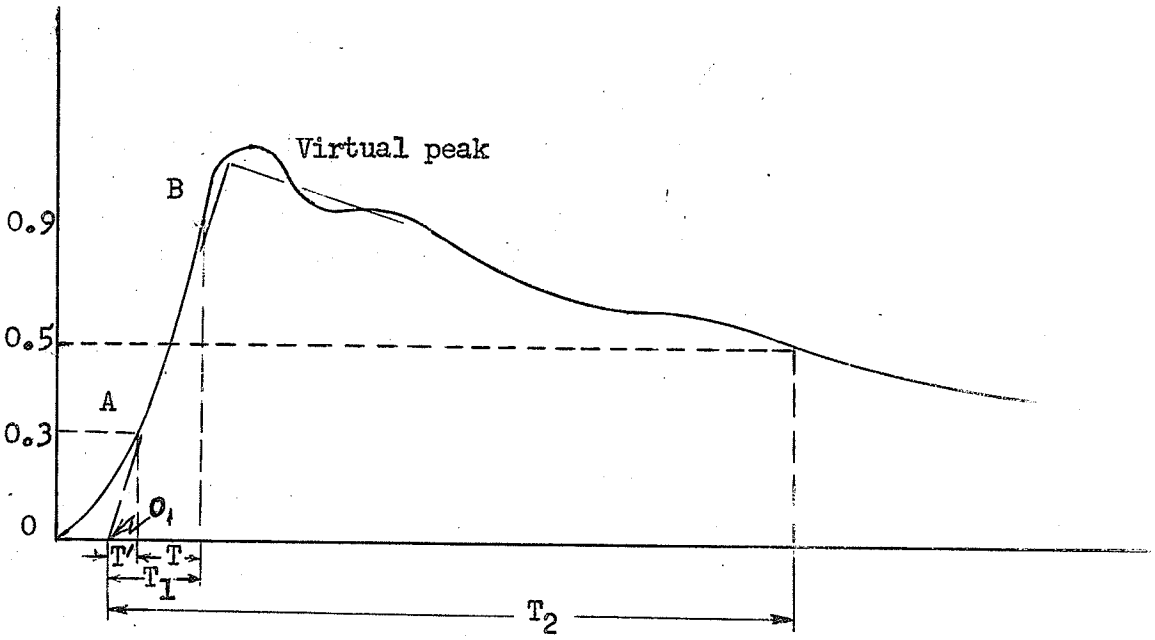

FIGURE 2-2

IMPULSE WAVEFORM SLIGHTLY UNDERDAMPED

(d) Virtual time to half-value, T_2. This is defined as "The time interval between 0, and the instant on the tail, where the voltage has decreased to half its (virtual) peak value".

The standard A.S.A. impulse is described as a $1\frac{1}{2}$ by 40 wave, whereas the International Electrotechnical Commission recommends a 1.2 by 50 wave. The values describing the impulse are measured in microseconds. A $1\frac{1}{2}$ by 40 impulse would then mean an impulse with a rise time of $1\frac{1}{2}$ usec. (microseconds) and a virtual time to half-value of 50 usec. The A.S.A. tolerances allowed on the shape of the wave is 30% on the front time and 20% on the time to half value. Due to these liberal tolerances, the front time was measured as the time between the 30% and maximum points of the impulse amplitude. The tail was measured from virtual zero to the point where the voltage decreased to one-half its maximum value.

II - II FAILURE DETECTION TECHNIQUES

A common procedure of failure detection for transformer windings consists of applying a reduced voltage impulse to the terminals of the test coil, testing the coil with the desired high voltage impulse, then reapplying the reduced impulse (references 6, 20, 31, 33). Oscillograms of the reduced voltage impulses are recorded and later compared for discrepancies. An insulation puncture tending to transient arc-over will cause a high frequency oscillation somewhere along the reduced impulse wave; any insulation failures, accompanied by a permanent carbonized path between portions of the winding, will cause a deformation in the

waveshape of this impulse wave. Very often differences are detectable only if the oscillograms are superimposed upon each other. The best results have been obtained by using a loosely coupled generator, that is, a generator of small capacitance so as to have an inherently high regulation to changes in the impedance of the test piece. When this method was extended to the Impulse Generator Simulator for a study on relay coils, the reduced voltage was limited by the generator capacitance to a maximum peak voltage of 400 volts. Voltage oscillograms of the impulse applied to the coil from the generator must first be recorded for the coil in its natural or undamaged state. After completion of the desired endurance tests, oscillograms of the generator output impulse are again recorded across the coil terminals and compared to those recorded previous to the endurance test. Any decrease in the tail of the voltage impulse indicates a reduction in the coil impedance, resulting from internal failures, in the same manner that was observed on the reduced impulse during tests on transformers. Since the voltage waveshape across different coils are usually different even when the generator settings are identical, it is necessary to compare a pair of oscillograms from each coil. Detection of permanent failures by this technique is examined in detail in Chapter V entitled "Experimental Results for the Voltage Oscillogram Fault Detection Method".

A more sensitive detection test for transformers is obtained by observing the current waveform across a shunt placed between the low voltage terminal of the test piece and the grounded terminal of the high voltage impulse generator (references 4, 5, 16, 20, 25, 26). Normally this current waveform is observed during the actual high voltage

impulse tests, but tests have been performed by reduced full wave impulses. However, at reduced voltages this test is less effective for detecting transient arc-over that may occur in the winding. Oscillograms illustrating winding failures as low as 0.1 percent of the total transformer winding have been presented in a number of technical papers. This current test was altered to suit the Impulse Generator Simulator and involved basically the same procedure as the voltage oscillogram method, except that a current shunt was added to the coil circuit. This current shunt may be a resistor, capacitor, or inductance. The value is not as critical as for transformer testing, since relay coils have a relatively larger resistance and low value shunts are not essential to retain the balance of surge currents. When the two low voltage current oscillograms obtained before and after the high voltage impulse test are compared, deviations in the second oscillogram waveshape will result from permanent internal failures incurred in the coil winding. It is important that the same voltage is applied when recording both oscillograms, since the inductive current is proportional to the integral of the applied voltage, and any increase in the applied voltage will increase the current flow accordingly.

This method fails entirely for chopped waves since at the instant of chop, the time at which the fault is most likely to occur, the voltage drops to zero and no rise in current can result to indicate a decreased winding impedance.

The more complex oscillographic techniques were not exploited since, in general, they could not be applied directly to the Impulse Generator Simulator. A new approach was examined instead: a study of the effect of

changes in the coil winding structure upon the induced oscillation within the coil. The impulse is applied between one of the coil terminals and the coil shell, and the output observed either between the remaining terminal and the coil shell or directly across the coil terminals. In the former method the observed impulse consists of the transmitted applied impulse, modulated by the induced internal oscillation, and is called the Transmitted Impulse Detection Method. In this method the transmitted impulse is unaffected, but the amplitude and frequency of the modulating oscillation are sensitive to changes in the coil winding. The experimental results for this method are included in Chapter VII. In the latter method the internal oscillation is monitored directly and is called the Induced Oscillation Detection Method. The experimental results for this method are included in Chapter VIII.

In order to study the impulse-failure-detection methods for single turn and layer failures, it was necessary to provide coils with controlled faults. The following chapter describes the preparation of these coils, and the experimental technique employed during the tests.

CHAPTER III

PREPARATION OF COILS AND MEASUREMENT TECHNIQUES FOR THE RECURRENT SURGE IMPULSE GENERATOR

III - I PREPARATION OF COILS TESTED

As previously stated, the objective of this thesis was to examine the detection sensitivity of a number of detection methods utilizing the Impulse Generator Simulator and to observe the impulse voltage distribution that resulted within the coil winding. Since this study required constant probing into the interior of the winding to simulate various failures, it was decided to position taps at the ends of the coil layers so as not to interfere significantly with the initial capacitive and inductive distributions. To determine if the tapping procedure, or in fact the taps themselves, altered the impulse test waveforms, oscillograms of voltage and current were recorded prior to tapping these coils and compared with the oscillograms recorded after the coil was tapped. The superimposed results are shown in figures 3-1 and 3-2 for 2200 and 4200 turn coils respectively, hereafter designated as coils (1) and (2); the oscillograms recorded before and after these coils were tapped correspond in each case. The grid visible on all oscillograms enclosed in this thesis represents a 1 cm. square grid on the oscilloscope screen. The technique used in photographing and developing these oscillograms is described in Appendix "B".

In order to gain access to this winding the bobbin end and protective tape were removed from one end of the core and a number of layer

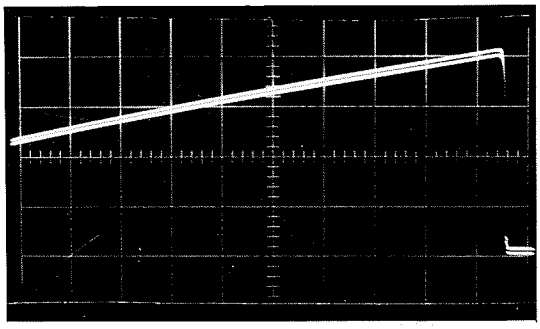

50 usec./cm. sweep; 100^{V}/cm. defl.

$1\frac{1}{2}$ by 200 applied impulse
positive potential measured downward

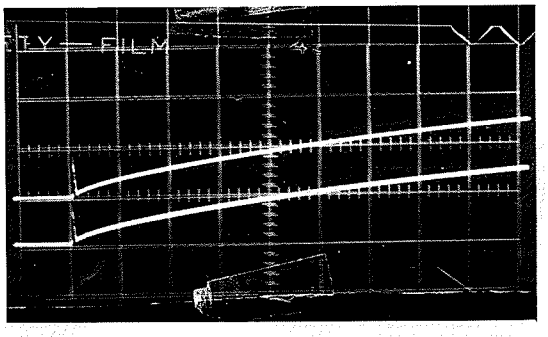

20 usec./cm. sweep; 5^{V}/cm. defl.

current impulse for
$1\frac{1}{2}$ by 200 applied impulse
positive potential measured upwards

OSCILLOGRAMS FOR TAPPED AND UNTAPPED 2200-TURN COIL

FIGURE 3-1

The lower oscillogram represents the waveform after the coil was
ıpped. Armature core contained in coil shell.

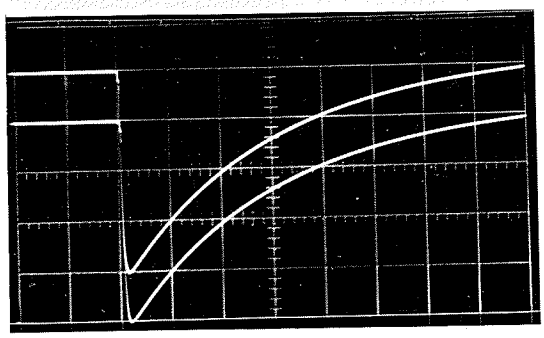

20 usec./cm. sweep; 100V/cm. defl.

1½ by 40 applied impulse

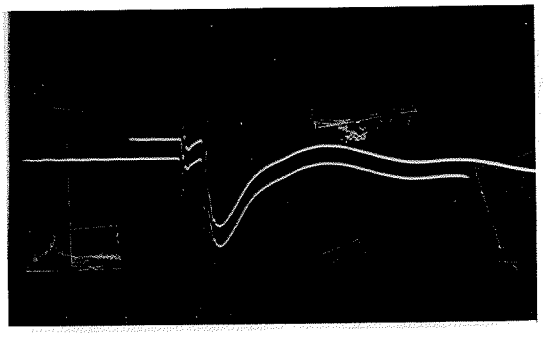

1 usec./cm. sweep; 2V/cm. defl.

charging current pulse

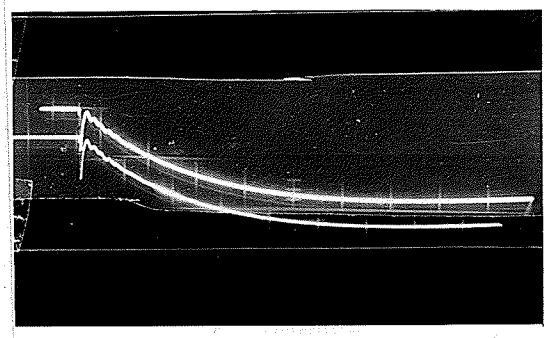

20 usec./cm. sweep; 5V/cm. defl.

current waveform
armature core contained in
coil shell

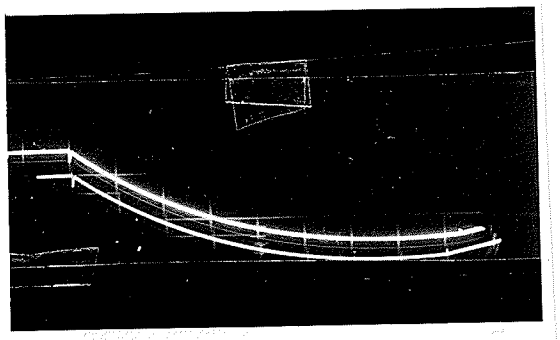

20 usec./cm. sweep; 10V/cm. defl.

current waveform
armature core removed from
coil shell

OSCILLOGRAMS FOR TAPPED AND UNTAPPED 4200-TURN COIL

FIGURE 3-2

The lower oscillogram represents the waveform after the coil was
ped. Positive potential measured downward. The current waveforms
wn are recorded for the 1½ by 40 applied impulse shown.

ends were separated from the remainder of the coil. Taps composed of wire identical to that used in the coil winding were soldered to randomly selected layers, and the soldered joints insulated by a coat of glyptal. The location of these taps was not known till after the completion of all tests as this information could not be obtained without dismantling and unwinding the coil. The tapped turns, numbered from the top layer, were:

Coil 1 26, 205, 409, 475, 480, 674, 845, 900, 1100, 1302.

Coil 2 267, 582, 590, 914, 917, 1239, 1246, 1584, 1918.

Only one type of coil, classified as Q12280A by Pioneer Electric Limited, was considered in this study. A photograph of one of these coils, along with its component parts, is illustrated in figure 3-3, and an illustration of a tapped coil is shown in figure 3-4.

Since coils were not systematically wound a diagram was constructed which indicated the positions of the turns and layers, and the size and type of coil irregularities. The diagrams for coils (1) and (2) are shown in figures 3-5(a) and 3-5(b) respectively, and reveal the inconsistencies between coils, and more specifically, the inconsistencies between the layers in one coil.

When these coils were unwound it was found that no information had been obtained concerning small failures, and another coil had to be prepared to complete these tests. However, this coil was not tapped but the protective tape and insulation were removed to expose the top layer of the coil, in order that shorts involving adjacent turns and similar combinations could be tested.

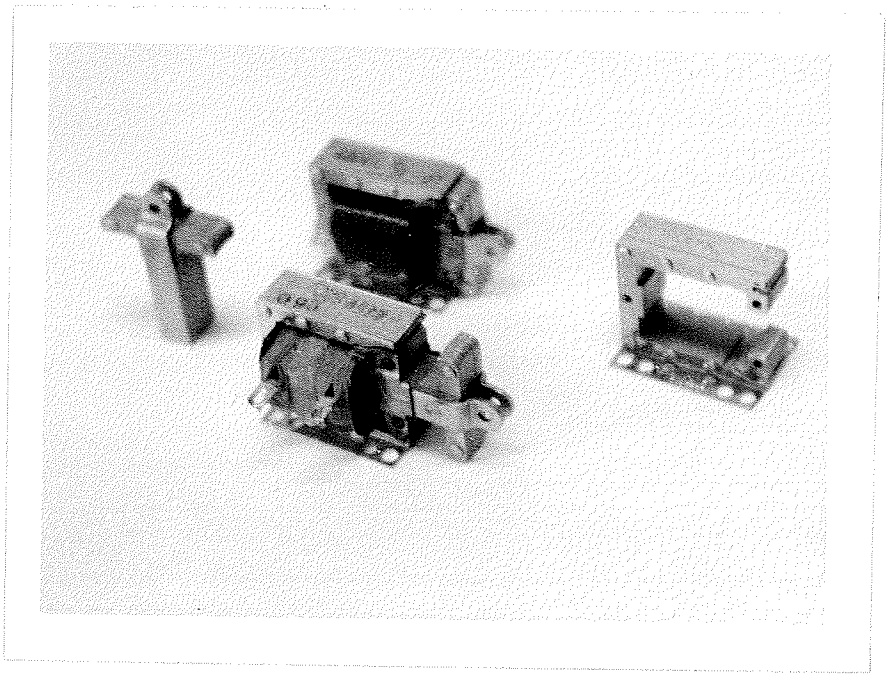

TEST COIL AND COMPONENTS

FIGURE 3-3

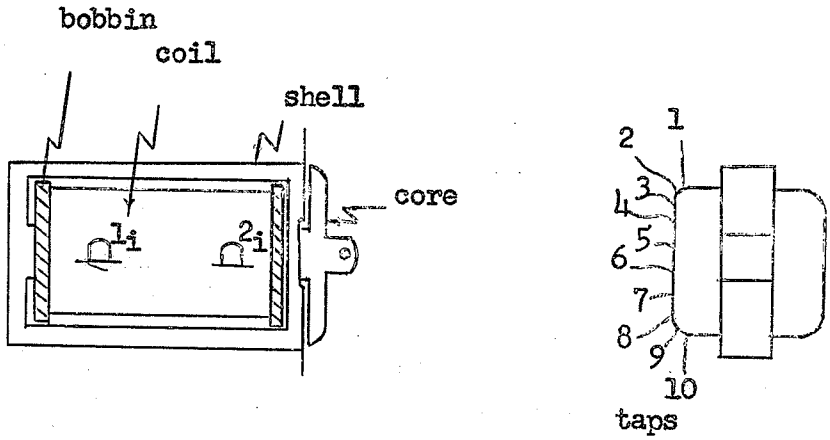

DIAGRAM OF TAPPED COIL

FIGURE 3-4

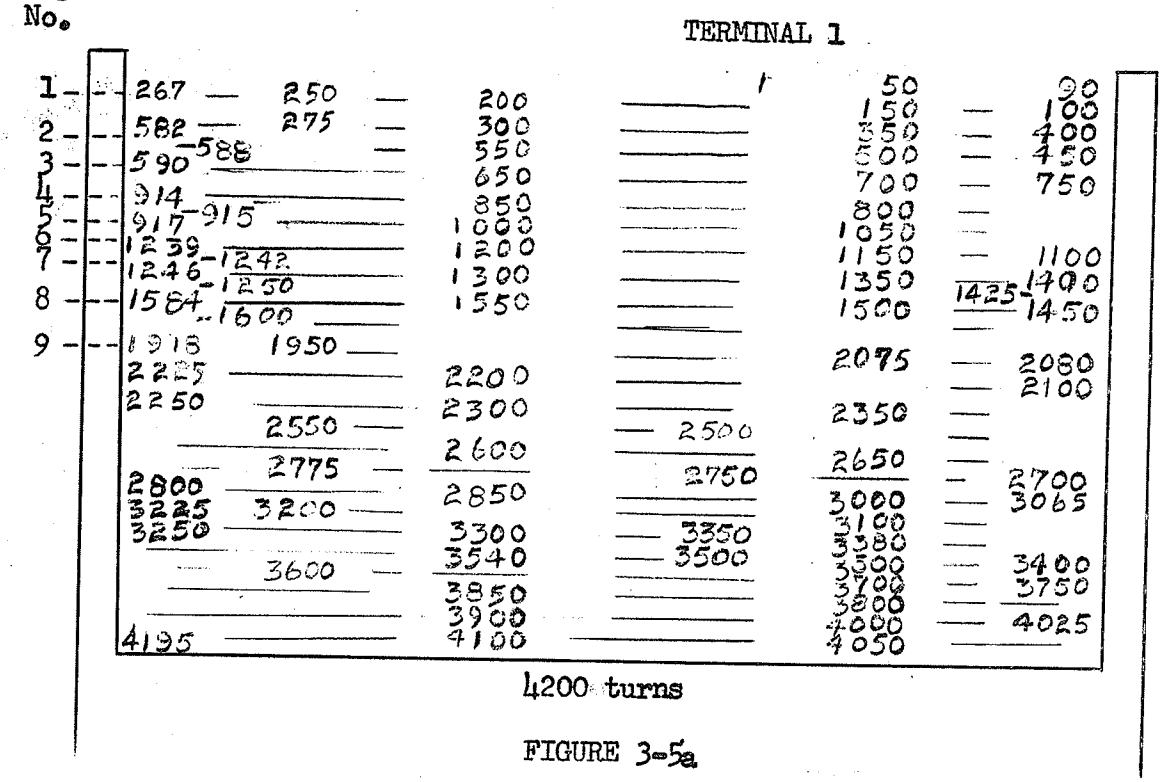

4200 turns

FIGURE 3-5a

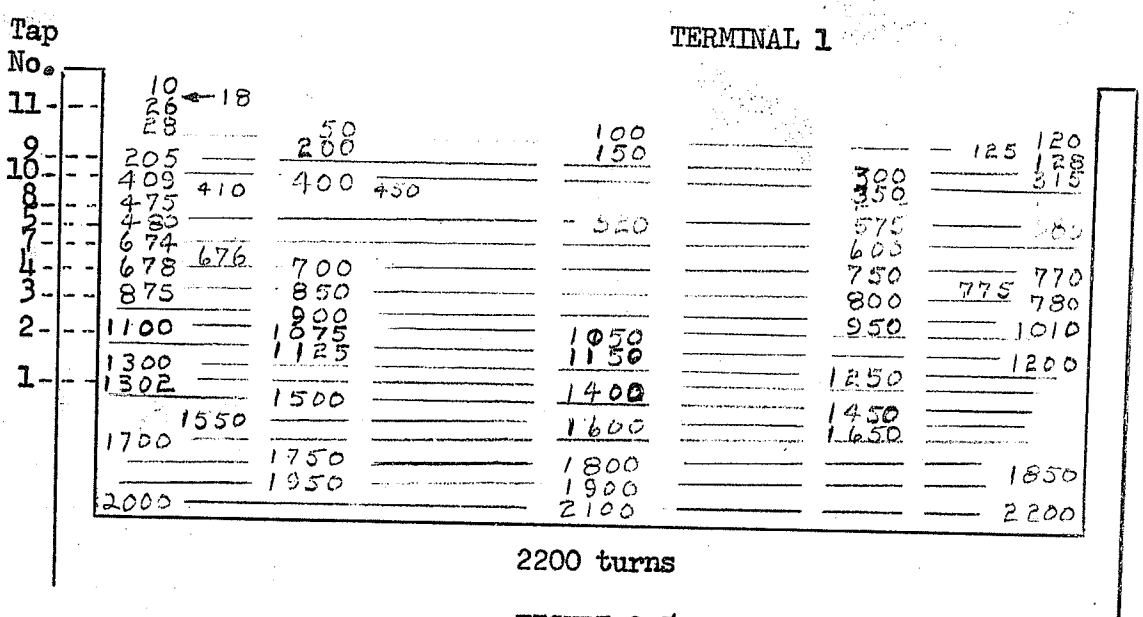

2200 turns

FIGURE 3-5b

DIAGRAMATIC REPRESENTATION OF UNSYSTEMATIC WINDING

OF RELAY COILS

FIGURE 3-5

Since the outer layer was only a part layer, another coil was stripped to permit the voltage distribution to be examined along a complete layer. The winding of the coil was removed from the core and sufficiently unwound to expose a complete layer. The winding was replaced on the core shell and the insulation of a number of turns was removed to allow the voltage distribution to be probed along this layer.

III - II EXPERIMENTAL TECHNIQUE EMPLOYED DURING THE TESTS AND MEASUREMENT INVOLVING THE IMPULSE GENERATOR SIMULATOR

An impulse voltage was applied to the coil by the Impulse Generator Simulator, as directed by the particular test or measurement, nd the output transferred by means of a calibrated high frequency robe to a Tektronix type 533 oscilloscope. To minimize the effects f lead inductance and capacitance, the tapped coils were mounted on a igh block close to the generator terminals. Any stray capacitance urrounding this apparatus was kept as constant as possible by preserving ıe positions of the coil, generator, and oscilloscope for all tests. picture of the apparatus is shown in figure 3-6.

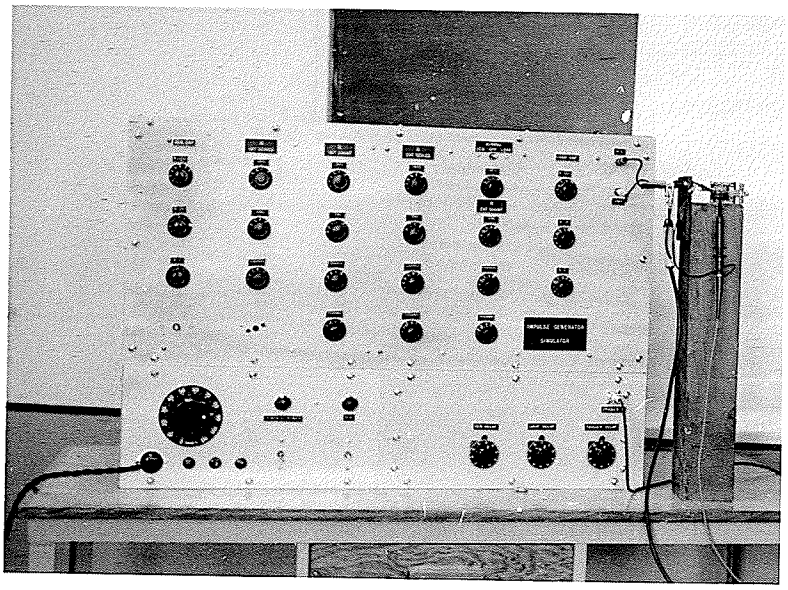

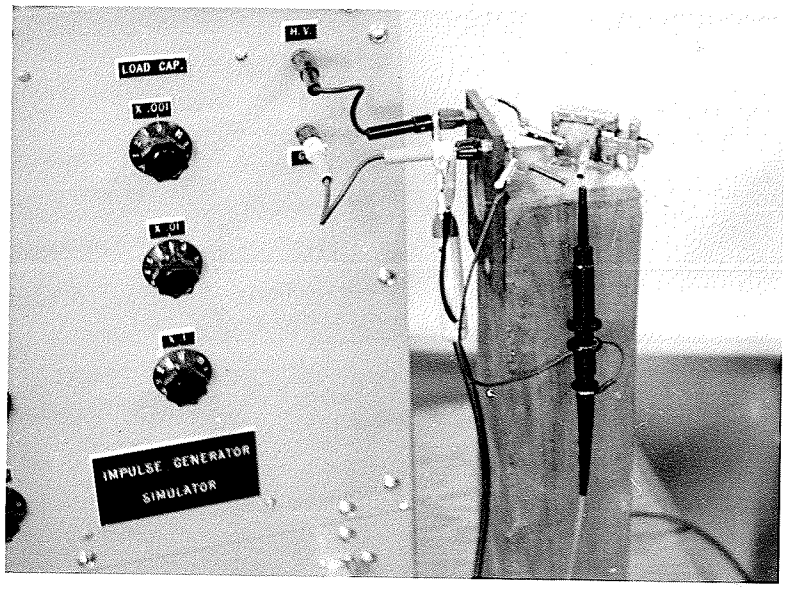

IMPULSE GENERATOR SIMULATOR WITH COIL TEST APPARATUS

FIGURE 3-6

CHAPTER IV

HIGH VOLTAGE IMPULSE TESTING

Two coils were subjected to high voltage impulses until they collapsed, in order that they could be tested for internal damage by the fault detection methods described in Chapter II. To evaluate the reliability of the fault detection methods would require testing large numbers of coils, since many coils fail at high voltages without leaving enough carbon to produce a permanent failure at low voltages. Since a sufficient supply of the coils was not available for proper evaluation, some of the existing problems could only be indicated.

IV - I PREVIOUS HIGH VOLTAGE IMPULSE TESTS ON THESE RELAY COILS

High voltage impulse tests were performed by Pioneer Electric Limited to establish the breakdown insulation level for the relay coils. When the coils were subjected to $1\frac{1}{2}$ by 40 impulses, signs of insulation breakdown were observed in the range 4-7 kv. (kilovolts), and complete collapse of the coils was noted in the range 10-15 kv. The failure indications in the 4-7 kv. range consisted of high frequency oscillations at the beginning of the current waveform, while total failures were accompanied by a collapse of the voltage waveforms, usually at the time when the applied voltage had just reached peak value. After total breakdown, the coils seldom withstood more than 5 kv. impulse. The most frequent form of breakdown of the coil was either

insulation failure between the coil terminals, or insulation failure between a layer of the winding and the coil shell.

No technique was available to determine whether permanent failures were formed at the completion of any portion of the tests, but the fact that the coils would withstand impulses up to 5 kv. after total breakdown indicates that low voltage detection techniques may not be applicable. The extent of the coil damage produced by the tests was determined by dismantling and unwinding the coil.

The contact strength of the wire was tested by overlapping two pieces of wire and subjecting their intersection to a series of high voltage impulses. Flashover occurred at approximately 17 kv., but the coils were expected to fail well below this value, since the poor technique used for winding the coils would weaken the insulation and intensify the voltage distribution.

IV - II HIGH VOLTAGE IMPULSE TESTS PERFORMED DURING THIS STUDY ON TWO 2200 TURN COILS

Two 2200 turn coils were subjected to high voltage impulse tests and oscillograms were recorded for both coils before and after these tests by each type of detection method discussed previously, and later compared for discrepancies. Particular caution was employed to maintain the same amplitude for the detection impulse for the initial and final oscillograms to permit a detailed comparison between these oscillograms. This difficulty could be overcome by assuming the behaviour of the coil linear for small variations in the input detection impulse and normalizing the results with respect to the applied voltage. The circuit

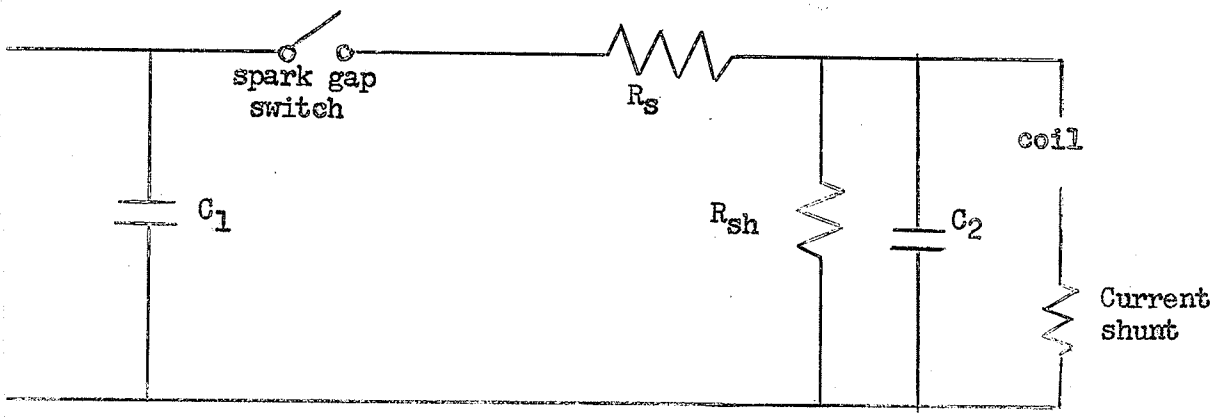

C_1 = input capacitance

C_2 = output capacitance

R_c = current shunt

R_s = series resistance

R_{sh} = shunt resistance

Voltage oscillogram recorded across R_{sh}

Current oscillogram recorded across R_c

HIGH VOLTAGE IMPULSE APPARATUS

FIGURE 4-1

diagram of the apparatus used for the high voltage tests is illustrated in figure 4-1 (reference 14).

The first coil, designated coil (4), was subjected to a series of high voltage impulses which initiated at 2 kv., increased by 2 kv. steps till 8 kv., then by 1 kv. steps till 10 kv., at which time the coil failed. A 3 kv. impulse was then applied successfully to the coil; however, the coil failed when the impulse was increased to 5 kv. When the 3 kv. impulse was reapplied, the coil again withstood the impulse. Oscillograms illustrating these results are shown in figure 4-2 and 4-3 for voltage and current impulse waveforms respectively. The set of waveforms at the bottom of the figures illustrate the conditions before the coil had failed; those at the center illustrate the waveforms just before and during failure at the 10 kv. level; and those at the top illustrate failure at the 5 kv. level. The current and voltage waveforms of figures 4-2 and 4-3 correspond directly.

When the coil was unwound, burnt particles and carbon dust were found around the turns at the end of the first three layers. The voltage probably flashed from this point in the winding to the low potential coil terminal. The type of permanent failure that remained in the coil was estimated from the results of the detection tests, illustrated in the respective succeeding chapters of the various detection tests, to consist of a number of turns in one, or possibly all three, layers.

A second coil, designated coil (5), was subjected to a series of similar high impulse tests, but did not collapse until a 15 kv. impulse was applied to the coil. The voltage was reduced to 3 kv., and then increased by 1 kv. increments till breakdown; however, unlike the first

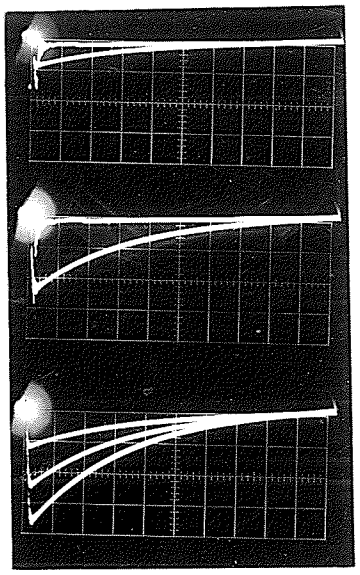

-3 kv. applied voltage impulse
-chopped 5 kv. voltage impulse
due to coil failure

-9 kv. applied voltage impulse
-chopped 10 kv. voltage impulse
due to coil failure

-4, 6 and 8 kv. voltage impulse
waveforms before coil failure

FIGURE 4-2

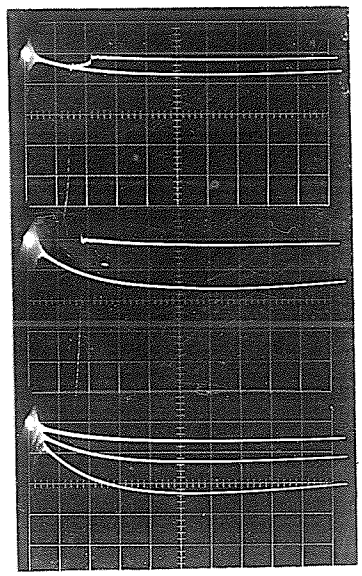

-3 kv. current impulse
-chopped current due to coil
failure when 5 kv. voltage
impulse applied

-current impulse for 9 kv. voltage
impulse
-chopped current due to coil
failure when 10 kv. voltage
impulse applied

-current waveforms corresponding
to above 4, 6 and 8 kv. voltage
impulses

FIGURE 4-3

VOLTAGE AND CURRENT OSCILLOGRAMS FOR HIGH VOLTAGE

IMPULSE STRESS ON FIRST COIL

All oscillograms have a sweep speed of 20 usec./cm.
Positive potential measured downward.

coil, this coil did not fail until a 12 kv. impulse was reached. This procedure, beginning with the 3 kv. impulse, had to be repeated a considerable number of times before failure could be attained by a 5 kv. impulse. Further repetition of 3 kv. and 4 kv. impulses would not lower this breakdown potential.

Figures 4-4 and 4-5 illustrate the voltage and current waveforms before and during coil failure. The two current waveforms shown at the bottom of figure 4-5 illustrate the current before the coil had collapsed under a high voltage impulse. The center illustration corresponds to the 14 kv. voltage impulse shown in figure 4-4. The current waveform, illustrating coil failure in figure 4-5, corresponds to the voltage waveform at the center of figure 4-4; likewise, the two remaining waveforms correspond.

A current waveform was recorded at two oscilloscope sweep speeds for a 4 kv. impulse, at the stage when the coil required an impulse of 7 kv. for breakdown. The first oscillogram, figure 4-6 , illustrates the current waveform for a sweep speed of 10 usec./cm. and the second oscillogram illustrates this same waveform at a sweep speed of 50 usec./cm. As stated in the previous section, the initial oscillation at the beginning of the current waveform is believed to act as a fault detector during high voltage tests, but no further information was obtained during this study because there were no more coils available.

When the coil was unwound the only signs of damage were burnt spots on the edges of both coil terminals and a light sprinkling of carbon dust on the top layer between and near the coil terminals. It appeared that the impulse current flashed between the coil terminals.

Two types of coil failure were produced by these high voltage tests. The first type, indicated by coil (4), was a minor failure in the coil winding which would undoubtedly extend to layer failures and eventually progress to adjacent layers with further applied impulses, until the coil was completely inoperative at low voltages. The second type of failure, indicated by coil (5), would develop slower than the first type, but eventually would carbonize a path between the coil terminals sufficient to short the coil even at low voltages. The coil could probably be protected from this latter type of failure by a spark gap placed between the coil terminals.

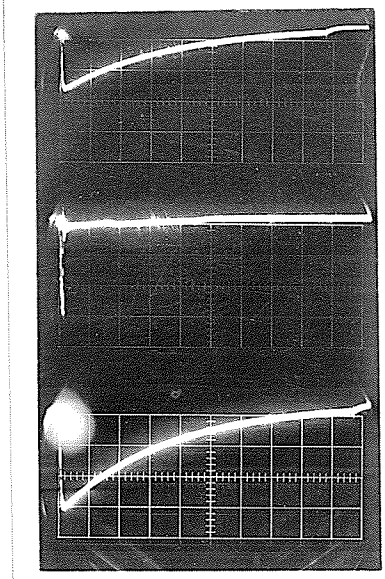

3 kv. voltage impulse after
first coil failure
2 kv./cm. vert. defl.

chopped voltage impulse during
first coil failure
2 kv./cm. vert. defl.

14 kv. voltage impulse before
first coil failure
5 kv./cm. vert. defl.

voltage waveforms

FIGURE 4-4

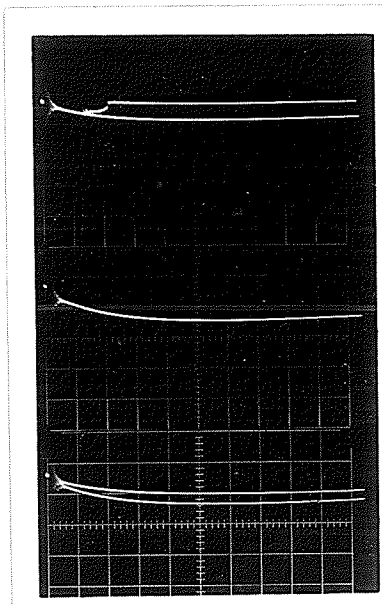

current waveforms during and
after first coil failure
5 volts/cm. vert. defl.

current waveform corresponding
to voltage impulse at bottom
of figure 4-4
5 volts/cm. vert. defl.

current waveforms before
first coil failure
5 volts/cm. vert. defl.

voltage waveforms

FIGURE 4-5

HIGH VOLTAGE IMPULSE TEST RESULTS

All oscillograms have a 20 usec./cm. sweep speed.
Positive potential measured downward.

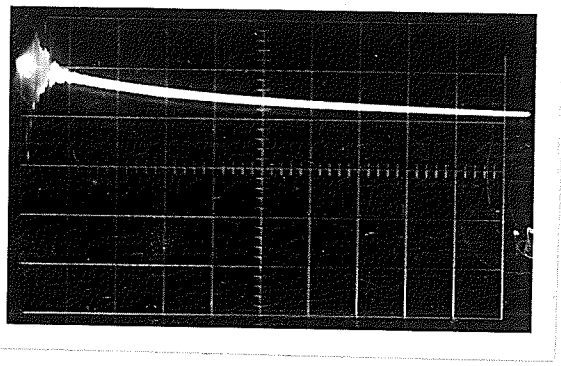

Current waveform for
a 4 kv. $1\frac{1}{2}$ by 40
high voltage impulse
5V/cm. vert. defl.
10 usec./cm. sweep speed

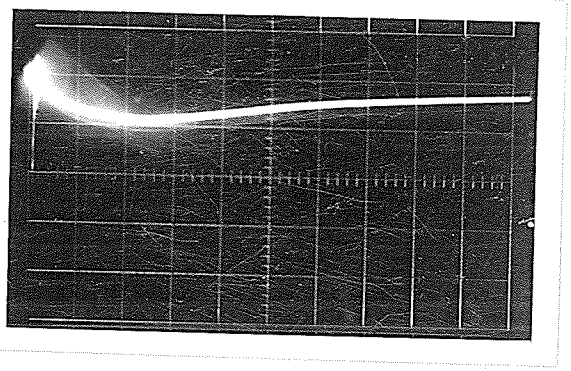

Current waveform for
a 4 kv. $1\frac{1}{2}$ by 40
high voltage impulse
5V/cm. vert. defl.
50 usec./cm. sweep speed

CURRENT WAVEFORM DURING HIGH VOLTAGE TESTS

FIGURE 4-6

CHAPTER V

EXPERIMENTAL RESULTS FOR THE VOLTAGE OSCILLOGRAM FAULT DETECTION METHOD

V - I FACTORS GOVERNING SENSITIVITY OF DETECTION

The output voltage impulse, E_o, from the Impulse Generator Simulator can be used to detect coil failure because the discharge rate of the output capacitor of the generator pulse-forming network is affected by changes in the coil impedance. The sensitivity of this method was found to depend on the equivalent circuit of the simulator, on the value of the capacitor in the circuit, and on the shape of the impulse voltage across the terminals of the coil. These effects were studied and pertinent results are illustrated in figures 5-2 to 5-7. The three waveforms in these figures are arranged as follows: the top waveform represents the output voltage without the coil; the second and third waveforms illustrate the output voltage for the coil with the armature core in the coil shell and removed respectively. Impulse waveforms for both circuits were adjusted to yield the prescribed shape when the armature core was placed in the coil shell and the coil was connected across the generator terminals.

The Impulse Generator Simulator can apply an impulse voltage to the terminals of the coil by either of the circuits shown in figure 5-1, or a combination of these circuits. The voltage waveform produced by the circuit of figure 5-1$_a$ was found to be more susceptible to changes in coil impedance than the waveform from circuit 5-1$_b$, since the former circuit including the coil has a higher output impedance. Figures 5-5 and 5-6 illustrate this difference between the two circuits.

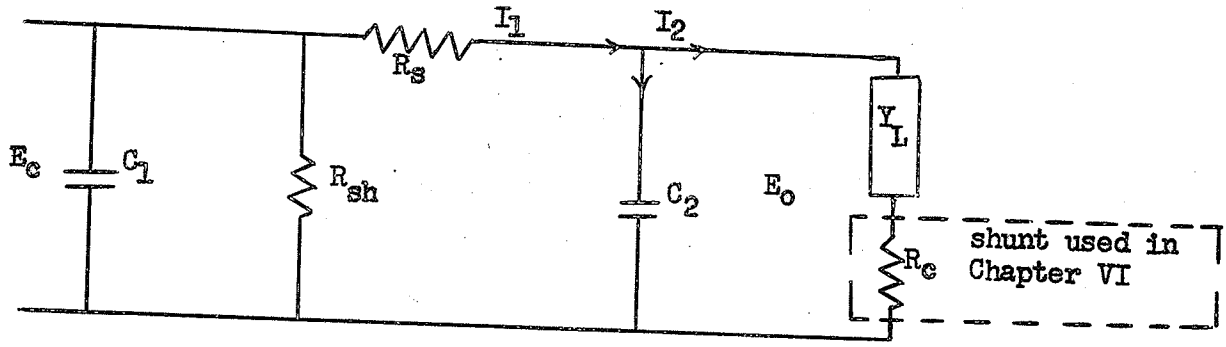

FIGURE 5-1a

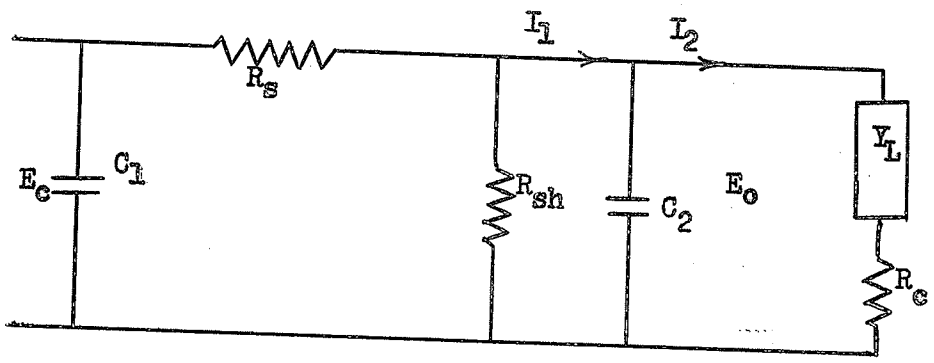

FIGURE 5-1b

C_1 = input capacitance

C_2 = output capacitance

E_o = output impulse voltage

R_c = current shunt

R_s = series resistance

R_{sh} = shunt resistance

E_c = capacitor supply voltage

Y_L = output load (relay coil)

FIGURE 5-1

EQUIVALENT CIRCUITS FOR IMPULSE SIMULATOR GENERATOR AND TEST PIECE

The amount of distortion in the output impulse for an impedance change in the coil was found to depend on the value of the capacitors used in the generator circuit, that is, on the energy available from the generator. Comparison of figure 5-2 for C_1 equal to 0.124 uf. (microfarads) and figure 5-5 for C_1 equal to 0.25 uf. showed that a larger deflection in the output waveform occurred with the smaller input capacitor. The same effect on the voltage waveshape by the output capacitor is illustrated for a $1\frac{1}{2}$ by 200 wave by comparing figure 5-3 for C_2 equal to 0.01 uf. to figure 5-4 for C_2 equal to 0.11 uf. A similar result is illustrated for a $1\frac{1}{2}$ by 40 wave by figures 5-5 and 5-7. Therefore, if the energy level is increased across the coil terminals, by either C_1 or C_2, the variation in the impulse voltage for changes in the coil impedance should be reduced. Capacitor C_1 had a greater effect on the sensitivity of the impulse than capacitor C_2, since the reduction of the distortion in the impulse waveform when C_1 was doubled was approximately equivalent to the change when C_2 was increased by tenfold. It was found that a generator capacitor less than about 0.05 uf. was impractical because successive impulse waveforms were not identical.

The detection sensitivity was also controlled by the impulse waveshape across the coil terminals. A $1\frac{1}{2}$ by 40 wave showed less deviation from the unfaulted waveform than a $1\frac{1}{2}$ by 200 wave for identical input and output circuit capacitors, since the coil impedance affects the decay of the charge on the output capacitor. These waveforms are illustrated in figures 5-2 and 5-3. Since detection of failures depended on sensing a variation in the tail of the applied impulse, the $1\frac{1}{2}$ by 200 impulse should prove to be better for failure detection than the $1\frac{1}{2}$ by 40 impulse.

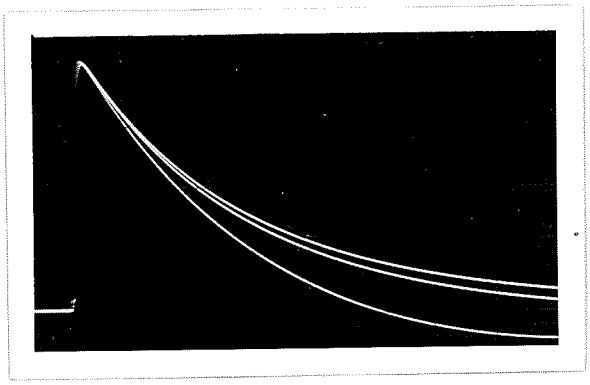

FIGURE 5-2

circuit of figure 6-1$_a$
1½ by 40 impulses
C_1 = 0.124 uf.
C_2 = 0.01 uf.

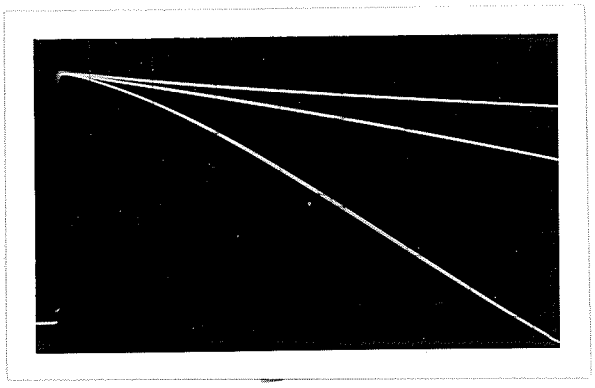

FIGURE 5-3

circuit of figure 6-1$_a$
1½ by 200 impulses
C_1 = 0.124 uf.
C_2 = 0.01 uf.

FIGURE 5-4

circuit of figure 6-1$_a$
1½ by 200 impulses
C_1 = 0.124 uf.
C_2 = 0.11 uf.

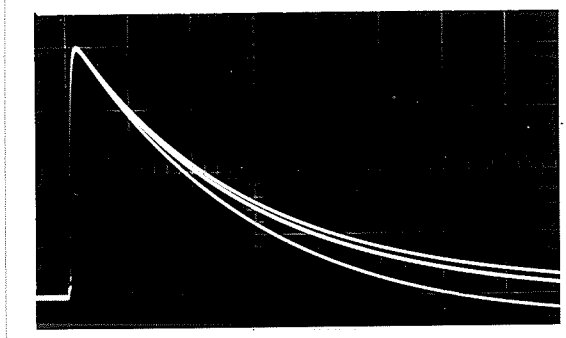

FIGURE 5-5

circuit of figure 6-1$_a$
1½ by 40 impulses
C_1 = 0.25 uf.
C_2 = 0.01 uf.

OUTPUT IMPULSE WAVEFORMS FOR NO LOAD, COIL WITH CORE IN, AND COIL WITH CORE OUT RESPECTIVELY FROM TOP TO BOTTOM

All oscillograms have a vert. defl. of 100 volts/cm. and a sweep speed of 20 usec./cm.

The test results cited in the following section are obtained from voltage studies for simulated permanent failures made on three tapped relay coils, and indicate the capabilities and limitations of the voltage oscillogram fault detection method.

V - II TESTS ON COILS WITH CONTROLLED FAULTS

These tests were performed to study the distortion in the low voltage impulse for various simulated permanent failures. The following three coils were used for the tests:

(1) 2200 turn tapped coil,

(2) 4200 turn tapped coil and

(3) 2200 turn untapped coil.

Although oscillograms are included in each section to illustrate pertinent points, a number of oscillograms are enclosed in Appendix "C" for added reference, along with a table listing the tap combinations used for each illustration and a table compiling all the tested tap combinations for coils (1) and (2), with their respective size expressed as the number of turns affected and the percentage of the total winding involved.

V - III TESTS PERFORMED ON A TAPPED 2200 TURN COIL

The winding structure of this coil is illustrated in figure 3-4(a) nd a list of tapped turns is contained on page 14.

1½ by 40 applied impulse. The generator was set to correspond to he circuit shown in figure 5-1(a), and the circuit parameters were djusted to the following values: C_1 = 0.124 uf., R_s = 74 ohms, R_s = 430 ohms.,

and C_2 = 0.01 uf. These settings for the generator yielded a $1\frac{1}{2}$ by 40 impulse across the coil terminal when no taps were shorted and the armature core was placed inside the coil shell. The impulse was applied to terminal two of the coil, and terminal one was grounded directly to the generator.

In all oscillograms the top waveform illustrates the impulse across the coil when no failure was simulated, while the remaining waveforms represent typical failures simulated by shorting specific taps. For instance, the second wave in figure 5-8 illustrates the reduction in the tail of the wave formed when taps 1 and 2 were connected to simulate a layer fault involving 202 turns or 9% of the winding.

Distortions produced in the voltage wave by a simulated fault affecting approximately 9% of the winding, such as the second wave in figures 5-8 and 5-10, indicated that detection of layer-to-layer faults was independent of the position along the winding. The resulting waveforms were sufficiently distorted that layer-to-layer failures should be easily detected.

As the percentage of the winding failures was increased, the tail of the wave was reduced until, when about 50% of the winding was affected, the tail was almost totally removed and the latter part of the wave developed a sinusoidal component. In all cases, the initial rise was unaffected, but the amplitude of the applied impulse was reduced.

Although failures involving less than 8.5% of the winding were not tested, it appears from a comparison of simulated failures of various magnitude that a 1.2% failure may possibly be detected from voltage

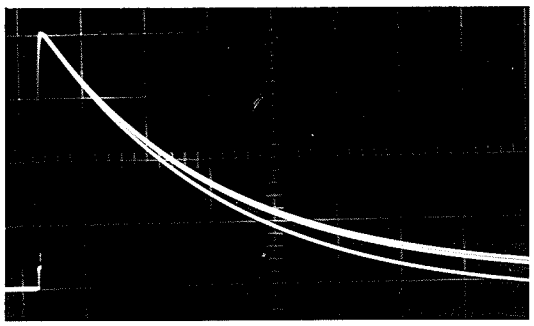

FIGURE 5-6

circuit of figure 6-1$_b$
1½ by 40 impulses
C_1 = 0.25 uf.
C_2 = 0.01 uf.

FIGURE 5-7

circuit of figure 6-1$_a$
1½ by 40 impulses
C_2 = 0.25 uf.
C_2 = 0.04 uf.

Figures 5-6 and 5-7 display output waveforms

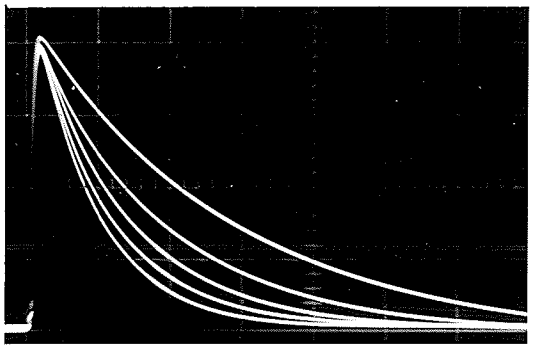

FIGURE 5-8

1½ by 40 impulse for no failure
9.6, 20, 21.8 and 34.4 percent
failures respectively

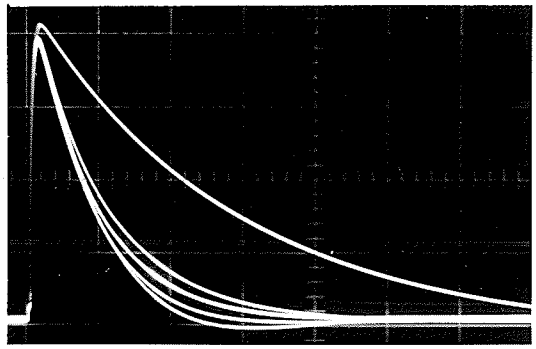

FIGURE 5-9

1½ by 40 impulse for no failure
29.9, 39.9, 42.5 and 52.3 percent
failures respectively

All oscillograms have a vert. defl. of 100 volts/cm. and a sweep speed of 20 usec./cm.

oscillograms. Comparison of the distorted voltage waveforms for 20% and 21.8% failures, shown as the third and fourth waveforms respectively in figure 5-8, illustrates that an increase of 1.8% in the winding failure resulted in a definite increase in the distortion of the impulse waveform. Other comparisons, such as the third and fourth waveforms in figure 5-9, indicate that winding failures involving 3% of the winding should produce a definite deformation in the applied impulse. When oscillograms were compared for failures which differed by only about 0.25%, the difference between the waveforms was difficult to observe. The sensitivity of the test is considered further in the section for coil (3).

Since the tests performed in section V - I indicated that detection sensitivity should depend on the shape of the impulse waveform, a $1\frac{1}{2}$ by 200 impulse was applied across the coil terminals.

$1\frac{1}{2}$ by 200 applied impulse. The values of the parameters of the impulse generator were changed to: C_1 = 0.124 uf., R_s = 47 ohms, R_{sh} = 2200 ohms, and C_2 = 0.1 uf.

An increase in sensitivity for the $1\frac{1}{2}$ by 200 wave, versus the $1\frac{1}{2}$ by 40 wave, is shown by a comparison of the 9.6% failure indication of figures 5-1 and 5-10. The $1\frac{1}{2}$ by 200 impulse results in a greater distortion in the tail of the wave, and a lower peak amplitude. This indication was similar for all simulated layer failures examined, irregardless of their position within the coil. As the percentage of the coil involved in the failures was increased in magnitude, the tail of the impulse decreased accordingly, developing a sinusoidal shape when

approximately 35% of the winding was shorted. Again, the initial rise was unaffected, but the peak amplitude was reduced.

Although the waveform for these tests was produced with a generator output capacitor of 0.11 uf., the results indicated that an increase of 0.6% in the winding failure produced a definite increase in the distortion of the current waveform. The detection sensitivity for this waveform is examined further in section V - V for a smaller output generator capacitor.

V - IV TESTS PERFORMED ON A TAPPED 4200 TURN COIL

The winding structure of this coil was illustrated in figure 3-5(b) and a list of tapped turns is given on page 14.

The detection sensitivity was reduced considerably for the tests on this coil; this reduction can be attributed to the increased generator output capacitor used during the tests, and to the increased impedance of the coil compared to that for the 2200 turn coil.

1½ by 40 applied impulse. The value of the generator parameters for the circuit shown in figure 5-1(a) were: C_1 = 0.25 uf., R_s = 74 ohms, R_{sh} = 430 ohms, and C_2 = 0.03 uf. The tests were performed as described in section V - III of this chapter.

The layer-to-layer failure, approximately 7.75% of the winding for this coil, was easily detected and independent of the location of the fault within the winding. An illustration of a 7.95% failure is shown in figure 5-16. The reduction in detection sensitivity for simulated layer failures in the 4200 turn coil can be seen by comparing figure 5-16 and figure 5-8. The results for a 16.5 and 26.5 percent failure are shown in

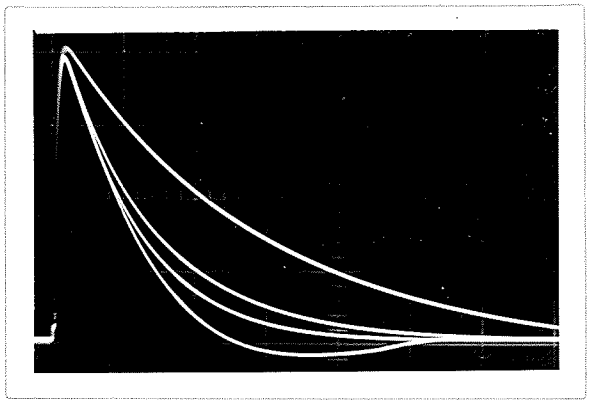

FIGURE 5-10

$1\frac{1}{2}$ by 40 impulse for no failure, 9.6, 20.3, and 51.2 percent failures respectively

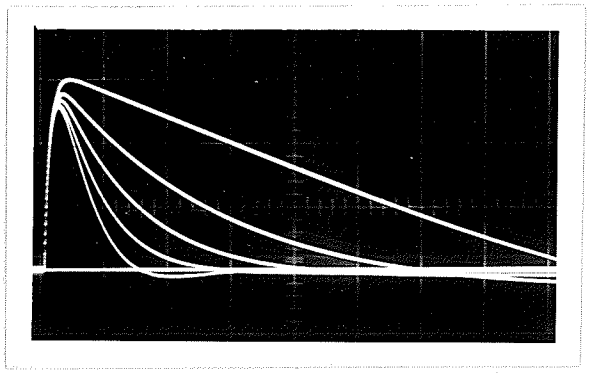

FIGURE 5-11

$1\frac{1}{2}$ by 200 impulse for no failure, 9.6, 20, and 34.4 percent failures respectively

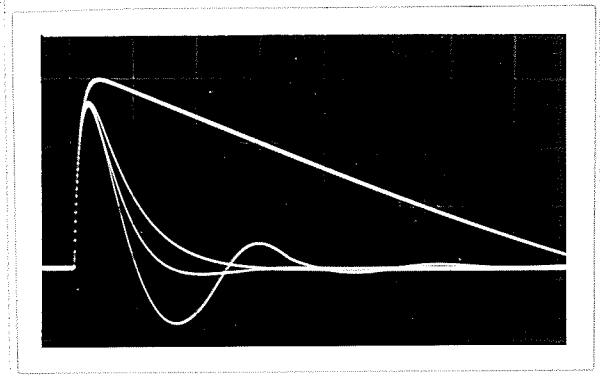

FIGURE 5-12

$1\frac{1}{2}$ by 200 impulse for no failure, 29.9, 39.4, and 52.3 percent failures respectively

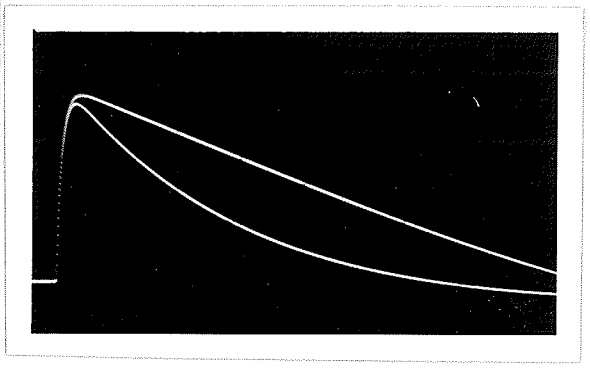

FIGURE 5-13

$1\frac{1}{2}$ by 200 impulse for no failure and 8.8 percent failures respectively

DISTORTION IN OUTPUT VOLTAGE WAVEFORM FOR FAULTS SIMULATED ON A 2200-TURN COIL

All oscillograms have a vert. defl. of 100 volts/cm. Figure 5-10 is a sweep speed of 20 usecs./cm. while the remaining figures have a sweep speed of 50 usecs./cm.

figure 5-17. An 8-turn, or 0.195%, failure is illustrated in figure 5-14 and did not show any distortion in the voltage waveshape. A 7.68% failure is compared to a 8.05% failure in figure 5-15 and illustrates a slight increase in the distortion of the impulse during the 8.05% failure.

The impulse voltage was applied to terminal one of the coil and the results disclosed that the distortions in the voltage impulse for layer failures were identical to those observed when the coil was excited through terminal two.

1½ by 300 applied impulse. The generator parameters were set at the following values: C_1 = 0.25 uf., R_s = 19 ohms, R_{sh} = 2391 ohms, and C_2 = 0.05 uf.

The waveform could not be formed with a smaller input capacitor and, as a result, the detection sensitivity was not improved by use of the longer impulse.

Detectability is demonstrated in figures 5-18 and 5-19 for failures of 0.19 and 7.5 percent of the coil winding. These oscillograms were formed by superimposing the waveforms of the unfaulted coil with the one obtained when the coil was faulted. This method was not as accurate as photographing both waves on the same film, although in the actual test for failure, superimposition of oscillograms would be required. The 0.19% failure was not detectable, whereas the 7.5% failure produced approximately the same distortion in the impulse test waveform as was observed for the 1½ by 40 impulse.

FIGURE 5-14

1½ by 40 impulse for no failure and 0.195 percent failure respectively

FIGURE 5-15

1½ by 40 impulse for no failure 7.68, and 8.05 percent failures respectively

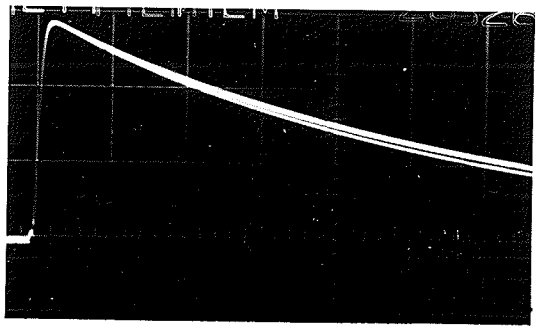

FIGURE 5-16

1½ by 40 impulse for no failure and 7.95 percent failure respectively

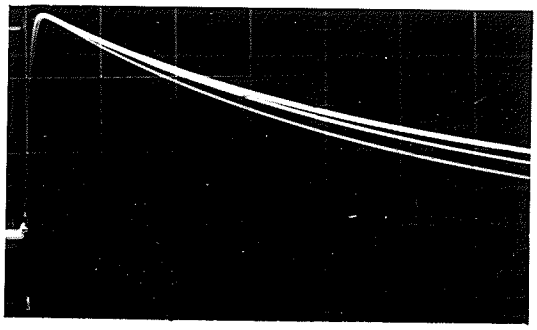

FIGURE 5-17

1½ by 40 impulse for no failure 16.5, and 26.5 percent failures respectively

DISTORTION IN OUTPUT VOLTAGE WAVEFORM FOR SIMULATED FAILURES ON A 4200 TURN COIL

All oscillograms have a vert. defl. of 100 volts/cm. and a sweep eed of 10 usec./cm.

3 by 350 applied impulse. The generator was reset using the same circuit capacitors as were used to yield the 1½ by 300 impulse. Figures 6-20 and 6-21 contain illustrations of 0.19 and 7.5 percent failures. The reduction in the rise time of the applied impulse did not appear to make any usual difference on failure detection, and there appeared to be no improvement over the 1½ by 300 impulse.

V - V DETECTION OF SIMULATED FAILURES INVOLVING ONLY A FEW TURNS IN A 2200 TURN COIL

For the tests a 1½ by 200 impulse, produced from a low capacitance circuit, was applied across the terminals of the coil. The generator variables were adjusted to yield: C_1 = 0.124 uf., R_s = 47 ohms, R_{sh} = 7200 ohms, and C_2 = 0.01 uf. The outer layer of the coil was exposed by removing the protective tape and insulation off the wire to insure good contact.

Systematic shorts, beginning with two adjacent turns, were produced and the waveform for the faulted and unfaulted winding photographed on one oscillogram. The deviation formed by shorting three adjacent turns could be detected on the oscilloscope, if carefully examined, but was difficult to reproduce on the oscillogram. This failure is illustrated in figure 5-22, and if the initial portions of these waveforms are adjusted properly, a distortion can be seen in the tail of the waveform. The results for several larger failures are shown in the remaining figures and indicate that failures of approximately 0.3% were detectable as predicted by the earlier tests.

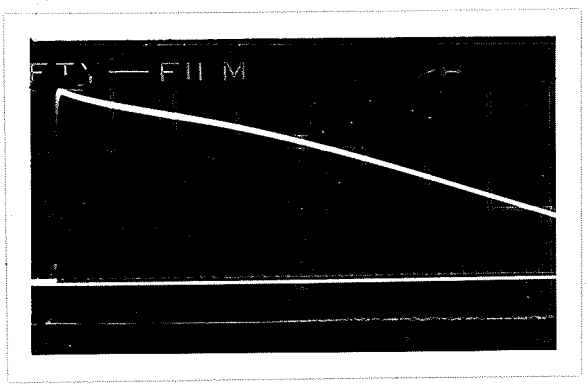

FIGURE 5-18

1½ by 300 impulse for no failure and 0.19 percent failure respectively

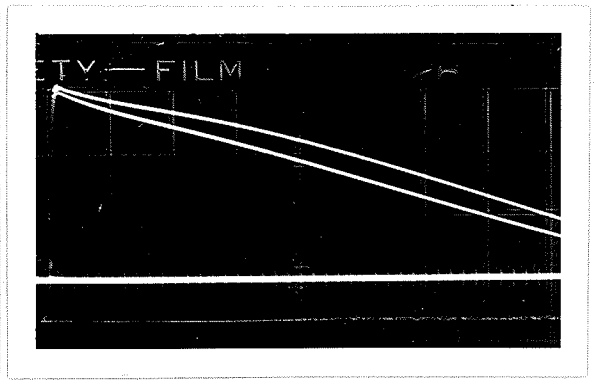

FIGURE 5-19

1½ by 300 impulse for no failure and 7.5 percent failure respectively

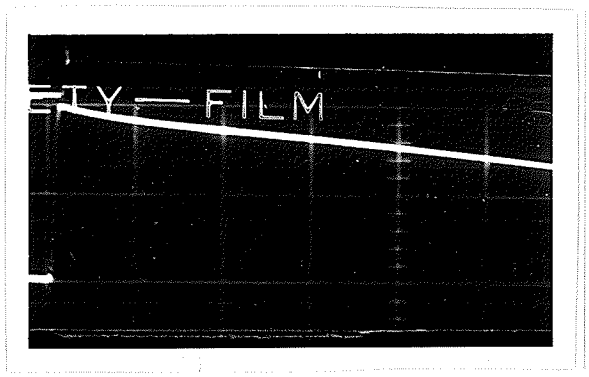

FIGURE 5-20

3 by 350 impulse for no failure and 0.19 percent failure respectively

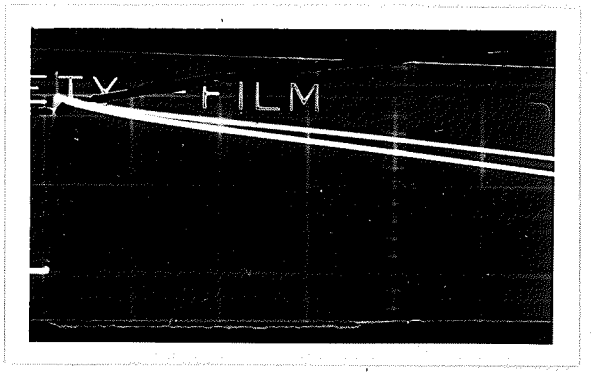

FIGURE 5-21

3 by 350 impulse for no failure and 7.5 percent failure respectively

DISTORTION TO OUTPUT VOLTAGE WAVEFORM FOR SIMULATED FAILURE ON A 4200 TURN COIL

All oscillograms have a vert. defl. of 100 volts/cm. and a sweep speed of 50 usec./cm.

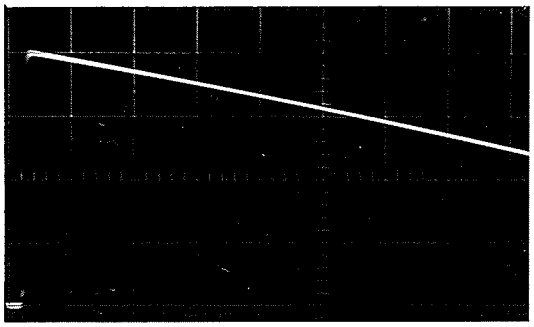

FIGURE 5-22

$1\frac{1}{2}$ by 200 impulse for no failure and a 3-turn failure respectively

FIGURE 5-23

$1\frac{1}{2}$ by 200 impulse for no failure and a 7-turn failure respectively

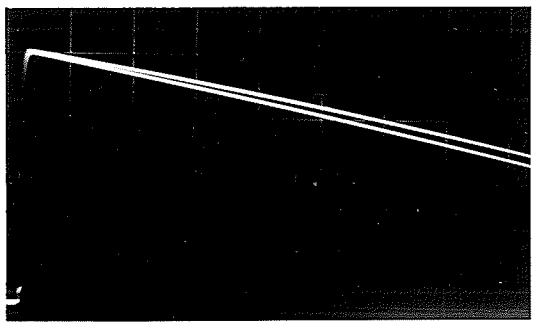

FIGURE 5-24

$1\frac{1}{2}$ by 200 impulse for no failure and a 15-turn failure respectively

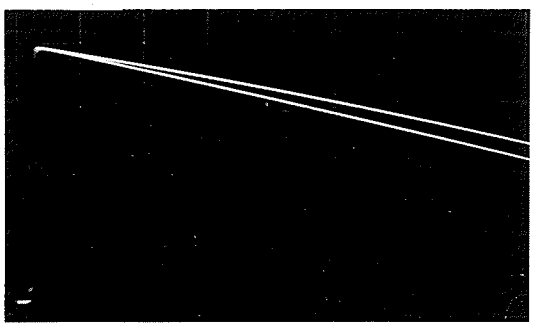

FIGURE 5-25

$1\frac{1}{2}$ by 200 impulse for no failure and a 25-turn failure respectively

DISTORTIONS IN OUTPUT VOLTAGE WAVEFORM FOR COIL WINDING FAILURES

All oscillograms have a vert. defl. of 100 volts/cm. and a sweep speed of 50 usec./cm.

V - VI TESTS ON COILS FAULTED BY HIGH VOLTAGE TESTS

The voltage oscillogram fault detection technique failed completely to indicate that the coil had failed during the high voltage tests. Oscillograms taken before and after the high voltage tests on coil (4) are shown in figures 5-26 and 5-27 for the $1\frac{1}{2}$ by 40 detection impulse and in figures 5-28 and 5-29 for the $1\frac{1}{2}$ by 200 detection impulse. Both impulses were generated with a low generator capacitor. Although carbon particles between a number of turns in the winding were found when the coil was examined, these results could be interpreted to mean either that a permanent failure did not remain after the tests, or that the failure was too small to be detected. If a permanent failure did result, the tests performed on simulated failures would suggest that the failure would not involve more than about five turns. To summarize, the tests indicated that the coil winding could fail without the failure being detected by the Voltage Oscillogram Fault Detection Method.

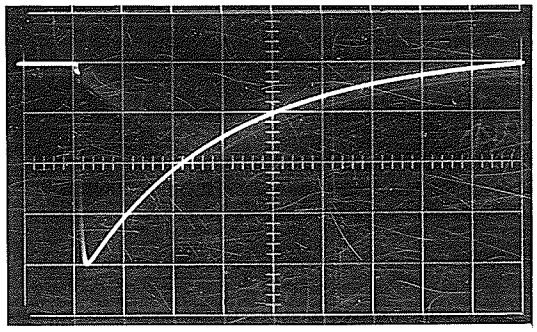

FIGURE 5-26

$1\frac{1}{2}$ by 40 impulse
voltage across terminals
of untested coil

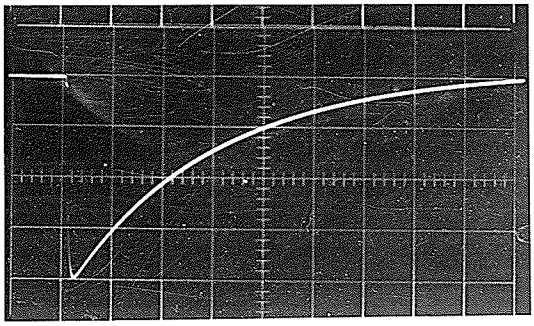

FIGURE 5-27

$1\frac{1}{2}$ by 40 impulse
voltage across terminals
of tested coil

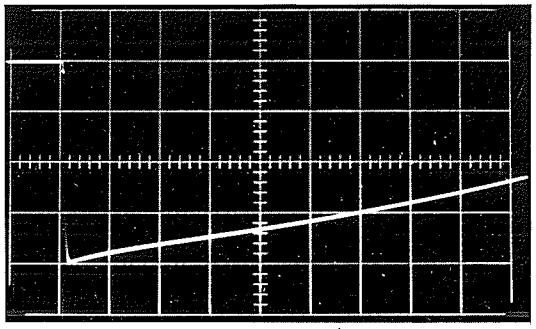

FIGURE 5-28

$1\frac{1}{2}$ by 200 impulse
voltage across terminals
of untested coil

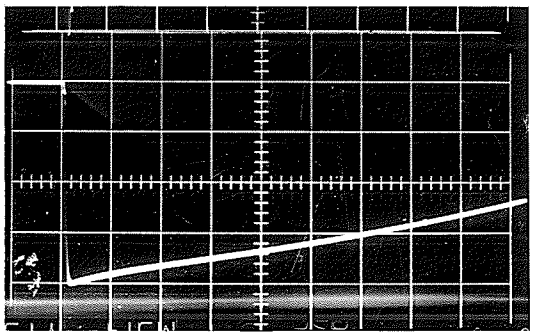

FIGURE 5-29

$1\frac{1}{2}$ by 200 impulse
voltage across terminals
of tested coil

OSCILLOGRAMS FOR VOLTAGE IMPULSE DETECTION METHOD

All oscillograms have a vert. defl. of 100 volts/cm. and a sweep peed of 20 usec./cm. Positive potential measured downward.

CHAPTER VI

EXPERIMENTAL RESULTS FOR THE CURRENT OSCILLOGRAM FAULT DETECTION METHOD

This system may be represented by one of the equivalent circuits shown in figure 5-1, except that a current shunt is required in the ground lead of the coil circuit. Two resistive shunts, of 151.0 ohms and 15.1 ohms respectively, were used during the tests to illustrate the effect of the shunt size on detection sensitivity. Both resistors were found to be free of reactive components to a frequency of 1.5 megacycles, but could not be checked beyond this frequency. The capacitors used in the resistor-capacitor shunt combinations were assumed to be of their nominal value. The voltage observed across this shunt is a measure of the coil current and the detection of failure by observation of this voltage is called the current oscillogram fault detection method.

VI - I TESTS ON COILS WITH CONTROLLED FAULTS

The sensitivity of the current waveforms to permanent failures in the coil winding was observed from simulated failures on the three coils used for the tests in the previous chapter. Although pertinent oscillograms are illustrated in each section, additional oscillograms are included in Appendix "D", along with a table specifying the tap combinations used for each simulated fault. Refer to Appendix "C" for a table specifying the size of the simulated failures resulting from the tap combinations on coils (1) and (2).

VI - II TESTS PERFORMED ON A TAPPED 2200 TURN COIL

$1\frac{1}{2}$ by 40 applied impulse. Oscillograms were recorded with a vertical deflection of 10 volts/cm. and a sweep speed of 20 usec./cm. The magnitude and location of the coil failure had a greater influence on the current waveshape than on the corresponding voltage waveform. Whereas the distortion in the voltage impulse was almost identical for all failures involving the same percentage of the winding, the current waveshape behaved in a more complicated fashion. This difference in the waveshape for layer failures is evident by comparing the 9% failure shown in figures 6-1 and 6-2 for a layer near the surface to figure 6-3 for a layer near the center of the coil. The waveform shown in figure 6-3 had a longer rise time, smaller peak, and a greater tail height. This property is not peculiar to layer failures, but affects two and three layer failures in the same manner. This is illustrated by comparing the upper waveforms in figures 6-1 and 6-2 to the waveform in figure 6-4. The latter waveform was smaller and broader than the first two. Especially obvious was the fact that the waveform for a two-layer failure did not differ greatly from a single-layer failure near the center of the coil in comparison to the striking difference between these two failures when they involved layers near the surface.

The indications for layer failures for the current oscillogram method were more obvious and convincing than those during similar tests by the voltage oscillogram technique. Comparison of figures 6-3 and 6-8 will exemplify this observation.

To determine the effect of the applied impulse voltage waveform on the current detection technique, tests were extended to a $1\frac{1}{2}$ by 200 impulse.

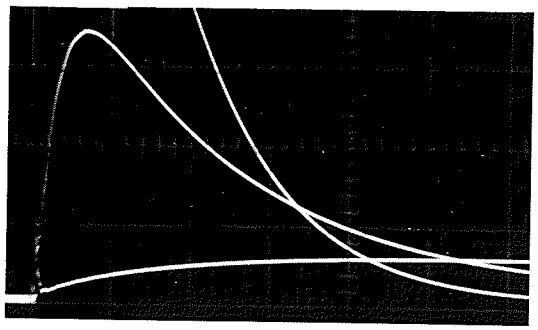

20 usec./cm. sweep; 10^{V}/cm. defl.

FIGURE 6-1

$1\frac{1}{2}$ by 40 current impulse
lower - no failure
center - failure of 9.85% of wdg.
upper - failure of 20.2% of wds.

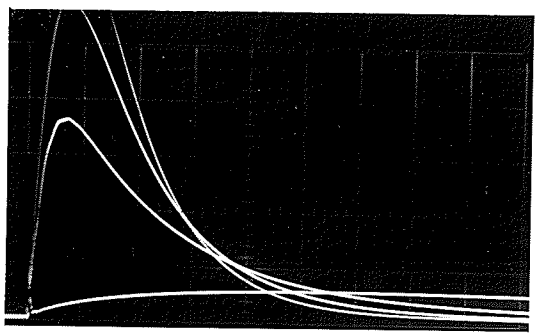

20 usec./cm. sweep; 10^{V}/cm. defl.

FIGURE 6-2

$1\frac{1}{2}$ by 40 current impulse
lower - no failure
center - failure of 9.6% of wdg.
upper - failure of 20.8% of wdg.
peak of failure of 28% of wdg.

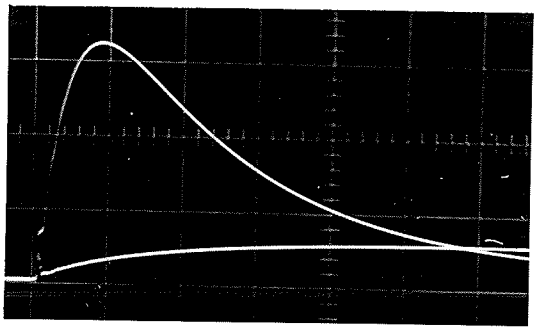

20 usec./cm. sweep; 10^{V}/cm. defl.

FIGURE 6-3

$1\frac{1}{2}$ by 40 current impulse
lower - no failure
upper - failure of 9.5% of wdg.

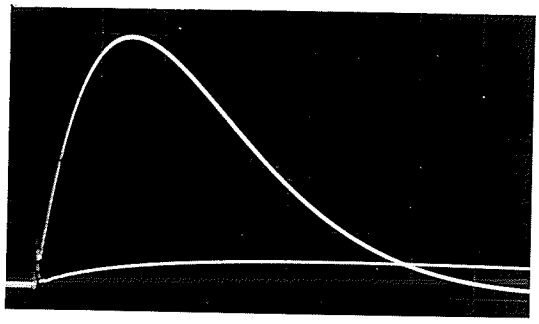

20 usec./cm. sweep; 10^{V}/cm. defl.

FIGURE 6-4

$1\frac{1}{2}$ by 40 current impulse
lower - no failure
upper - failure of 18.2% of wdg.

DISTORTIONS IN CURRENT IMPULSE WAVEFORMS DUE TO SIMULATED PERMANENT FAILURES IN 2200-TURN COIL

1½ by 200 applied impulse. The sweep speed for the oscillograms was decreased to 50 usec./cm. The current waveforms were distorted in a similar manner except that the current waveform for the 1½ by 200 impulse was on a different scale. The peak amplitudes were approximately equal but a greater difference between the original and faulted wave did exist in the latter portion of the applied 1½ by 200 impulse. Comparison of figures 6-1 and 6-5 indicates that the faulted current during the 1½ by 200 impulse was reduced below normal current sooner and produced a larger distortion over the remaining portion of the wave than that observed for the 1½ by 40 wave, resulting in greater detectability of failure. Failures involving 9% of the winding are illustrated in figures 6-5 and 6-6 for layers near the surface, in figures 6-7 for a layer failure one-quarter of the way into the winding, and in figure 6-8 for a layer failure near the center of the winding. Two-layer failures are illustrated in figures 6-5 and 6-6 for layers near the surface. The dependence of the current waveform on the location of the fault within the winding in the 1½ by 200 impulse detection test was the same as that observed during the 1½ by 40 impulse test.

VI - III TEST PERFORMED ON A TAPPED 4200-TURN COIL

1½ by 40 applied impulse. The oscillograms were recorded with a sweep speed of 10 usec./cm. and a vertical deflection of 5 volts/cm.

A failure of 0.165%, or 7 turns, shown in figure 6-9, produced a distortion in the tail of the waveform sufficient to give a definite indication of failure. An example of a layer failure is shown in figure 6-10 for a 7.5 percent failure and indicated that the detection

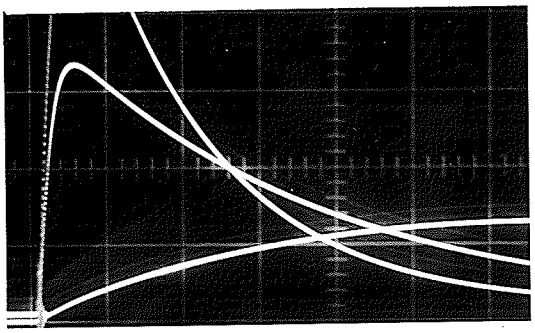

50 usec./cm. sweep; 10^{V}/cm. defl.

FIGURE 6-5

$1\frac{1}{2}$ by 200 current impulse
lower - no failure
center - failure of 9% of wdg.
upper - failure of 20% of wdg.

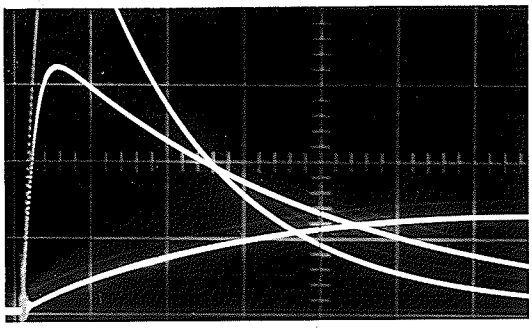

50 usec./cm. sweep; 10^{V}/cm. defl.

FIGURE 6-6

$1\frac{1}{2}$ by 200 current impulse
lower - no failure
center - failure of 9.5% of wdg.
upper - failure of 19% of wdg.

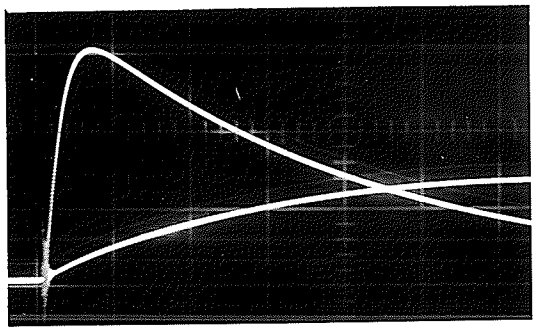

50 usec./cm. sweep; 10^{V}/cm. defl.

FIGURE 6-7

$1\frac{1}{2}$ by 200 current impulse
lower - no failure
upper - failure of 9.25% of wdg.

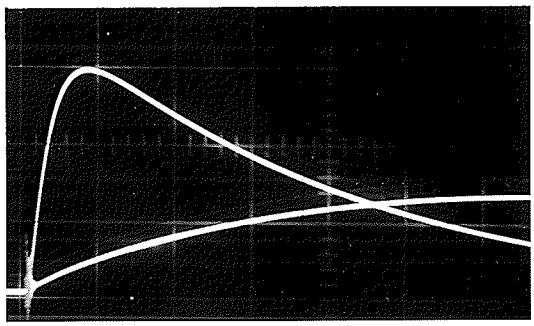

50 usec./cm. sweep; 10^{V}/cm. defl.

FIGURE 6-8

$1\frac{1}{2}$ by 200 current impulse
lower - no failure
upper - failure of 9% of wdg.

DISTORTIONS IN A $1\frac{1}{2}$ BY 200 CURRENT IMPULSE WAVEFORM DUE TO SIMULATED PERMANENT FAILURES IN THE 2200-TURN COIL

sensitivity was approximately equal to that demonstrated during the tests on the 2200 turn coil. The current waveform indicated only a slight dependency on the location of the fault within the coil winding, unlike the results obtained with the 2200 turn coil. When large failures, of the order of 20% of the winding, were simulated, very large currents were produced and demonstrated the improvement in failure detection by this method compared to the voltage oscillogram method.

Simulated failures, for the impulse applied to terminal two of the coil, showed identical distortions to those produced when the coil was excited through terminal one.

Layer failures were examined with the armature core removed from the coil and a 7.5% failure is reproduced in figure 6-11. Although the current was approximately four times as great, the detection sensitivity was not visibly increased over that when the armature core was kept inside the coil. The discontinuity in the waves was formed when the input impulse was chopped to prevent the total current from exceeding the rated value of the current shunt.

Various combinations of resistor-capacitor current shunts were tested but did not appear to improve failure detection. Further tests performed on current shunts are described in the following section. Distortions for a 0.165% failure, using 0.0067 and 0.1 uf. capacitors, are shown in figures 6-12 and 6-13 respectively.

1½ by 300 impulse. The oscillograms were recorded with a deflection of 5 volts/cm. and a sweep speed of 50 usec./cm. The tests

10 usec./cm. sweep; 5V/cm. defl.

FIGURE 6-9

$1\frac{1}{2}$ by 40 current impulse
lower - no failure
upper - failure of 0.165% of wdg.

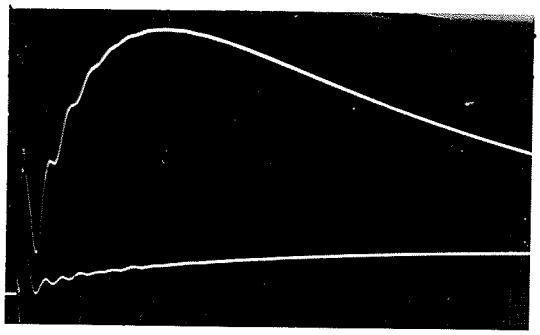

10 usec./cm. sweep; 5V/cm. defl.

FIGURE 6-10

$1\frac{1}{2}$ by 40 current impulse
lower - no failure
upper - failure of 7.5% of wdg.

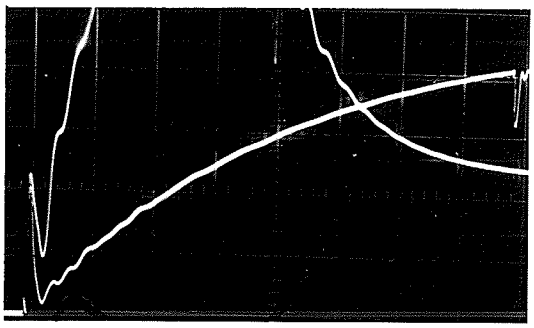

10 usec./cm. sweep; 5V/cm. defl.

FIGURE 6-11

$1\frac{1}{2}$ by 40 current impulse
lower - no failure
upper - failure of 7.5% of wdg.

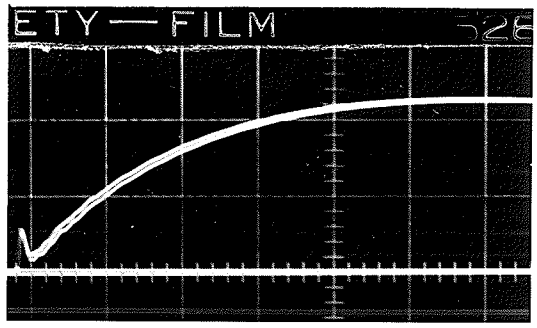

10 usec./cm. sweep; 2V/cm. defl.

FIGURE 6-12

$1\frac{1}{2}$ by 40 current impulse
lower - no failure
upper - failure of 0.165% of wdg.
shunt capacitor - 0.0067 uf.

DISTORTIONS IN $1\frac{1}{2}$ BY 40 CURRENT IMPULSE FOR SIMULATED PERMANENT FAILURES IN 4200-TURN COIL

did not illustrate any great improvement over the 1½ by 40 wave. Large values of capacitors had to be used to produce the 1½ by 300 impulse and resulted in a reduced detection sensitivity. A 0.165% failure is illustrated in figure 6-14, and when compared with figure 6-9 for the 1½ by 40 impulse, indicates that the distortion was produced over a greater portion of the total wave, yielding a more obvious display. A 15.9% failure produced a distorted waveform, approaching a square wave, and is illustrated in figure 6-15.

3 by 350 applied impulse. The generator was set with the same input and output capacitors that were used to produce the 1½ by 300 impulse. In the illustration shown in figure 6-16 for a 16 percent failure, the faulted current had a vertical deflection of 10 volts/cm., whereas the unfaulted current has a vertical deflection of 5 volts/cm. Comparison of figures 6-15 and 6-16 illustrates that the rise time of the current waveform with the coil faulted is proportional to the rise time of the applied impulse.

VI - IV DETECTION OF FAILURES INVOLVING ONLY A FEW TURNS IN A 2200 TURN COIL

The 2200 turn coil whose outer layer was exposed for simulated failures during the detection tests by the voltage oscillogram method was tested with similar simulated faults by the current method. All oscillograms were recorded with a 20 usec./cm. sweep speed.

Oscillograms of a one-turn fault are illustrated in figure 6-17 for a 150 ohm shunt and a 1½ by 40 applied impulse and in figure 6-18

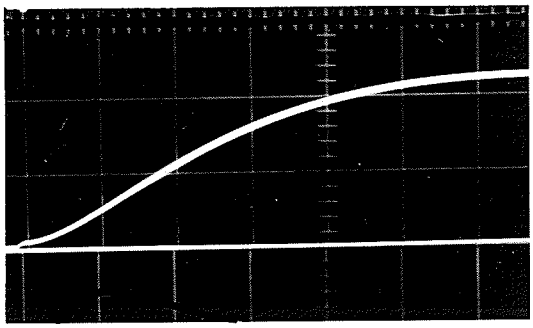

10 usec./cm. sweep; 2V/cm. defl.

FIGURE 6-13

$1\frac{1}{2}$ by 40 current impulse
lower - no failure
upper - failure of 0.165% of wdg.
shunt capacitor - 0.1 uf.

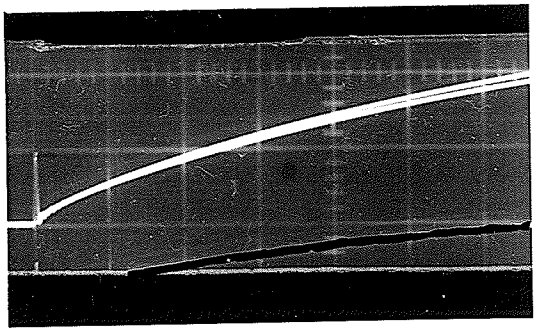

50 usec./cm. sweep; 5V/cm. defl.

FIGURE 6-14

$1\frac{1}{2}$ by 300 current impulse
lower - no failure
upper - failure of 0.165% of wdg.

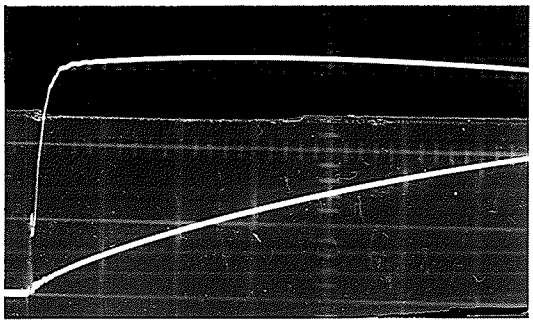

50 usec./cm. sweep; 5V/cm. defl.

FIGURE 6-15

$1\frac{1}{2}$ by 300 current impulse
lower - no failure
upper - failure of 15.9% of wdg.

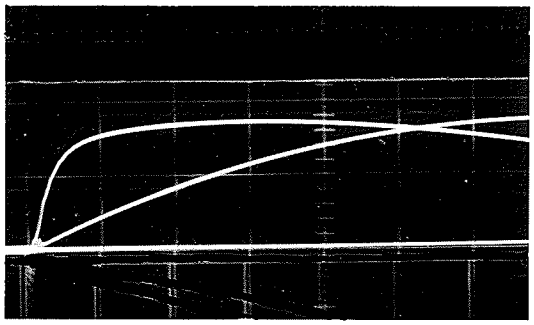

50 usec./cm. sweep; 5V/cm. defl.

FIGURE 6-16

3 by 350 current impulse
lower - no failure
upper - failure of 16% of wdg.

DISTORTIONS IN THE CURRENT IMPULSE WAVEFORMS FOR SIMULATED PERMANENT FAILURES IN 4200-TURN COIL

for a 15 ohm shunt and a 1½ by 200 impulse. A slight distortion was detected at the beginning of the wave in figure 6-17 as a result of the expanded vertical scaling and the differences in intensity between the two waveforms. However, this distortion was very slight and was not perceptible from the results of the 1½ by 200 impulse recorded with a normal vertical deflection, as shown in figure 6-18.

Failures involving more turns were examined and the occurrence of a 4-turn or larger failure is easily detectable. A 5-turn failure, recorded across a 15 ohm resistor, is shown in figure 6-19 for the 1½ by 40 impulse and in figure 6-20 for the 1½ by 200 impulse. The oscillogram in figure 6-20 indicates a distortion over a greater portion of the current wave and suggests that the current waveform was a better detector when a 1½ by 200 impulse was applied across the coil terminals.

A number of capacitor-resistor current shunts were examined, and a 0.25 uf. capacitor in parallel with a 15 ohm. resistor was found to improve detection slightly.

Two-turn failures are illustrated for the armature core within the coil shell in figure 6-21 and with the core removed in figure 6-22. Detection sensitivity was not improved when the armature was removed from the coil shell. The impulse generator was reset for the 1½ by 200 impulse with a low circuit capacitance and 1- and 2-turn failures were examined for this shunt combination. These failures are illustrated in figures 6-23 and 6-24 respectively and indicate that a slight distortion occurred for a 1-turn short. Although this distortion is not sufficient to enable this failure to be detected by superimposition of oscillograms

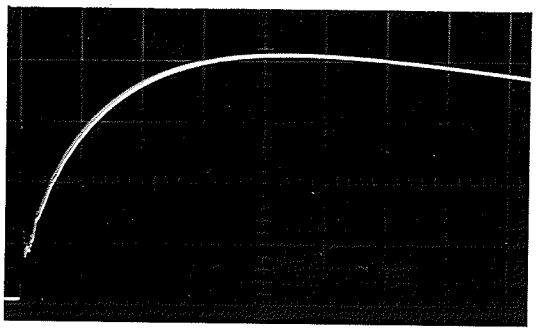

20 usec./cm. sweep; 1V/cm. defl.

FIGURE 6-17

$1\frac{1}{2}$ by 40 current impulse
lower - no failure
upper - 1 turn wdg. failure
150 ohm shunt resistor

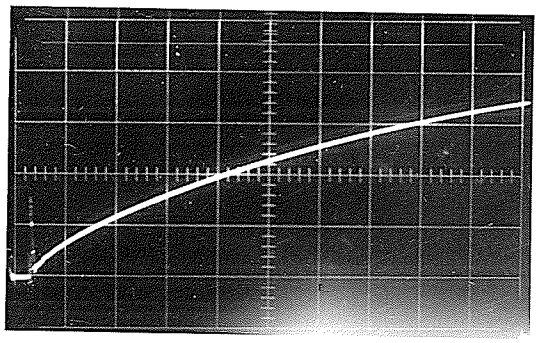

20 usec./cm. sweep; 5V/cm. defl.

FIGURE 6-18

$1\frac{1}{2}$ by 200 current impulse
lower - no failure
upper - 1 turn wdg. failure
15 ohm shunt resistor

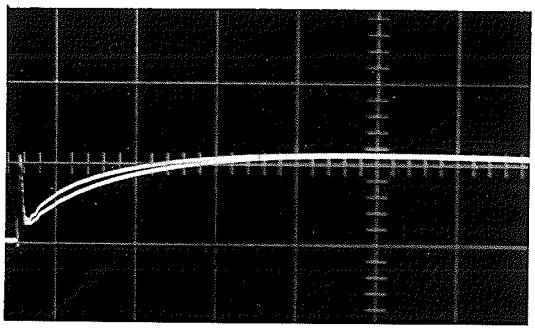

20 usec./cm. sweep; 5V/cm. defl.

FIGURE 6-19

$1\frac{1}{2}$ by 40 current impulse
lower - no failure
upper - 5 turn wdg. failure
15 ohm shunt resistor

20 usec./cm. sweep; 5V/cm. defl.

FIGURE 6-20

$1\frac{1}{2}$ by 200 current impulse
lower - no failure
upper - 5 turn wdg. failure
15 ohm shunt resistor

DISTORTIONS IN THE CURRENT IMPULSE WAVEFORMS FOR SIMULATED PERMANENT FAILURES IN 2200-TURN COIL

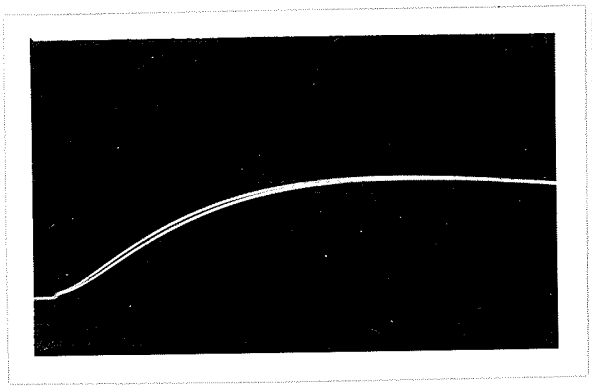

20 usec./cm. sweep; 2V/cm. defl.

FIGURE 6-21

$1\frac{1}{2}$ by 40 current impulse
lower - no failure
upper - 2 turn wdg. failure
shunt - 15 ohm and .25 uf.
armature core contained in coil

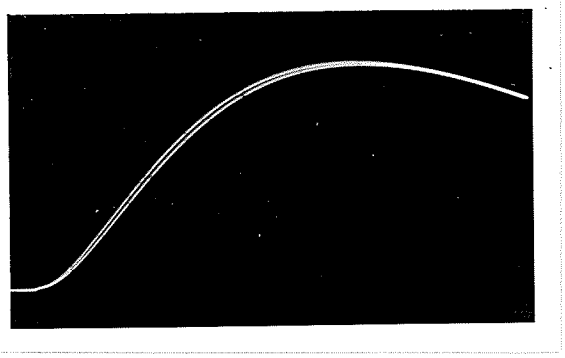

20 usec./cm. sweep; 2V/cm. defl.

FIGURE 6-22

$1\frac{1}{2}$ by 40 current impulse
lower - no failure
upper - 2 turn wdg. failure
shunt - 15 ohm and .25 uf.
armature core removed from coil

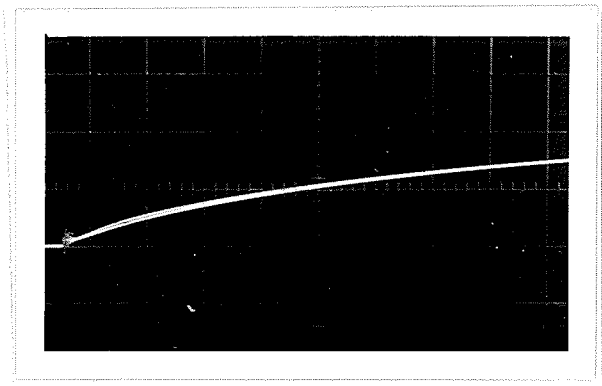

20 usec./cm. sweep; 10V/cm. defl.

FIGURE 6-23

$1\frac{1}{2}$ by 200 current impulse
lower - no failure
upper - 1 turn wdg. failure
shunt - 15 ohm and .25 uf.

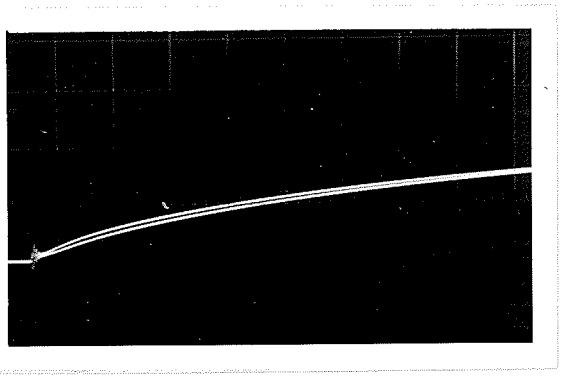

20 usec./cm. sweep; 10V/cm. defl.

FIGURE 6-24

$1\frac{1}{2}$ by 200 current impulse
lower - no failure
upper - 2 turn failure
shunt - 15 ohm and .25 uf.

DISTORTIONS IN THE CURRENT IMPULSE WAVEFORMS FOR SIMULATED PERMANENT FAILURES IN 2200-TURN COIL

with any confidence, it does illustrate the gain in sensitivity over the voltage oscillogram fault detection method.

VI - V FAILURE INDICATION FROM CAPACITIVE PULSE

Since neither the voltage nor current oscillogram method of fault detection provided conclusive evidence of minor failure, tests were repeated to examine the possibility of using the capacitive pulse at the beginning of the current waveform for fault detection. Figures 6-25 and 6-26 illustrate the deformation in the charging pulse, when a $1\frac{1}{2}$ by 40 impulse was applied across the coil terminals for simulated 1-turn and 7-turn failures respectively. Figures 6-27 and 6-28 present similar results for a $1\frac{1}{2}$ by 200 applied impulse. The oscillograms show the considerable change that exists in the latter portion of the oscillograms compared to that visible in the pulse. The pulse did not depend on the shape of the waveform nor on whether the impulse was chopped or not.

VI - VI TESTS ON COILS FAULTED BY HIGH VOLTAGE IMPULSES

When the current oscillogram fault detection method was applied to the coils subjected to the high voltage impulses, only the results for coil (4) indicated that a winding failure had occurred. Current oscillograms taken before and after the high voltage tests for this coil are shown in figures 6-29 and 6-30 for the $1\frac{1}{2}$ by 40 detection impulse, and in figures 6-31 and 6-32 for the $1\frac{1}{2}$ by 200 impulse. Both impulses were produced with the generator set with low values for capacitors C_1 and C_2 of figure 5-1(a). The results indicated that the waveforms taken

after the high voltage tests were slightly larger in magnitude and were representative of a failure involving about four turns.

Besides this indication of permanent failure, the capacitive pulse was accompanied by a high frequency oscillation after the high voltage tests. Since previous tests on simulated permanent failures indicated that this pulse was unaffected by permanent failures, this high frequency oscillation suggested that the pulse was affected by voltage flashover that occurred in carbonized portions of the coil winding.

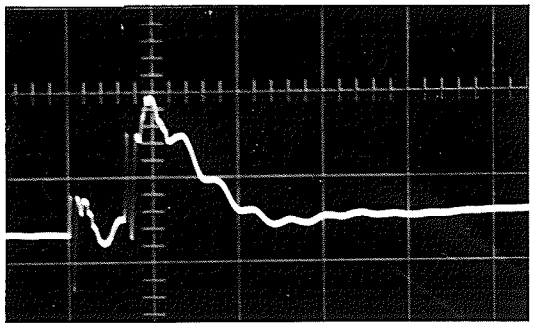

FIGURE 6-25

1 turn fault
$1\frac{1}{2}$ by 40 applied impulse

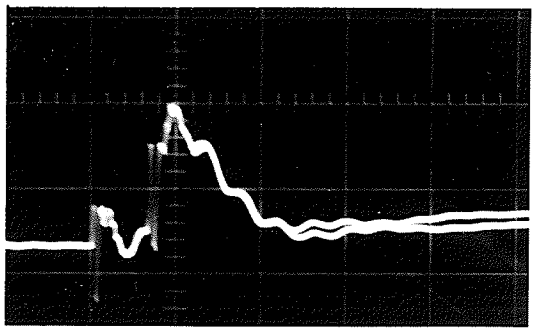

FIGURE 6-26

7 turn fault
$1\frac{1}{2}$ by 40 applied impulse

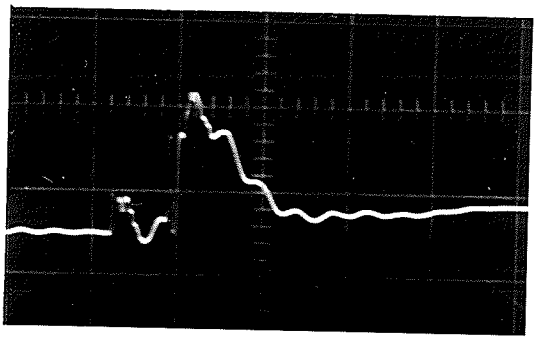

FIGURE 6-27

1 turn fault
$1\frac{1}{2}$ by 200 applied impulse

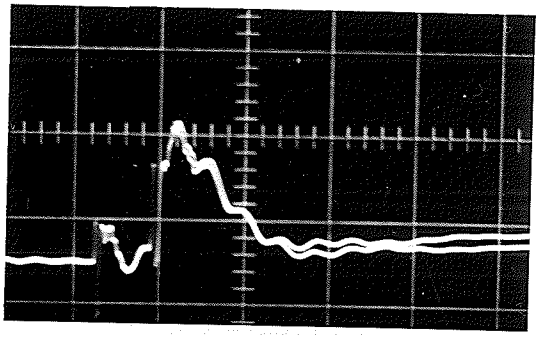

FIGURE 6-28

7 turn fault
$1\frac{1}{2}$ by 200 applied impulse

FAULTED AND UNFAULTED WAVEFORMS OF THE

CHARGING CURRENT PULSE

The lower waveform represents the pulse for an unfaulted coil. All oscillograms taken with a vert. defl. of 2 /cm. and a sweep speed of 1 usec./cm.

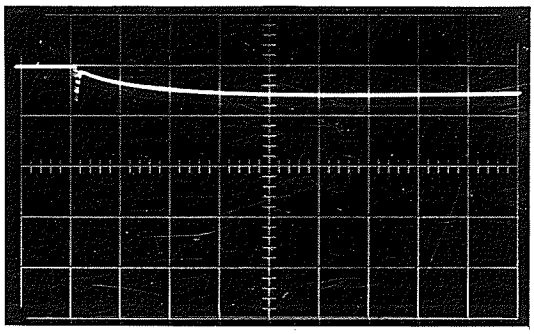

FIGURE 6-24

$1\frac{1}{2}$ by 40 impulse
voltage across terminals
of untested coil
current waveform shown

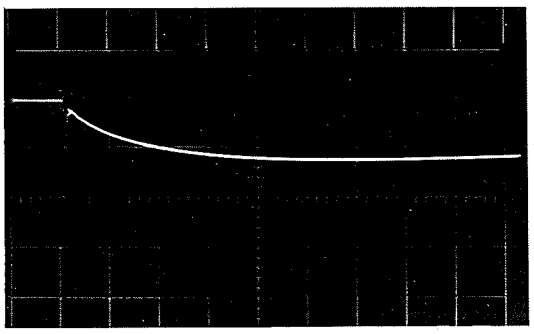

FIGURE 6-30

$1\frac{1}{2}$ by 40 impulse
voltage across terminals
of tested coil
current waveform shown

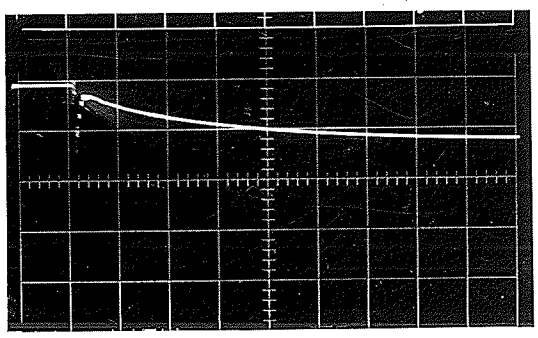

FIGURE 6-31

$1\frac{1}{2}$ by 200 impulse
voltage across terminals
of untested coil
current waveform shown

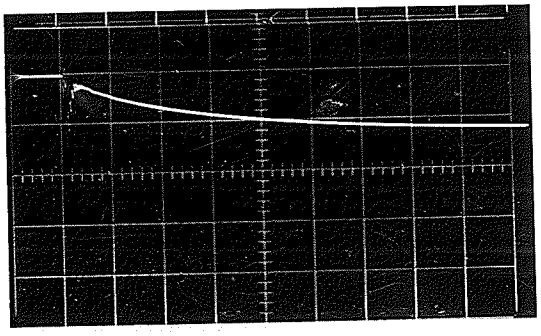

FIGURE 6-32

$1\frac{1}{2}$ by 200 impulse
voltage across terminals
of tested coil
current waveform shown

OSCILLOGRAMS FOR CURRENT IMPULSE DETECTION METHOD

All oscillograms have a sweep speed of 20 usec./cm. Figures 6-24, 6-31 and 6-32 have a vertical defl. of 2^{V}/cm. and figure 6-30 has a vert. defl. of 1^{V}/cm. Positive potential measured downward.

CHAPTER VII

EXPERIMENTAL RESULTS FOR THE TRANSMITTED IMPULSE DETECTION METHOD

VII - I DETECTION BY COIL TRANSMISSION OF VOLTAGE IMPULSE

Since neither the voltage nor current oscillogram fault detection method provided conclusive evidence of minor winding failures, further study in this problem was required and a number of techniques were investigated: promising results were realized for the coil conceived as a two-terminal-pair network. The input terminal-pair was chosen as one of the coil terminals and the coil shell, while the output terminal-pair constituted the remaining coil terminal and the coil shell. The applied voltage impulse excited the fundamental frequency of the coil which modulated this impulse as it travelled to the output terminals.

When a permanent failure develops in the coil, a portion of the winding is shorted in which eddy currents are generated by the active flux. These eddy currents are accompanied by an opposing flux which indirectly alters the amplitude and frequency of the internal oscillations. This failure detection technique concentrates on detecting these changes in the fundamental frequency of the coil, caused by winding failures, rather than changes in the applied impulse as examined by the former detection methods studied.

VII - II SIMULATED FAILURES WHEN COIL EXCITED THROUGH TERMINAL (1)

Terminal (1) was defined in figure 3-5 of Chapter III as the terminal leading to the outer layer of the winding. Initial tests were

performed on a 4200-turn coil, with the armature core in and out of the coil shell respectively, and were extended to the 2200-turn coil to examine the detection sensitivity and its dependence on the applied impulse waveforms. The oscillograms for this test and those in the remaining sections of this chapter were recorded with a vertical deflection of 100 volts/cm. and a sweep speed of 20 usec./cm. Only pertinent oscillograms are included in the discussion, but additional oscillograms are included in Appendix "E".

4200-Turn Coil

The parameters of the impulse generator were set with low values for the generator capacitors to produce a 1½ by 40 voltage impulse across the coil terminals. The tests were performed with the coil shell grounded to the impulse generator through a 150 ohm resistor.

Armature core contained in coil shell. The transmitted 1½ by 40 impulse was modulated by a highly damped oscillation of approximately 16 kilocycles when the coil was free from any failures. When a failure of 0.165%, or 7 turns, of the winding was simulated by shorting taps number 2 and 3, a definite change was present in the modulating oscillation. Superimposition of the unfaulted and faulted waveforms for 0.165% and 0.195% failures is shown in figures 7-1 and 7-2 respectively. Larger failures were accompanied by an increase in the oscillation frequency, as well as the reduction in amplitude, and resulted in well defined indication of coil failure. Figure 7-3 illustrates a 7.73% failure, which is typical of any layer failure for the coil. The failure indications were found to

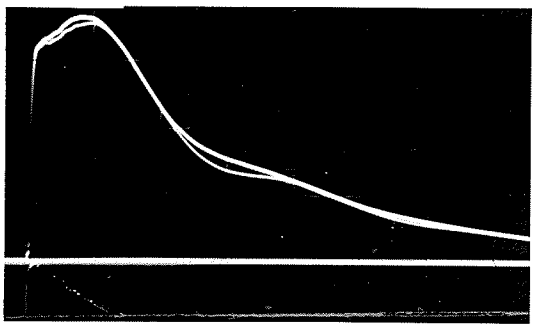

FIGURE 7-1

failure involving .165 percent
of the total winding
armature core contained in
coil shell

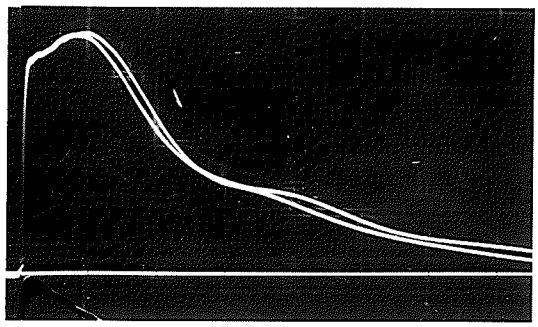

FIGURE 7-2

failure involving .195 percent
of the total winding
armature core contained in
coil shell

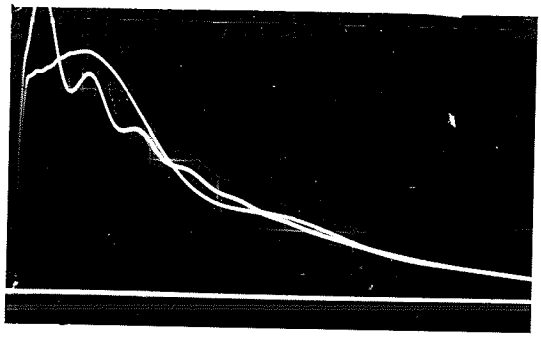

FIGURE 7-3

failure involving 7.73 percent
of the total winding
armature core contained in
coil shell

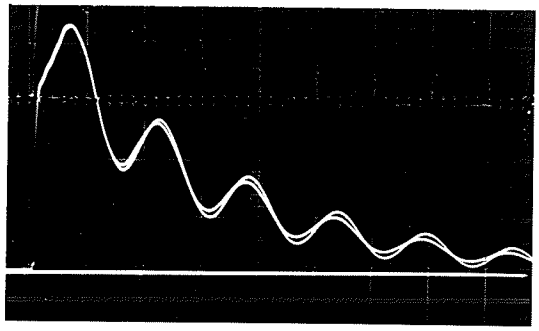

FIGURE 7-4

failure involving 2 loosely coupled
turns of identical wire
armature core removed from
coil shell

FAULTED AND UNFAULTED WAVEFORMS FOR A $1\frac{1}{2}$ BY 40 IMPULSE

APPLIED BETWEEN TERMINAL (1) AND CORE

OF 4200-TURN COIL

be independent of the location of the failure within the coil winding.

Armature core removed from the shell. When the armature core was removed from the coil shell, the amplitude and frequency of the induced oscillation were increased and the detection sensitivity for these oscillations was improved considerably. The detection sensitivity inherent in this method is exemplified by the distortion for a 2-turn failure, produced by looping two turns of wire around the coil and shorting the ends, shown in figure 7-4. Since these turns were only loosely coupled to the coil winding, a 2-turn failure within the winding should be easily distinguished.

The 0.165 and 7.73 percent failures were re-examined for the armature core removed from the coil, and indicated a greater deviation between the unfaulted and faulted oscillograms over a larger portion of the waveform than was observed during the previous tests when the armature core was kept in the coil shell. These failures are illustrated in figures 7-5 and 7-6 respectively.

In order to compare the detection sensitivity of this method with that available by the current and voltage oscillogram methods, tests were conducted on coil (1).

?200-Turn Coil

The tests were performed with the resistance removed from the oil circuit and the armature core placed in the coil shell. The induced oscillation was similar to the oscillation observed with the resistance n the coil circuit and the armature core removed from the coil shell.

Failures of 1 and 2 turns were examined and an illustration of a 1-turn failure is shown in figure 7-7 for an applied $1\frac{1}{2}$ by 40 impulse. The waveform with the larger oscillation is representive of the unfaulted coil. The 1- and 2-turn failures did not produce any noticeable change in the frequency, but did damp the existing oscillation sufficiently to produce failure indications which are easily distinguished from the unfaulted waveform. When failures were observed for chopped applied impulses, the corresponding change in amplitude and frequency in the coil oscillation was easier to distinguish. The result of a single-turn failure for an applied $1\frac{1}{2}$ by 40 impulse, chopped at 10 usec., is illustrated in figure 7-8. Tests showed that the amplitude of the oscillation after the impulse was chopped depended directly on the phase at the instant of chop. The 1-turn illustrations, shown in figures 7-9 and 7-10 for the unchopped and chopped $1\frac{1}{2}$ by 200 impulse respectively, indicated that a $1\frac{1}{2}$ by 200 impulse yielded a greater contrast between the faulted and unfaulted impulses than a $1\frac{1}{2}$ by 40 wave. This difference is apparent from a comparison of figures 7-7 and 7-9. Larger failures are indicated by a marked frequency shift. These chopped $1\frac{1}{2}$ by 40 and $1\frac{1}{2}$ by 200 waves are compared in figure 7-11; their results are compared in figures 7-12. The chopped $1\frac{1}{2}$ by 200 impulse approached a square wave and energized oscillations of larger amplitude.

A comparison of the results of the two coils shows that the 4200-turn coil had a lower natural frequency than the 2200-turn coil: the former was recorded as approximately 31 kilocycles, whereas the latter had a frequency in the neighbourhood of 50 kilocycles. However, there did not seem to be any difference in the detection sensitivity. The

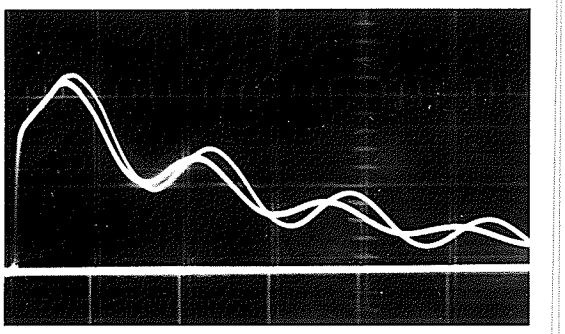

FIGURE 7-5

failure involving .165 percent
of the total winding
armature core removed from
coil shell

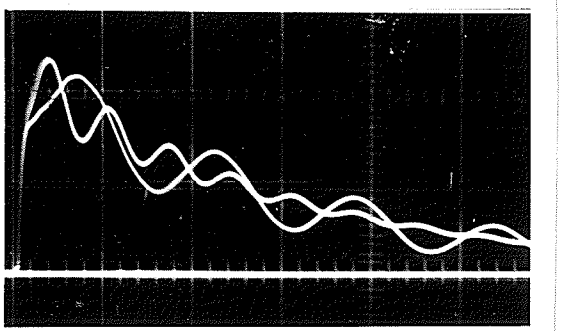

FIGURE 7-6

failure involving 7.72 percent
of the total winding
armature core removed from
coil shell

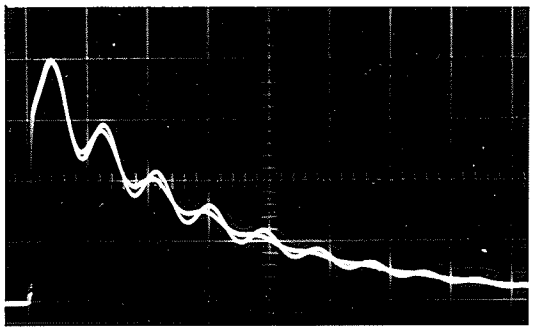

FIGURE 7-7

failure of 1 turn in 2200
turn coil
armature core contained in
coil shell

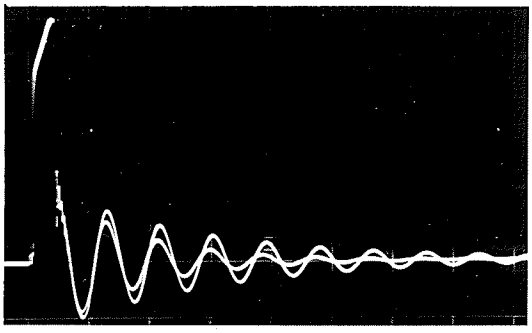

FIGURE 7-8

failure of 1 turn in 2200
turn coil
armature core contained in
coil shell
chopped input impulse

FAULTED AND UNFAULTED WAVEFORMS FOR AN $1\frac{1}{2}$ BY 40 IMPULSE

APPLIED BETWEEN TERMINAL 1 AND CORE

The waveform with the largest amplitude at 20 usec. represents the unfaulted waveform. All oscillograms have a vert. defl. of 100V/cm. and a sweep speed of 20 usec./cm.

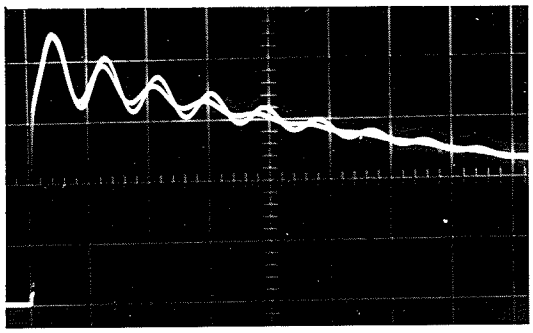

FIGURE 7-9

failure of 1 turn in
2200 turn coil
$1\frac{1}{2}$ by 200 input impulse

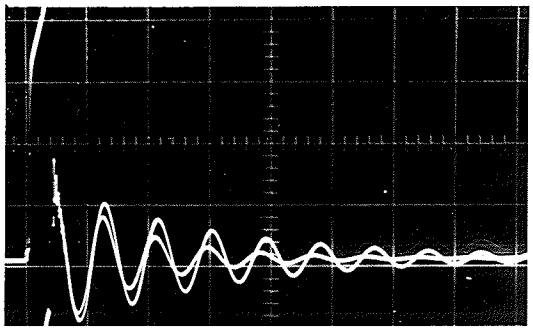

FIGURE 7-10

failure of 1 turn in
2200 turn coil
chopped $1\frac{1}{2}$ by 200 impulse

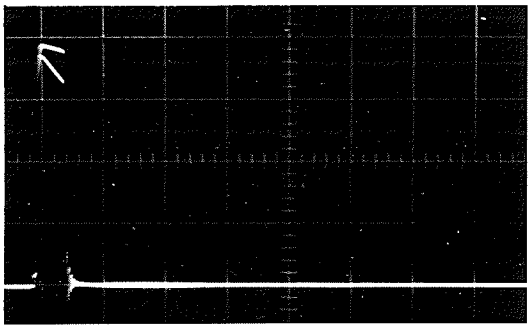

FIGURE 7-11

comparison between a chopped
$1\frac{1}{2}$ by 40 and a $1\frac{1}{2}$ by 200
impulse

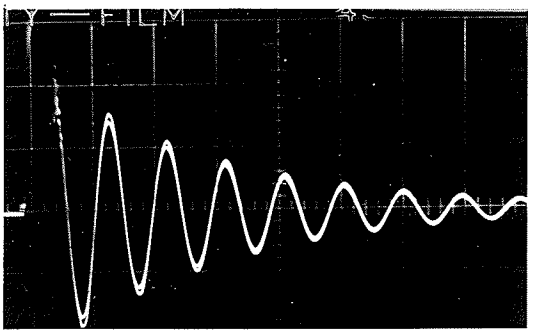

FIGURE 7-12

comparison of the results of
a $1\frac{1}{2}$ by 40 and a $1\frac{1}{2}$ by 200
impulse

FAULTED AND UNFAULTED WAVEFORMS FOR AN IMPULSE APPLIED

BETWEEN TERMINAL 1 AND CORE

All oscillograms have a vert. defl. of 100^{v}/cm. and a sweep speed of 20 usec./cm. Armature core contained in coil shell.

frequencies were altered slightly when the coils were energized through the other terminal.

Comparison of the oscillation with and without the resistance and with and without the armature core in the circuit suggests that this oscillation is dependent on the resonance between the coil inductance and the coil and generator capacitance.

VII - III EXCITATION OF THE COIL THROUGH TERMINAL (2)

The amplitude of the induced oscillation and the change in amplitude due to coil failure were both increased by exciting the coil through terminal (2). Initial tests were observed on a 4200-turn coil for an unchopped and chopped 1½ by 40 input impulse and the results disclosed that a 2-turn failure could be identified without superimposing the oscillograms (see Appendix "E"). A change in frequency, as well as the amplitude, was easily visible when the failures involved more than four turns. The amplitude of the oscillations was found to depend directly on the magnitude of the applied impulse, however no change in frequency could be detected for variation of the applied impulse. The tests were completed by simulating minor failures on the exposed outer layer of coil (3).

The results of a 2-turn failure for an applied normal and chopped 1½ by 40 impulse are shown in figures 7-13 and 7-14 respectively, and illustrated more positive failure indications than were observed during the tests for the coil energized through terminal (1). These failures were duplicated for an applied 1½ by 200 impulse, shown in figures 7-15 and 7-16, and produced better indications than those observed for the 1½ by 40 impulse. Figure 7-17 illustrates the results for a 1½ by 15 impulse

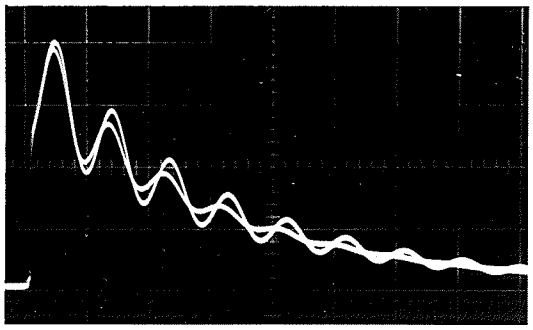

FIGURE 7-13

2 turn failure
1½ by 40 applied impulse

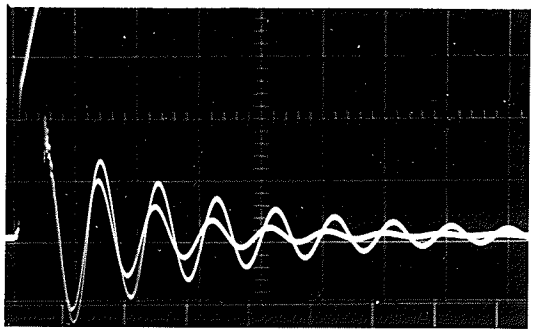

FIGURE 7-14

2 turn failure
1½ by 40 chopped impulse

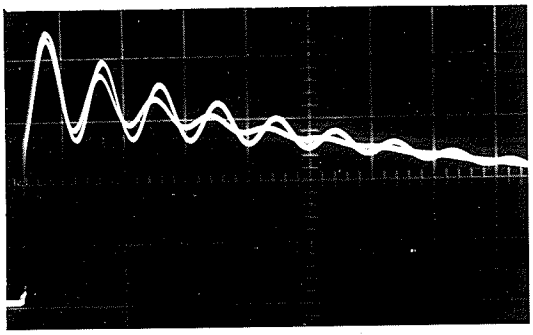

FIGURE 7-15

2 turn failure
1½ by 200 applied impulse

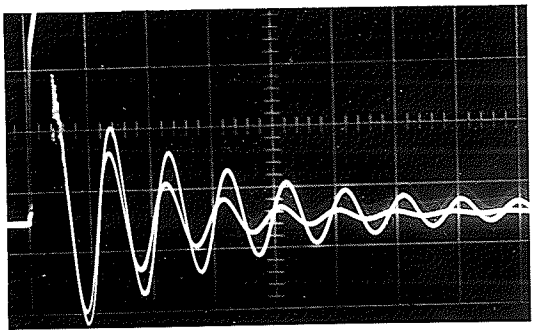

FIGURE 7-16

2 turn failure
1½ by 200 chopped impulse

FAULTED AND UNFAULTED WAVEFORMS FOR AN IMPULSE APPLIED BETWEEN

TERMINAL 2 AND CORE OF 2200 TURN COIL

All oscillograms have a vert. defl. of 100^{v}/cm. and a sweep speed of 20 usec./cm. Armature core contained in coil shell.

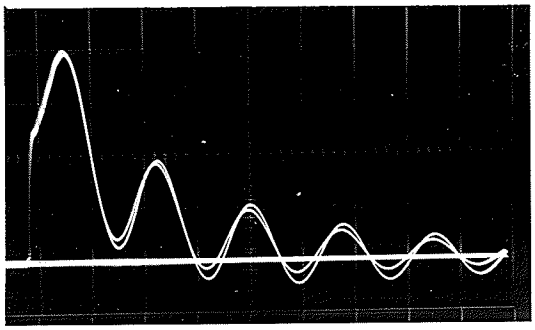

FIGURE 7-17

$1\frac{1}{2}$ by 15 applied impulse
loosely coupled two-turn
failure

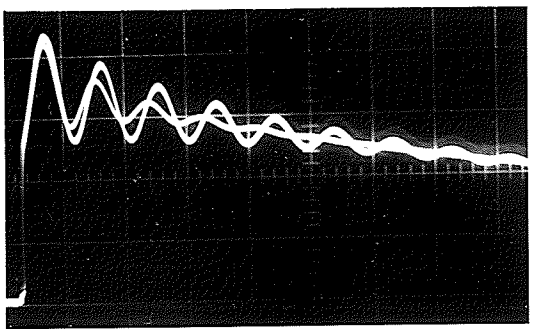

FIGURE 7-18

3 turn failure
$1\frac{1}{2}$ by 200 applied impulse

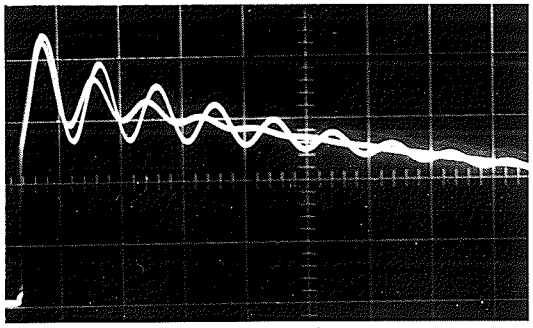

FIGURE 7-19

4 turn failure
$1\frac{1}{2}$ by 200 impulse

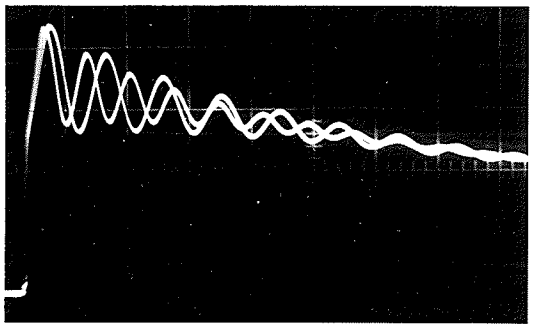

FIGURE 7-20

7 turn failure
$1\frac{1}{2}$ by 200 applied impulse

FAULTED AND UNFAULTED WAVEFORMS FOR AN IMPULSE APPLIED BETWEEN

TERMINAL 2 AND CORE OF 2200 TURN COIL

All oscillograms have a vert. defl. of 100^{v}/cm. and a sweep speed of 20 usec./cm. Armature core contained in coil shell.

and indicates that, although the induced oscillations were of greater amplitude, the change in the oscillation during coil failure was reduced. It appears that failure indication depends upon either the rate at which the energy is delivered to the coil, or upon the total energy supplied to the coil.

A 1-turn, 4-turn and a 7-turn failure are illustrated in figures 7-18, 7-10 and 7-20. Failures in the order of seven turns, or greater, changed the induced oscillation sufficiently to eliminate the need for superimposition of oscillograms.

When the output terminals of the coil were terminated, the coil oscillations were damped and the failure indications reduced considerably.

Comparison of the results for the chopped and unchopped applied impulses indicated that the applied impulse added nothing to the detectability of a failure and, moreover, obscured any change that had occurred in the amplitude and frequency of the coil oscillation. The problem was to excite this winding and independently measure this oscillation. The results of one method of observing this oscillation separately is discussed in the following chapter.

VII - IV TESTS ON COILS FAULTED BY HIGH VOLTAGE IMPULSES

When the transmitted impulse method of failure detection was applied to the two coils that were subjected to the high voltage impulse tests, only the results for coil (4) showed that a failure had occurred during the high voltage impulse tests. Figure 7-21 illustrates the output waveforms for the $1\frac{1}{2}$ by 40 and the $1\frac{1}{2}$ by 200 applied impulses for

coil (4) before the high voltage tests, whereas figures 7-22 and 7-23 illustrate the results for these impulses after coil (4) was subjected to the high voltage impulses. The reduction in amplitude of the modulating oscillation was evident by visual inspection of the oscillograms; the results of the $1\frac{1}{2}$ by 200 impulse being particulary clear. The results for coil (5) did not indicate any signs of failure and are not included.

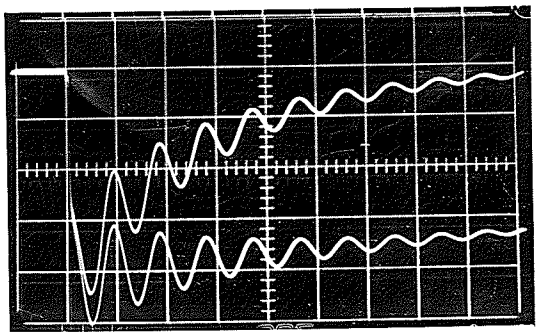

FIGURE 7-21

$1\frac{1}{2}$ by 40 and $1\frac{1}{2}$ by 200 modulated outputs of untested coil

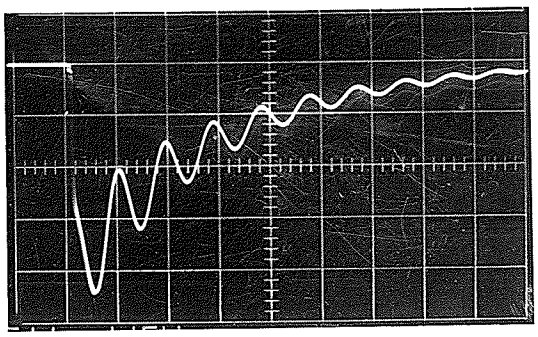

FIGURE 7-22

$1\frac{1}{2}$ by 40 modulated output impulse of tested coil

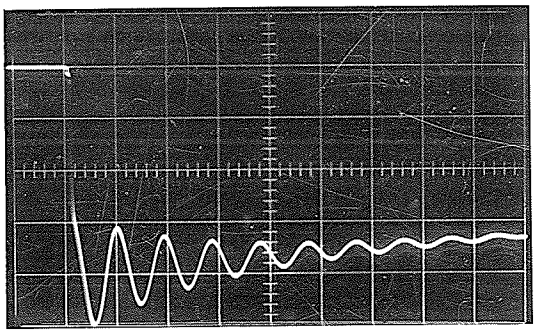

FIGURE 7-23

$1\frac{1}{2}$ by 200 modulated output impulse of tested coil

FAILURE DETECTION FOR COIL SUBJECTED TO HIGH VOLTAGE TESTS

All oscillograms have a vert. defl. of 100^{V}/cm. and a sweep speed of 20 usec./cm. Positive potential measured downward. Armature core contained in coil shell.

CHAPTER VIII

EXPERIMENTAL RESULTS FOR THE INDUCED OSCILLIATION DETECTION METHOD

VIII - I DETECTION BY EXCITATION AT THE NATURAL COIL FREQUENCY

When an impulse was applied between either of the coil terminals and the coil shell, an induced oscillatory voltage, similar to the oscillation that modulated the transmitted impulse for the tests in the previous chapter, was obtained across the coil terminals. The bottom illustration of figure 8-1 indicates the oscillations produced across the output terminals - terminal two and the coil shell - when a chopped $1\frac{1}{2}$ by 40 impulse was applied to the input terminals - terminal one and the coil shell. The center illustration of figure 8-1 indicates the oscillation observed across the coil terminals when the same chopped $1\frac{1}{2}$ by 40 impulse was applied to the input terminals. The oscillation observed across the coil terminals was larger in amplitude and displaced in time from the oscillation observed across the output terminals of the coil.

The top waveform in figure 8-1 illustrates the oscillation observed across the coil terminals when this chopped $1\frac{1}{2}$ by 40 impulse was applied to the input terminals of the coil and a 4-turn fault was simulated on the coil. Note that the positive voltage is measured downward in these figures, and in a number of other figures contained in the thesis, since the negatives were printed in reverse by error. Figure 8-4 illustrates the resulting waveforms for the induced oscillation when a

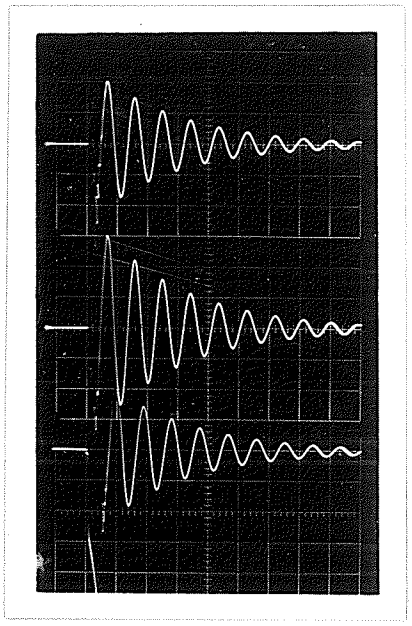

FIGURE 8-1

top - $1\frac{1}{2}$ by 40 chopped impulse result for a 4 turn coil failure

center - $1\frac{1}{2}$ by 40 chopped impulse result for no coil failure

bottom - Transmitted pulse for a chopped $1\frac{1}{2}$ by 40 impulse (see previous section)

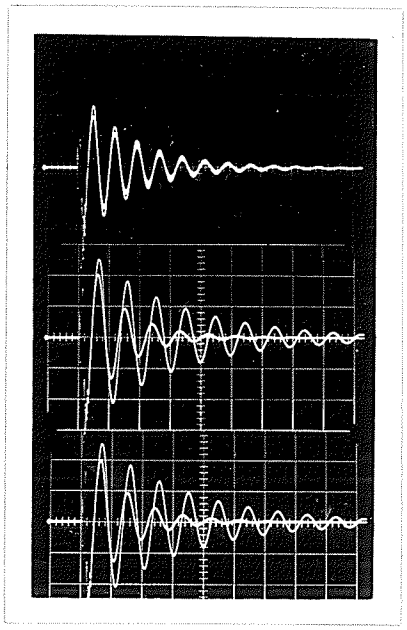

FIGURE 8-2

top - $1\frac{1}{2}$ by 200 impulse result (larger waveform) compared to that for a $1\frac{1}{2}$ by 40 impulse
7 turn coil failure

center - $1\frac{1}{2}$ by 200 chopped impulse results for no failure and a 12 turn coil failure

bottom - $1\frac{1}{2}$ by 200 impulse results for no failure and a 12 turn coil failure

FAILURE DETECTION FROM INDUCED COIL OSCILLATIONS

All oscillograms have a vert. defl. of 5^{V}/cm. and a sweep speed of 20 usec./cm. Positive measured downward.

$1\frac{1}{2}$ by 200 impulse was applied to the input terminals of the coil and 4- and 5-turn faults were simulated on the coil; the waveform with the reduced intensity represents the simulated 4-turn failure. When the simulated failure was increased from 4 to 5 turns, the damping factor was increased considerably and the frequency was altered slightly. The waveforms in this figure cannot be compared to those in figure 8-1 because the amplitude of the applied impulses was different. The waveforms at the top of figure 8-2 illustrate the results for 7-turn failures when the coil was excited by $1\frac{1}{2}$ by 200 and $1\frac{1}{2}$ by 40 impulses of equal peak amplitude, produced with the same circuit capacitors in the generator simulator. The oscillations excited by the $1\frac{1}{2}$ by 200 impulse had a greater amplitude and damping factor than those excited by the $1\frac{1}{2}$ by 40 impulse. The center and bottom illustrations in figure 8-2 represent 12-turn failure indications for chopped and unchopped $1\frac{1}{2}$ by 200 impulses respectively. The unchopped impulse excited an oscillation of a slightly larger amplitude for the unfaulted coil, and an oscillation of a slightly smaller amplitude for the faulted coil, resulting in a slight increase in detection sensitivity. These illustrations show that the sensitivity of failure detection is susceptible to the total energy delivered by the impulse and to the impulse waveshape, or rate, by which this energy is delivered to the coil.

When the positive side of the impulse was applied to the coil shell and the coil terminal was grounded, the induced oscillation was reduced considerably.

Figure 8-3 summarizes the results of the tests performed on coil (1) with an applied $1\frac{1}{2}$ by 40 impulse. The sixth waveform illustrates the

FIGURE 8-3

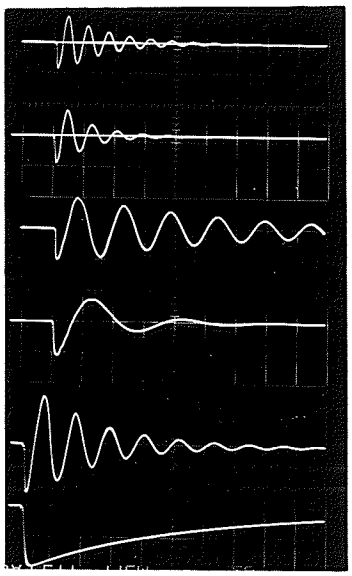

first - oscillation induced in the coil with the armature core out and a 20 turn fault

second - oscillation induced with the core in and a 20 turn failure

third - oscillation induced with the core removed and no failure simulation

fourth - oscillation induced with the core in the coil and a resistance in series with the coil terminal

fifth - same as the fourth, except the resistance is removed

sixth - $1\frac{1}{2}$ by 40 applied impulse. 200^{V}/cm. vert. defl.

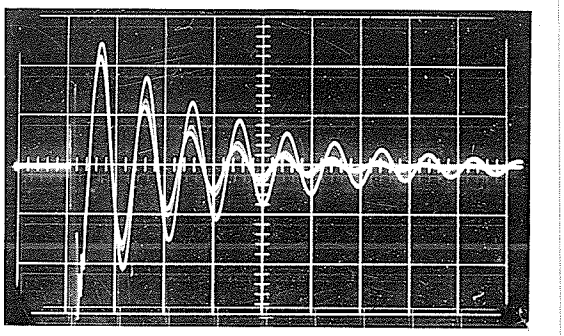

FIGURE 8-4

4- and 5-turn failure
$1\frac{1}{2}$ by 200 applied impulse

FAILURE DETECTION FROM INDUCED COIL OSCILLATIONS

All oscillograms have a sweep speed of 20 usec./cm. Figure 8-3 has a vert. defl. of 10^{V}/cm. and figure 8-4 has a vert. defl. of 5^{V}/cm. Positive potential measured downward.

applied $1\frac{1}{2}$ by 40 impulse while the fifth and third waveforms illustrate the induced oscillations for the coil with no simulated failure and the armature core in and out of the coil shell respectively. These comparisons indicate that both the frequency and damping factor of the induced oscillation were reduced when the armature core was removed from the coil shell. The fourth waveform illustrates the induced oscillation for the coil with the armature core contained in the coil, but with a 150 ohm resistor placed between the coil shell and the low voltage terminal of the impulse simulator. This oscillation is identical to that modulating the impulse in the tests performed in the previous chapter when the resistance was included in the coil circuit. This oscillation could be damped out completely by increasing this resistance and would suggest that this oscillation depends on the resonance between the combination of the output generator capacitor and distributed capacitance of the coil and the coil inductance. The second and first waveforms represent the results for a 20-turn failure and the armature core in and out of the coil shell respectively.

VIII - II TESTS ON COIL FAULTED BY HIGH VOLTAGE TESTS

The resonant method of failure detection also yielded favourable results when coil (4) was examined for coil failure, but along with the other methods, did not indicate failure for coil (5). Figures 8-5 and 8-6 illustrate the oscillograms taken before and after the tests for coil (5) and show a reduction in the amplitude of the coil oscillation equal to that for a 4- or 5-turn failure.

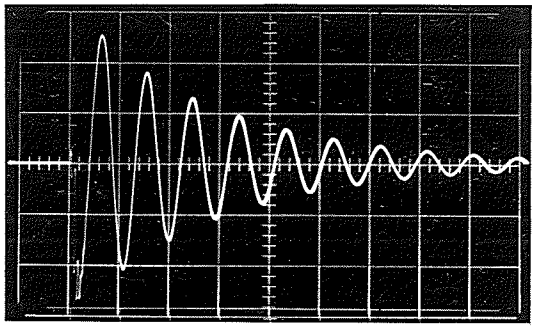

FIGURE 8-5

oscillation across terminals
of untested coil for
$1\frac{1}{2}$ by 40 applied impulse

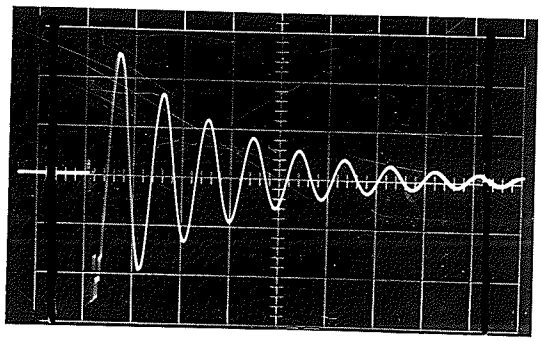

FIGURE 8-6

oscillation across terminals
of tested coil for
$1\frac{1}{2}$ by 40 applied impulse

FAILURE DETECTION FOR COIL SUBJECTED TO

HIGH VOLTAGE IMPULSE TESTS

All oscillograms have a vert. defl. of 5^{V}/cm. and a sweep speed of 20 usec./cm. Positive potential measured downward. Armature core contained in coil shell.

CHAPTER IX

DISCUSSION OF THE FAULT DETECTION METHODS

IX - I VOLTAGE OSCILLOGRAM FAULT DETECTION METHOD

The tests performed on controlled failures showed that the greatest detection sensitivity was obtained by voltage impulses with a long tail, produced with low values for the circuit capacitors in the Impulse Generator Simulator. A restriction is imposed by the generator on the minimum value for these capacitors since, if they are set too low, successive waveforms will not be identical, blurring the oscillograms.

The greatest detection sensitivity was obtained during these tests by a $1\frac{1}{2}$ by 200 impulse produced with the generator input capacitor set at 0.125 uf. and the output capacitor set at 0.01 uf. A failure involving 0.32% of the winding, that is 7 turns in a 2200-turn coil, was detected when the faulted and unfaulted impulse waveforms were photographed on the same oscillogram. In actual practice two oscillograms must be superimposed and very meticulous technique is required to retain this degree of accuracy.

Comparison of the results for both the 2200- and 4200-turn coils indicated that this method depended on the impedance of the coil tested, and that this method would only produce good results if the impedance of the coil was much less than the output impedance of the generator.

When this method was extended to coils faulted by high voltage impulses, it failed completely to indicate that the coils had failed, even though the other detection methods suggested a failure of the order of 3 or 4 turns. These tests justify the conclusion that the voltage impulse is inadequate as a primary detection for failures incurred during high voltage impulse testing.

IX - II CURRENT OSCILLOGRAM FAULT DETECTION METHOD

The detection sensitivity of this technique depended primarily on the same parameters as affected the voltage oscillogram technique; however, this method was more sensitive than the voltage oscillogram method. For instance, the distortion in the current waveform for failures involving 0.165% of the winding was comparable to the distortion in the voltage impulse waveform for failures involving 2% of the winding.

Tests performed on coil (3) showed that a two-turn fault in the outer layer of the 2200-turn coil was detectable when photographed on the same oscillogram across a 15 ohm resistor for a $1\frac{1}{2}$ by 200 impulse applied to the coil. This indication decreased when the shunt resistor was increased to 150 ohms. Although the total current increased considerably when the armature core was removed from the coil shell, the detection sensitivity was not affected. The results of the tests on the coils faulted by the high voltage impulses indicated that a permanent failure of the order of 3 or 4 turns remained in the coil.

The distortion in the current waveform depended on the position of the failure within the coil winding. Failures near the surface produced a distorted waveform with a faster rise time, indicating that the detection sensitivity would be greatest for failures near the surface and decreasing for failures near the center of the winding.

Although the amplitude of the current for the coil with no simulated failure was proportional to the impedance of the coil, the detection sensitivity decreased only slightly when the detection tests were extended from the 2200-turn coil to the 4200-turn coil.

The current pulse at the beginning of the current waveform was shown to be of little value in detecting permanent failures and was reduced by placing a capacitor in parallel with the 15-ohm shunt. The greatest improvement in failure detection by the tail of the impulse was observed with a capacitor of 0.25 uf., yielding a time constant of 4 usec. for the shunt. When this time constant was increased to 15 usec., the failure indication was poorer. Although this pulse had no value for permanent failures, Pioneer Electric Limited found this pulse useful in detecting whether the winding was susceptible to transient arc-over failures. This property was also shown during the tests on the coils faulted by the high voltage impulses, and indicated that further study should be directed to this pulse as a failure detector.

IX - III INDUCED OSCILLATION FAULT DETECTION METHOD

Although the Current Oscillogram Detection Method possessed sufficient sensitivity to detect most minor permanent failures, the indication was not of a form to permit small failures to be easily apparent from comparison of the oscillograms. Failure detection techniques, based on the induced coil oscillation, were examined and were found to yield clearer indications of failure. Two methods for monitoring this oscillation were discussed - the Transmitted Impulse Detection Method and the Induced Oscillation Detection Method. Both methods had similar detection sensitivity, but the latter method made minor changes more readily visible.

Tests on controlled failures indicated that a one-turn failure in a 2200-turn coil was accompanied by a reduction in the amplitude and an increase in the damping rate of the oscillations; larger failures were

accompanied by a change in frequency as well. From the results illustrated in the preceding chapters, it can be easily appreciated that the sensitivity inherent in this type of detection exceeds that available by the conventional current and voltage methods of failure detection. The tests performed on the coils faulted by high voltage impulses verified these findings, but also indicated that the current waveform may have more potential if the current pulse is sensitive to failure by transient arc-over.

Comparison of the results for a $1\frac{1}{2}$ by 40 impulse and a $1\frac{1}{2}$ by 200 applied impulse showed that the amplitude of the induced oscillation depended on the waveshape of the impulse and on the energy delivered by the impulse. Before any definite conclusions can be drawn about the optimum detection sensitivity, further tests on simulated failures are required in which the capacitors of the simulator are varied while the applied impulse is kept constant.

The amplitude of the induced oscillation was proportional to the amplitude of the applied impulse, but this dependence was not as serious as in the conventional methods of failure detection, since the rate of decay of this oscillation, affected by failure, was not affected by the waveshape.

Further studies were not undertaken to exploit the possibility of increasing the detection sensitivity over that already indicated in the previous chapters. One possibility would be to test if the spectrum analyzer could be used to determine the difference in energy available or the frequency shift in the induced oscillation before and after the coil was faulted.

CHAPTER X

VOLTAGE DISTRIBUTION ALONG COIL WINDINGS

X - I VOLTAGE DISTRIBUTION IN TRANSFORMERS AND SINGLE LAYER COILS

Theoretical studies, followed by experimental verification, have yielded an insight into the internal behaviour of single-layer coils, and have led to an understanding of the impulse voltage distribution in transformer windings. The initial distribution of voltage was found to be governed by the capacitive distribution within the winding since the magnetic field required a finite time to develop. Moreover, it was discovered that this initial distribution depended on a capacitive ratio, α, which was defined as the square root of the ratio of total capacitance to earth, C_g, to the total series capacitance of the full winding, C_s, that is

$$\alpha = \sqrt{C_g/C_s}$$

The initial voltage at any point x along the winding, $e_{(x)}$, measured from the neutral end of the coil could be calculated from the following equation (reference 12),

$$e_{(x)} = E_o \frac{(\sinh \alpha \, x/L)}{(\sinh \alpha)}$$

where

E_o = magnitude of the applied voltage

L = total length of the winding

x = distance measured from neutral end of winding.

It is important to note that if the capacitance is not uniformly distributed along the winding, then α will not be a constant.

This expression was derived for a unit-step of voltage applied across the coil terminals. Similar distributions result experimentally for waveforms with steep wavefronts, that is, the initial voltage gradient is dependent directly on the rise time.

After this voltage distribution is established, currents will be produced within the winding which depend directly on this voltage distribution. The natural tendency of this initial distribution of current growth, by redistributing the condenser charges, is towards a uniform distribution of voltage. A non-uniform distribution of current results, when the voltage becomes uniform, due to the presence of magnetic leakage. Further redistribution of voltage, yielding maximum voltage where the minimum voltage was previously, is required to bring about uniformity in the current distribution. These internal oscillations in resonant portions of the winding are gradually damped out resulting in a uniform voltage distribution. Since internal oscillations exist as a result of voltage redistribution caused by inductive currents, their amplitude is dependent on the decay time of the impulse. For short wavetails the amplitudesof the lower harmonics are decreased.

The total voltage to earth can then be represented by a harmonic series in space and time of the form

$$e_{(x,t)} = E_o \frac{L - x}{L} + E_o \sum_{m=1}^{\infty} U_m \sin (m \pi x/L) \cos \omega_m t$$

ω_m = angular frequency of the mth harmonic

U_m = amplitude of mth harmonic and is a function of the initial voltage distribution

These equations, derived from the unit-step function, can be modified by Duhamel's theorem to be applicable to a disturbing force of any

mathematical form. Duhamel's theorem states

$$r(t) = e_u(t)e(0) + \int_0^t e_u(x)e'(t-x)dx$$

$e_u(t)$ = response to an applied unit-step of voltage

$e(0)$ = value of applied voltage at t=0

$e'(t-x)$ = first derivative of the applied voltage function with variable t replaced by $(t-x)$.

$r(t)$ = response for an applied voltage $e_{(t)}$

The amplitude of the oscillations in practice is dependent on the voltage distribution accompanying a particular waveshape, approaching their maximum amplitude for unit-step waves.

X - II APPLICATION OF STANDARD WAVES TO MULTI-LAYER COILS

Knowledge of the impulse voltage distribution along the transformer windings has furnished information regarding the locations of highly stressed portions of the winding. Similar studies were pursued for the multi-layer coils in order to study the internal behaviour of their windings. The studies revealed a fairly uniform initial impulse stress distribution and subdued localized oscillatory stress regions, compared to those existing in transformers.

The voltage waveshape of particular interest is the standard $1\frac{1}{2}$ by 40 wave used in most impulse tests. This impulse was applied across the terminals of the coil and oscillograms of voltage recorded from the tapped points along the winding to the neutral. Both terminals were used respectively for the neutral in order that the tapped points would represent both

the top half and the bottom half of the coils. Graphs were plotted from these results to show the voltage distribution throughout the coil.

Figure 10-1 illustrates the applied 1½ by 40 wave along with the voltages observed at the various taps for coil (1) with the core in. Figure 10-2 illustrates similar results for coil (2). Figure 10-3 illustrates these voltages for coil (2) with the core out.

It was assumed that the first and last layers had approximately the same capacitance to core, thus the taps could be used to illustrate the voltage throughout the coil by reversing the coil terminals.

Graphs were plotted for voltage versus position throughout the coil at specific times after the impulse was applied to the coil terminals. For example, figure 10-4 illustrates the value of the voltage at the 75 percent position of the total winding at 2, 4 and 5 microseconds after the 1½ by 40 impulse was applied to the coil terminals. Graph 1 illustrates the voltage distribution for coil (1) with the core within the coil shell. Graphs 2 and 3 illustrate similar results for coil (2) with the armature core in and out of the coil shell respectively.

The voltage distribution along the top layer of the coil for the armature core inside and removed from the coil shell was examined for extreme variations of the voltage stress and is illustrated in figure 10-5. The top and bottom waveforms are indicative of the end turns in the layer while the remaining waveforms represent the distribution taken at approximately equal intervals along the top layer. This figure indicates that the voltage distributed along a layer decreases uniformly as shown on the graphs, but oscillates with time with the oscillation of greatest amplitude appearing at the center of the layer.

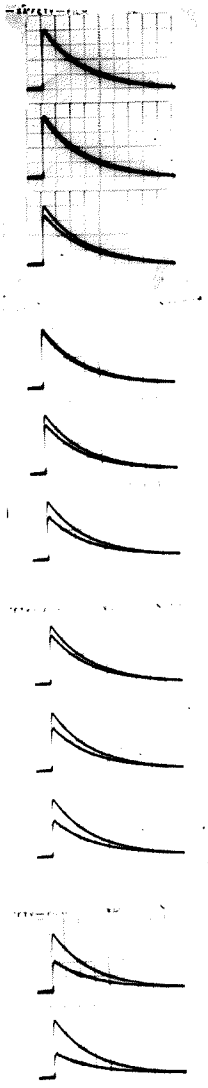

APPLIED VOLTAGE TERMINAL #1 100V/cm

VOLTAGE AT TAP #11 100V/cm

VOLTAGE AT TAP #10 100V/cm

VOLTAGE AT TAP # 9 100V/cm

VOLTAGE AT TAP # 8 100V/cm

VOLTAGE AT TAP # 7 100V/cm

VOLTAGE AT TAP # 5 100V/cm

VOLTAGE AT TAP # 4 100V/cm

VOLTAGE AT TAP # 3 100V/cm

VOLTAGE AT TAP # 2 100V/cm

VOLTAGE AT TAP # 1 100V/cm

1½×40 IMPULSE VOLTAGE DISTRIBUTION

FOR COIL I WITH CORE CONTAINED IN SHELL

APPLIED VOLTAGE REPRODUCED IN EACH OSCILLOGRAM
ALL OSCILLOGRAMS HAVE A SWEEP SPEED OF 20 μSEC/CM

FIGURE 10-1

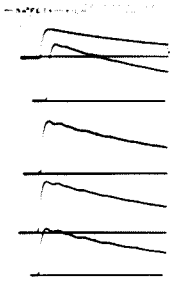

APPLIED VOLTAGE TERMINAL #1 200V/cm
VOLTAGE AT TAP #1 100V/cm
VOLTAGE AT TAP #2 100V/cm
VOLTAGE AT TAP #3 100V/cm
VOLTAGE AT TAP #4 100V/cm

OSCILLOGRAM DISPLAYING VOLTAGES AT TAPS #5, #6, #7, #8 & #9 IS MISSING

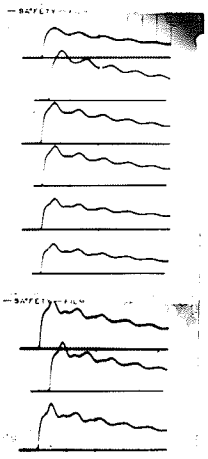

VOLTAGE AT TAP #9 100V/cm
VOLTAGE AT TAP #8 50V/cm
VOLTAGE AT TAP #7 50V/cm
VOLTAGE AT TAP #6 50V/cm
VOLTAGE AT TAP #5 50V/cm
VOLTAGE AT TAP #4 50V/cm
VOLTAGE AT TAP #3 20V/cm
VOLTAGE AT TAP #2 20V/cm
VOLTAGE AT TAP #1 20V/cm

ALL OSCILLOGRAMS HAVE 5 μSEC/CM SWEEP SPEED

1 ½ x 40 IMPULSE VOLTAGE DISTRIBUTION FOR COIL 2 WITH CORE CONTAINED IN SHELL

VOLTAGE APPLIED TO TERMINAL #1 FOR FIRST SET (#1 — #9)
VOLTAGE APPLIED TO TERMINAL #2 FOR SECOND SET (#9 — #1)

FIGURE 10-2

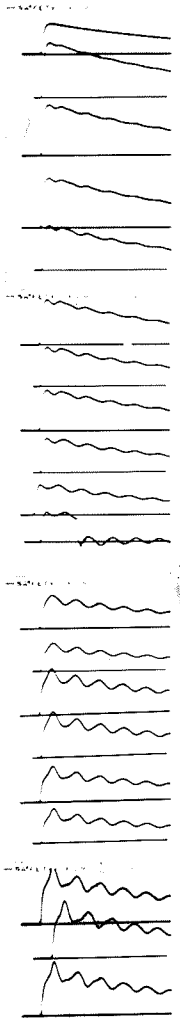

APPLIED VOLTAGE TERMINAL #1 200V/cm
VOLTAGE AT TAP #1 100V/cm
VOLTAGE AT TAP #2 100V/cm
VOLTAGE AT TAP #3 100V/cm
VOLTAGE AT TAP #4 100V/cm
VOLTAGE AT TAP #5 100V/cm
VOLTAGE AT TAP #6 100V/cm
VOLTAGE AT TAP #7 100V/cm
VOLTAGE AT TAP #8 100V/cm
VOLTAGE AT TAP #9 100V/cm
CHOPPED VOLTAGE AT TAP #9 f=125 kc
VOLTAGE AT TAP #9 100V/cm
VOLTAGE AT TAP #8 100V/cm
VOLTAGE AT TAP #7 50V/cm
VOLTAGE AT TAP #6 50V/cm
VOLTAGE AT TAP #5 50V/cm
VOLTAGE AT TAP #4 50V/cm
VOLTAGE AT TAP #3 20V/cm
VOLTAGE AT TAP #2 20V/cm
VOLTAGE AT TAP #1 10V/cm

ALL OSCILLOGRAMS HAVE A SWEEP SPEED OF 5 μSEC/CM

1 ½ x 40 IMPULSE VOLTAGE DISTRIBUTION

FOR COIL 2 WITH CORE REMOVED FROM SHELL

VOLTAGE APPLIED TO TERMINAL #1 FOR FIRST SET (#1 - #9)
VOLTAGE APPLIED TO TERMINAL #2 FOR SECOND SET (#9 - #1)

FIGURE 10-3

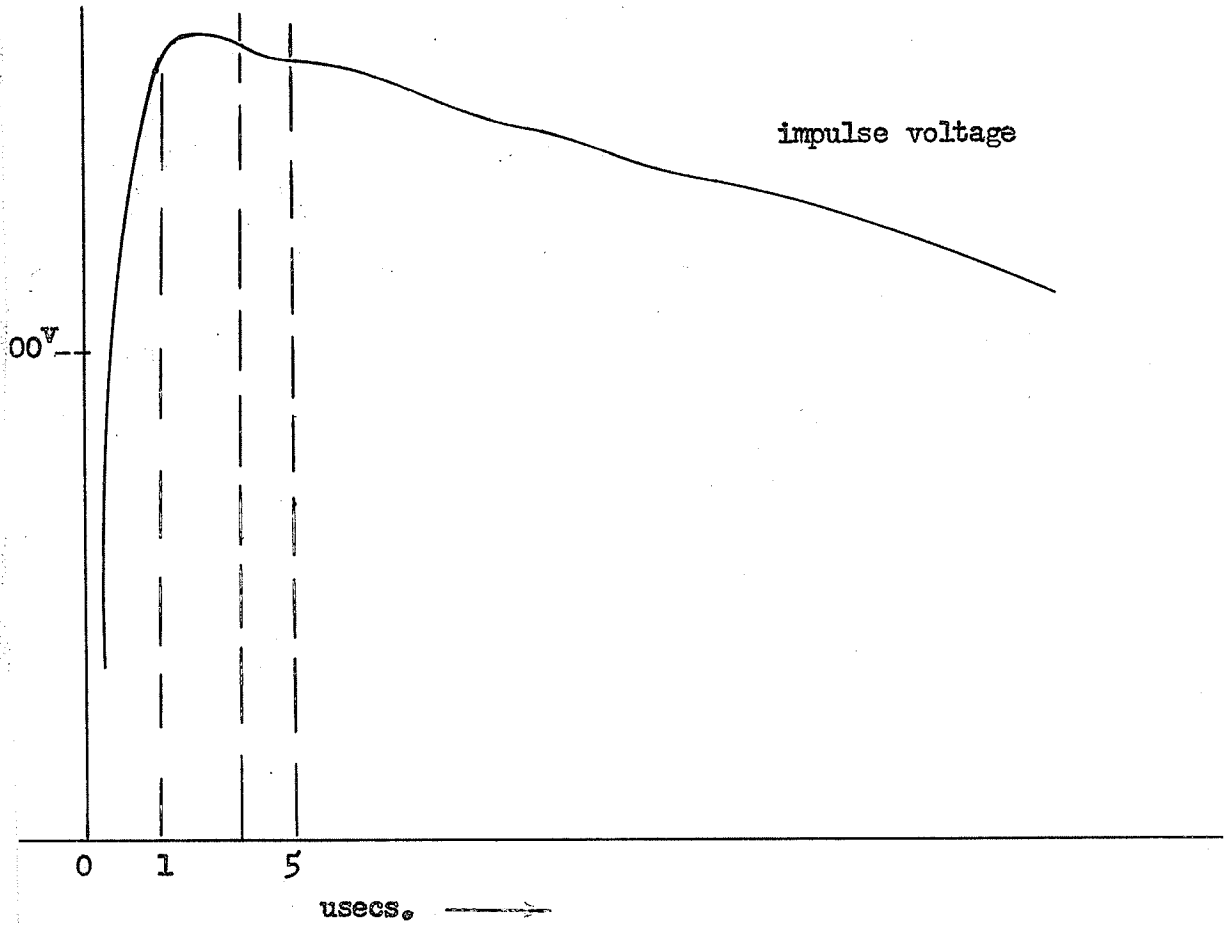

measured at the 75 percent position of the total winding

MEASUREMENT OF IMPULSE VOLTAGE FOR THE

IMPULSE VOLTAGE DISTRIBUTION CURVE

FIGURE 10-4

GRAPH 1

1½ × 40 IMPULSE VOLTAGE DISTRIBUTION

FOR COIL (1) WITH CORE CONTAINED IN SHELL

TAKEN AT 5 μSEC. AFTER IMPULSE APPLIED

TO COIL TERMINALS

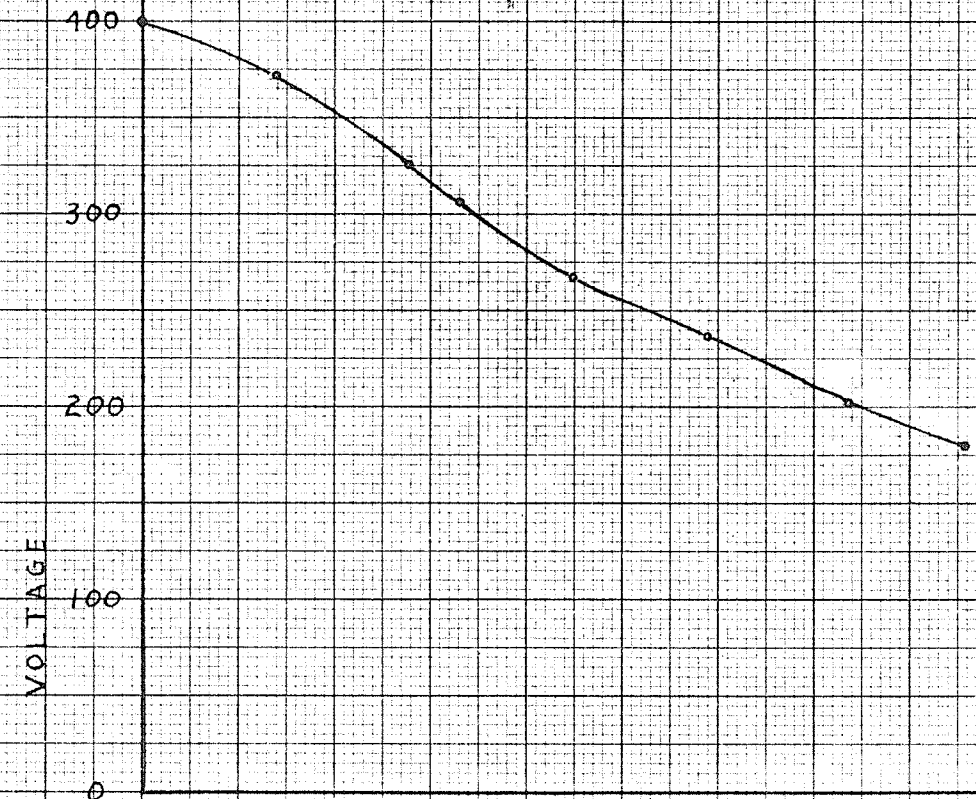

0 150 300 450 600 750 900 1050 1200 1350 1500 1650 1800 1950 2100 2250

TURN NUMBERS

92

8 FEB 1962

GRAPH 2

1½ x 40 IMPULSE VOLTAGE DISTRIBUTION

FOR COIL (2) WITH CORE CONTAINED IN SHELL
TAKEN AT VARIOUS INTERVALS AFTER IMPULSE
APPLIED TO COIL TERMINALS

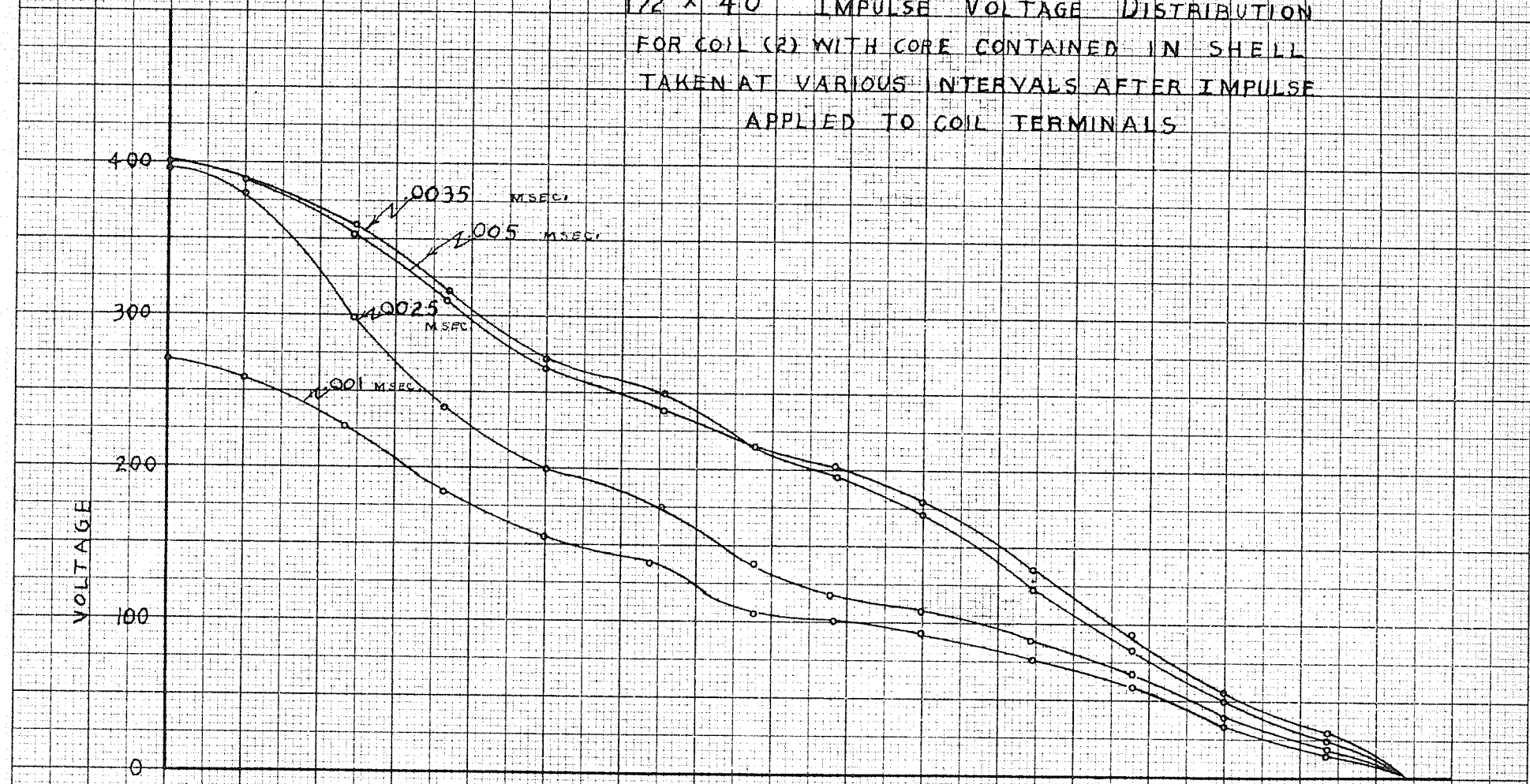

TL FEB 1962

GRAPH 3

½ × 40 IMPULSE VOLTAGE DISTRIBUTION
FOR COIL (2) WITH CORE REMOVED FROM SHELL
TAKEN AT .0035 AND .005 MSECS. AFTER IMPULSE
APPLIED TO COIL TERMINALS

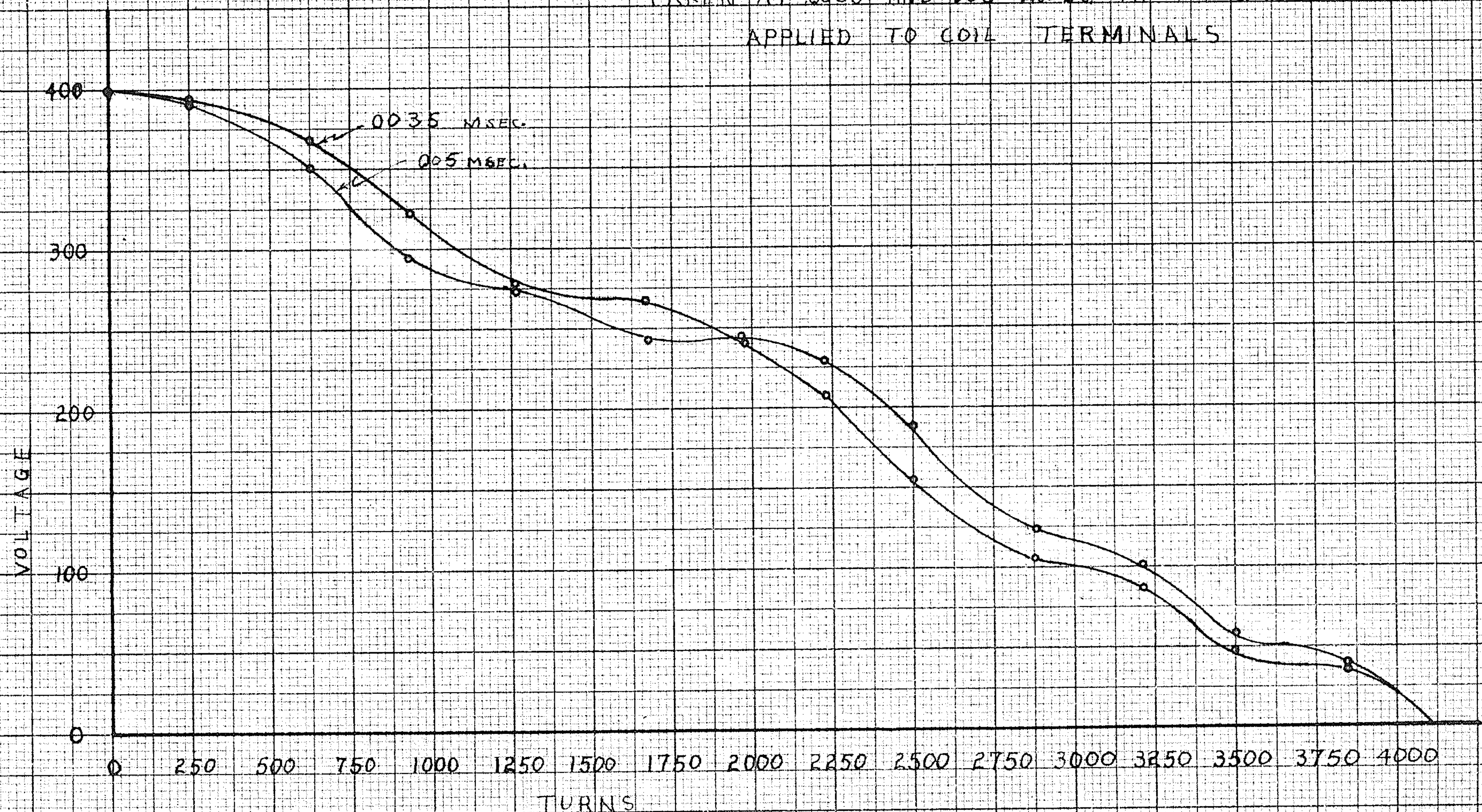

T E FEB 1962

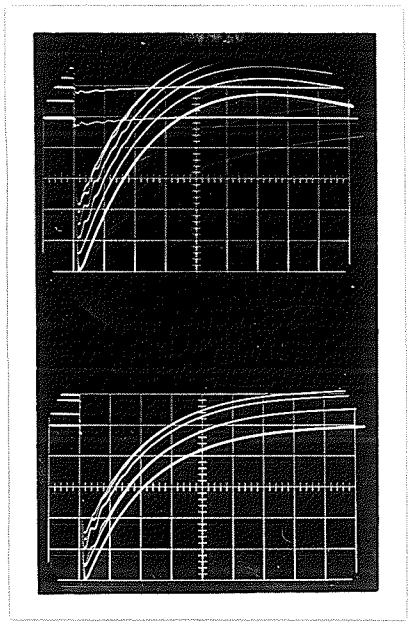

Samples of voltage distribution taken at approximately equal intervals along the top layer of the coil when the core is removed from the core

Samples of voltage distribution taken at approximately equal intervals along the top layer of the coil when the core is in the core of the coil

VOLTAGE DISTRIBUTION ALONG THE TOP LAYER OF THE COIL

FIGURE 10-5

All oscillograms have a 100^{V}/cm. vert. defl. and a sweep speed of 20 usec./cm.

X - III VOLTAGE DISTRIBUTION ALONG MULTI-LAYER COILS

Figures 10-1, 10-2 and 10-3 illustrate the oscillations that occurred at the tapped points during the application of the impulse. The oscillations were found to be most severe towards the grounded end of the winding. Graphs 1, 2 and 3, on the other hand, represent the voltage distribution along the winding at specific times. The transition of voltage distribution along the winding to the uniform state was not accompanied by the strong oscillations as shown by transformers. However, the oscillations were stronger when the core was removed from the coil shell. The graphs illustrate that the oscillations, which brought the voltage distribution to a uniform state, were in phase along the winding preventing severe voltage stress from developing over a portion of the winding.

It appears that the capacitance is so disposed through the winding that the initial voltage is fairly uniformly distributed throughout the winding. Comparison of this distribution to that for transformers would indicate a low capacitance ratio, α . This would indicate that the capacitance between layers is comparable to the capacitance of the winding to the core, or perhaps larger. This is true for all layers except the first few top layers. Their increased capacitance allows the voltage distribution near the top layer to attain a larger gradient during the initial portion of the applied impulse.

Moreover, the capacitance is distributed in such a manner that the initial voltage distribution is fairly uniform with respect to the turn-to-turn inductance. Since the winding of a coil has a small leakage inductance, the remaining non-uniformity in the turn currents would

redistribute itself without generating any extreme resonant oscillations within the winding. A still further reduction in the magnitude of the oscillations would occur due to the damping effect of the coil resistance. Experiments have indicated that the amplitude of the various harmonics is reduced exponentially, depending on the effective resistance of the coil at that harmonic frequency. This resistance depends on the skin effect of the copper and varies according to the frequency of oscillation. It was shown in Appendix A that the amplitude of the distribution for the harmonics depends on the resistance of the coil.

CHAPTER XI

CONCLUSIONS

The Voltage Oscillogram Fault Detection Method was found inadequate for detecting minor failures in the coils. The sensitivity of this method would be greater for coils with a smaller internal impedance, but even then would not be as sensitive as the other methods studied.

The Current Oscillogram Fault Detection Method was sufficiently sensitive to detect failures involving two turns in a 2200-turn coil when meticulous technique was employed in recording oscillograms before and during the production of a controlled failure in the coil. If the failure of coil (4) was typical of a coil failure from high voltage impulse tests, then the Impulse Generator Simulator would have to be modified to allow the applied impulse to be easily reproducable.

The two methods of failure detection based on the sensitivity of the induced oscillation to changes in the coil impedance yielded the best indications of permanent failure. Single-turn failures in a 2200-turn coil could be detected by superimposing the oscillograms; four-turn failures could be recognized without superimposing the oscillograms.

In some cases, it may be desired to determine if the coil has been damaged by the high voltage impulse tests even though the coil does not fail during this test. It is doubtful if any of these methods would detect insulation puncture by transient arc-over unless a carbonized path remained between the damaged portions. Possible methods of detecting this type of failure were indicated by the appearance of a high frequency oscillation superimposed on the charging current pulse of the detection

current waveform recorded for the faulted coil, and by the change in the oscillation at the beginning of the current waveform observed prior to coil failure during the high voltage impulse tests. Further study is required to determine if this high frequency oscillation can be used to detect transient arc-over failures.

The greatest voltage gradient within the coil winding during the application of an impulse voltage was found to occur between the outer layers of the coil. When the two coils were subjected to high voltage impulse tests, one of the coils failed by flashing from one end of the outer layer to the coil shell. These tests indicate that the coils may be most vulnerable at the outer layers, but a more detailed study of the voltage distribution is desirable before firm conclusions are drawn.

B I B L I O G R A P H Y

A. BOOKS

1. Bewley, L.V. Travelling Waves on Transmission Systems. New York: The McGraw Hill Book Company Inc., 1933.

2. Moore, R.K. Travelling-Wave Engineering. New York: The McGraw Hill Book Company Inc., 1960.

3. Skilling. Electric Transmission Lines. New York: The McGraw Hill Book Company Inc., 1951.

4. Williams, E.M. and Woodford, J.B. Transmission Circuits. The Macmillan Company Inc., 1957.

B. PERIODICALS

1. Abetti, P.A. and Maginniss, F.J. "Natural Frequencies of Coils and Windings Determined by Equivalent Circuit", The Transactions of the American Institute of Electrical Engineers, vol. 72, part III, p. 495.

2. Abetti, P.A. and Maginniss, F.J. "Fundamental Oscillations of Coils and Windings", The Transactions of the American Institute of Electrical Engineers, vol. 73, part III-A, p. 1.

3. Abetti, P.A. "The Use of Transformer Models for the Determination of Transient Voltage", CIGRE, 1954, session paper 131.

4. Aicher, L.C. "Experience with Transformer Impulse Failure Detection Method", The Transactions of the American Institute of Electrical Engineers, vol. 67, part III, 1948, p. 1621.

5. Aicher, L.C. "The Impulse Testing of Low Voltage High Kilovolt-Amp. Transformer Windings", The Transactions of the American Institute of Electrical Engineers, vol. 71, part III, 1952, p. 337.

6. Allibone, T.E., Hawley, W.G. and Perry, F.R. "Cathode-Ray Oscilloscope Studies of Surge Phenomena", The Journal of the Institution of Electrical Engineers, vol. 75, p. 1934.

7. Allibone, T.E. and Perry, F.R. "Standardization of Impulse-Voltage Testing", The Journal of the Institution of Electrical Engineers, vol. 78, 1936, p. 257.

8. Allibone, T.E., McKenzie, D.B. and Perry, F.R. "The Effects of Impulse Voltage on Transformer Windings", The Proceedings of the Institution of Electrical Engineers, vol. 18, 1937, p. 128.

9. Beardsley, K.D., McMorris, W.A. and Stewart, H.C. "Voltage Stresses in Distribution Transformers due to Lightning Currents in Low Voltage Circuits", The Transactions of the American Institute of Electrical Engineers, vol. 67, 1948, pp 1632-35.

10. Bellaschi, P.L. and Palermo, A.J. "Analysis of Transient Voltages in Networks", The Transactions of the American Institute of Electrical Engineers, vol. 59, 1940, pp 973-81.

11. Bewley, L.V., Hagenguth, H. and Jackson, F.R. "Methods of Determining Natural Frequencies in Coils and Windings", The Transactions of the American Institute of Electrical Engineers, vol. 60, 1941, p. 1145.

12. Blume, L.F. and Boyajian, A. "Abnormal Voltages within Transformers", The Transactions of the American Institute of Electrical Engineers, vol. 38, 1919, p. 577.

13. Boyajian, A. "Oscillation of a High Voltage Secondary Winding", The Transactions of the American Institute of Electrical Engineers, vol. 65, 1946, p. 1010.

14. Chiles, J.H. Jr. and Teague, W.L. "The Impulse Generator and its Uses", The Transactions of the American Institute of Electrical Engineers, vol. 71, part III, 1952, p. 431.

15. Descans, F. and Chevalier, H. "Surge Voltage Distribution in Transformer Windings; Transference of Surge of Adjacent Windings", CIGRE, 1946, session paper 322.

16. Elsner, R. "Detection of Insulation Failures during Impulse Testing of Transformers", CIGRE, 1954, session paper 101.

17. Foust, C.M. and Henderson, J.T. "Direct Measurement of Surge Currents", The Transactions of the American Institute of Electrical Engineers, vol. 54, April 1935, pp 373-78.

18. Froidevaux, J. and Rossier, C. "Impulse Testing of Large Transformers; the Maintenance of the Wave Shape and its Importance", CIGRE, 1956, session paper 118.

19. Goodlet, B.L. "Electro-Magnetic Phenomena in High-Voltage Testing Equipment", The Journal of the Institution of Electrical Engineers, vol. 74, May 1934.

20. Hagenguth, J.H. "Progress in Impulse Testing of Transformers", The Transactions of the American Institute of Electrical Engineers, vol. 63, 1944, p. 999.

21. Hazleton, T.H., Dalzell, J.W. and McMath, J.P.C. "Impulse Tests on Solenoids used in Pioneer Electric Street Lighting Relay", Report No. 61-545 of Pioneer Electric Brandon Limited.

22. Lech, W., Golinski, J. and Radziwill, J. "Impulse Ionization in Transformer Windings", CIGRE, 1956, session paper 116.

23. Paluev, K.K. and Hayenguth, H. "The Effect of Transient Voltage on Power Transformer Design IV", The Transactions of the American Institute of Electrical Engineers, vol. 51, September 1932, p. 601.

24. Paluev, K.K. "The Effect of Transient Voltages on Power Transformer Design III", The Transactions of the American Institute of Electrical Engineers, vol. 48, 1929, p. 681.

25. Peppon, E.C. and Hickling, G.H. "The Detection of Oscillographic Methods of Winding Failures during Impulse Tests on Transformers", The Journal of the Institution of Electrical Engineers, vol. 96, part II, p. 769.

26. Purvis, W.J. "Impulse Failure Detection Methods in Transformer Testing", The Proceedings of the High Voltage Symposium, National Research Council, Ottawa, September 1956, NRC No. 4314.

27. Provost, P.G. "Impulse Testing of Transformers", CIGRE, 1954, session paper 115.

28. Rabus, W. "The Impulse Voltage Difference Method for the Detection and Location of Faults during Full Wave Impulse Tests on Transformers", CIGRE, 1954, session paper 139.

29. Rudenberg, R. "Performance of Travelling Waves in Coils and Windings", The Transactions of the American Institute of Electrical Engineers, vol. 59, 1940, p. 1031.

30. Stenkirst, E. "Study of Fault Detection and Failure Location during Surge Testing of Transformers", CIGRE, 1952, session paper 129.

31. Stewart, H.C. and Holcomb, J.E. "Impulse-Failure-Detection Methods as Applied to Distribution Transformers", The Transactions of the American Institute of Electrical Engineers, vol. 64, 1945, pp 640-4.

32. Treanor, E.D., Stewart, H.C. and Holcomb, J.E. "The Production Impulse Testing of Distribution Transformers", The Transactions of the American Institute of Electrical Engineers, vol. 71, part III, 1952, pp 808-12.

33. Vogel, F.J. and Montainger, V.M. "Progress Report on Impulse Testing of Commercial Transformers", The Transactions of the American Institute of Electrical Engineers, vol. 52, 1933, pp 909-10.

34. Weed, J.M. "Prevention of Transient Voltages in Windings", The Journal of the Institution of Electrical Engineers, vol. 41, 1922, p. 14.

A P P E N D I C E S

APPENDIX A

MULTI-LAYER COILS

A - I OSCILLATIONS WITHIN COILS

A knowledge of the response of the coil winding to an impulse is of fundamental importance in a study of the effects of impulse voltages from switching transients or lightning surges. If the rise time of an applied impulse is very short, there is a negligible growth of magnetic flux during the rise time and the coil acts essentially as a capacitance. A period of continual energy interchange between the magnetic and electric fields modifies this initial voltage distribution into a distribution governed by both the capacitance and inductance of the winding. This energy interchange is the result of highly damped oscillations which can be represented by a complex series of standing or travelling waves of specific frequencies, wavelengths, and damping factors.

The response of the coil to the impulse function may be represented by a Fourier series in which each term of the series represents the response of a particular harmonic. The voltage in the coil for the n'th harmonic is a function of position and may be represented by the form

$$e_{(x,t)} = E_{n(x)} \cos (\omega_n t)$$

where $E_{n(x)}$ = space function of the n'th harmonic and depends on the waveform of the applied voltage and the characteristics of the coil

ω_n = frequency of n'th harmonic

t = time measured from the instant the impulse was applied to the coil terminals

A unique spectrum of frequencies can be derived for each coil from differential equations describing the internal behaviour of the coil. The space functions of the fundamental and second and third harmonics have been verified experimentally (reference 10, 11, 29).

A - II DIFFERENTIAL EQUATIONS

The differential equations describing this voltage-current relationship in coils assume very complex forms, if simplifying assumptions are not made in the analytical model. For a single-layer coil, R. Rudenberg used a model whereby a turn of this winding was bound to the remaining turns in the winding by a capacitive and inductive network, equivalent to that illustrated in figure A-1(b). The current equation was derived by setting the decrease in the current flow in the n'th turn equal to the charging current into the capacitance of this turn to ground and to the adjacent turns. The voltage equation was derived by considering the voltage of the n'th turn as that induced by the rate of change of current in all the turns of the coil. An effective inductance was defined as the self-inductance of the n'th turn plus the sum of the mutual inductances binding the remaining turn of the winding to this turn. The effect on the voltage of the n'th turn by the progressive variation in the rate of change of current along the winding was neglected. These simplified equations yielded a solution for the voltage and current in the form of standing or travelling waves, which agrees well with experiment, thus justifying the simplifying assumptions.

This approach by Rudenberg was modified in this study to apply to coil layers, rather than to turns, and two differential equations in two

variables resulted. In the derivation of these equations, simplifying assumptions about the behaviour of the voltage within a layer had to be made.

The difference in voltage between adjacent turns in the layer was assumed to be small and the voltage considered to vary linearly along the layer, so that the further simplifying assumption could be made that the layer was at a constant voltage equal to the average value of the voltage in the layer. However, the experimental measurements of the voltage distribution described in Chapter X showed that the voltage was not uniform along the top layer but oscillated, with oscillations of greatest amplitude occurring at the center of the layer.

The effect of conductance between turns and layers and the resistance along the layer was also neglected. Since the resistive component of the winding is large, the results from this model must be corrected for the effect of resistance.

The nomenclature used in the derivation of the equations was:

e_n = average voltage of n'th layer

$e_{\lambda n}$ = voltage induced in n'th layer by self-inductance of layer

e_{un} = voltage induced in n'th layer by mutual inductance to remaining layers of coil

W = length of one layer of the coil winding

C_g = ground capacitance per unit length of coil conductor

C_{gn} = ground capacitance per unit length of coil conductor for n'th layer

C_t = turn capacitance per unit length of coil conductor

C_{tn} = turn capacitance per unit length of coil conductor for n'th layer

i_{gn} = charging current to ground for n'th layer

i_{tn} = charging current to adjacent layers from n'th layer

λ = self-inductance per unit length of single turn

u_{mn} = mutual inductance between n'th and m'th layers

M_{mn} = mutual inductance between m'th and n'th layer. When m = n increments coincide and M_{mm} is the self-inductance of the layer

The charging current through the ground capacitance from the n'th layer is:

$$i_{gn} = C_{gn}W \frac{\partial e_n}{\partial t} \qquad \text{....A-1}$$

The charging current of the n'th layer to both its adjacent layers is:

$$i_{tn} = C_{tn}W \left[\frac{\partial (e_n - e_{n+1})}{\partial t} + \frac{\partial (e_n - e_{n-1})}{\partial t} \right]$$

$$i_{tn} = C_{tn}W \left[\frac{\partial \left[-(e_{n-1} - e_n) + (e_n - e_{n+1}) \right]}{\partial t} \right]$$

$$i_{tn} = -C_{tn}W \left[\frac{\partial \left[(e_{n-1} - e_n) - (e_n - e_{n+1}) \right]}{\partial t} \right]$$

$$i_{tn} = -C_{tn}W^3 \left[\frac{\partial \left[\frac{(e_{n-1} - e_n)}{W} - \frac{(e_n - e_{n+1})}{W} \right]}{W \, \partial t} \right] \qquad \text{....A-2}$$

The total charging current from the n'th layer is equal to the decrease in the current within the n'th layer:

$$-\Delta i_n = C_{gn} W \frac{\partial e_n}{\partial t} - C_{tn} W^3 \left[\frac{\partial \left[\frac{(e_{n-1} - e_n)}{W} - \frac{(e_n - e_{n+1})}{W} \right]}{\partial t} \right]$$

If this equation is divided by W and the limit as $W \to 0$ considered, then:

$$-\frac{\partial i_n}{\partial x} = C_{gn} \frac{\partial e_n}{\partial t} - C_{tn} W^2 \frac{\partial^3 e_n}{\partial t \, \partial x^2} \qquad \text{....A-3}$$

The voltage variation along the coil is caused by magnetic induction. The voltage induced within the n'th layer by the self-inductance of the n'th layer is:

$$e_{\lambda n} = \lambda_n W \frac{\partial i_n}{\partial t} \qquad \text{....A-4}$$

The voltage induced within the n'th layer by the mutual inductance to the adjacent layers is:

$$e_{un} = u_{n,n+1} W \frac{\partial (i_{n+1})}{\partial t} + u_{n,n-1} W \frac{\partial (i_{n-1})}{\partial t}$$

The total induced voltage by the mutual inductance to all the layers of the winding is:

$$e_{un} = \sum_m u_{nm} W \frac{\partial i_m}{\partial t} \qquad m \neq n \qquad \text{....A-5}$$

where m represents m'th layer.

Then the voltage induced in the n'th layer is:

$$-e_n = \lambda_n W \frac{\partial i_n}{\partial t} + \sum_{\substack{m \\ m \neq n}} u_{mn} W \frac{\partial i_m}{\partial t} \qquad \text{....A-6}$$

or

$$-e_n = \sum_{\substack{m \\ m=n}} M_{mn} \, W \frac{\partial i_m}{\partial t} \qquad \text{....A-7}$$

Dividing by W and considering the limit as $W \to 0$, then:

$$\frac{\partial e_n}{\partial x} = - \int M_{x,s} \frac{\partial i_{st}}{\partial t} \, ds \qquad \text{....A-8}$$

n'th layer reduces to increment x
m'th layer reduces to increment s

when x = s increments are coincident

$M_{x,s}$ becomes self-inductance

Equations similar to equations A-3 and A-8 have been solved by means of Fredholm integral equations for single layer windings and the results showed that the voltage and current distribution are sinusoided in time, but not necessarily in space (reference 2). The space distribution for single layer windings was shown to be determined by the form of the mutual inductance function. The solution accounted for the total mutual inductance and existed for either uniform or non-uniform winding parameters. Non-uniformities in the winding, such as axial gaps or breaks and portions with reduced turn density, were found to reduce the fundamental frequency of the coil. If the resistive effect were considered, a damping factor dependent on the position along the coil would result.

This method of solution for coil frequencies, if they were required, would be extremely difficult since the actual coils were not identically or even uniformly wound. If the winding parameters are considered constant, and the effect of the rate of change of the current differences between layers neglected, equivalent circuits could be constructed from the solution of these equations and then adjusted to compensate for the approximations made in the coil representation.

Equation A-3 can be rewritten as:

$$-\frac{\partial i}{\partial x} = C_g\frac{\partial e}{\partial t} - C_t W^2 \frac{\partial^3 e}{\partial t\, \partial x^2} \qquad \text{....A-9}$$

Equation A-6 is repeated for convenience:

$$-e_n = \lambda_n W \frac{\partial i_n}{\partial t} + \sum_m u_{mn} W \frac{\partial i_m}{\partial t} \qquad m \neq n$$

By adding and subtracting the term $u_{mn}W\frac{\partial i_n}{\partial t}$, equation A-6 can be written

$$-e_n = \lambda_n W \frac{\partial i_n}{\partial t} + \sum_m u_{mn} W \frac{\partial (i_m - i_n)}{\partial t} + \sum_m u_{mn} W \frac{\partial i_n}{\partial t} \qquad m \neq n$$

$$-e_n = \left[\lambda + \sum_m u_{mn}\right] W \frac{\partial i_n}{\partial t} + \sum_m u_{mn} W \frac{\partial (i_m - i_n)}{\partial t} \qquad \text{....A-10}$$

Note that the coupling effect of all layers with n'th layer is expressed as two terms; the first dependent on i_n and the second on the difference between the currents in the m'th layer and n'th layer. If this coefficient is evaluated, it can be shown that it is the sum of a number of elements of opposing sign and, except at high frequencies, the error in neglecting this term is very small. To this approximation, Equation A-10 then becomes

$$-e_n = L W \frac{\partial i_n}{\partial t} \qquad \text{....A-11}$$

where $L = \lambda + \sum_m u_{mn} \qquad m \neq n$

dividing by W and considering the limit as $W \to 0$, Equation A-11 reduces to

$$-\frac{\partial e_n}{\partial x} = L \frac{\partial i_n}{\partial t}$$

and if the parameters are considered the same for each layer

$$-\frac{\partial e}{\partial x} = L\frac{\partial i}{\partial t} \qquad \text{....A-12}$$

A - III REPRESENTATION BY AN EQUIVALENT CIRCUIT

If the effect of the mutual inductance is neglected, then equations A-9 and A-12 may be considered as approximate representations of the coil winding. The combination of these equations yields an equation for current or voltage of the form:

$$\frac{\partial^2 e}{\partial x^2} - lC_g\frac{\partial e}{\partial t} + C_s l\frac{\partial^4 e}{\partial t^2 \partial x^2} = 0 \qquad \text{....A-13}$$

This equation can be solved by separation of variables and yields a solution of the following form:

$$e = E\, e^{j\omega t}\quad e^{j\alpha x} \qquad \text{....A-14}$$

This voltage oscillates simusoidally in time and also in space along the extension x of the coil. Substituting this solution into the previous equation will yield an expression for the natural frequencies and for the wave density.

This solution may be expressed as a travelling wave by setting $\alpha = \frac{\omega}{v}$, that is,

$$e = E\, e^{j\omega\left[t - \frac{x}{v}\right]} \qquad \text{....A-15}$$

Since the solution can be reduced to a standing wave or travelling waveform, the coil may be represented by an artificial transmission line of the form shown in figure A-1$_a$. If mutual inductance is considered, then the circuit must take the form of figure A-1$_b$. As stated previously, the resistive component of the coil cannot be neglected and the complete equivalent circuit must take the form shown in figure A-1$_c$.

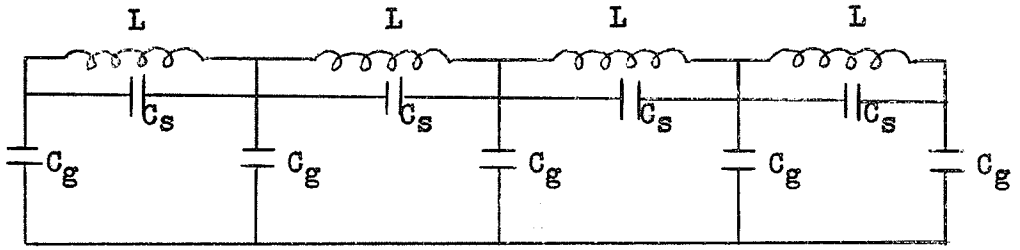

FIGURE A-1_a

LOSSLESS COIL

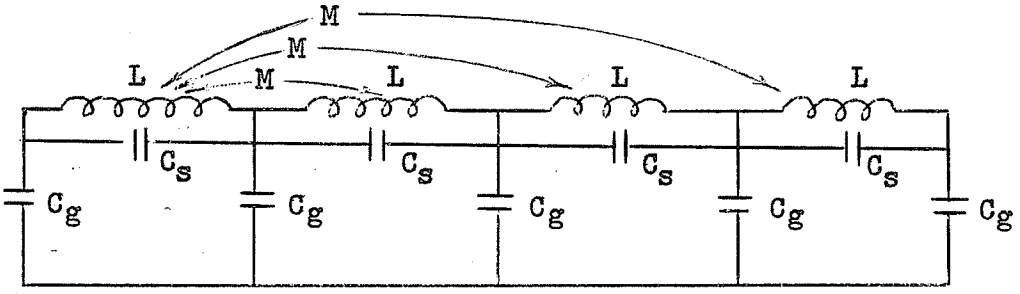

FIGURE A-1_b

LOSSLESS COIL WITH MUTUAL INDUCTANCE

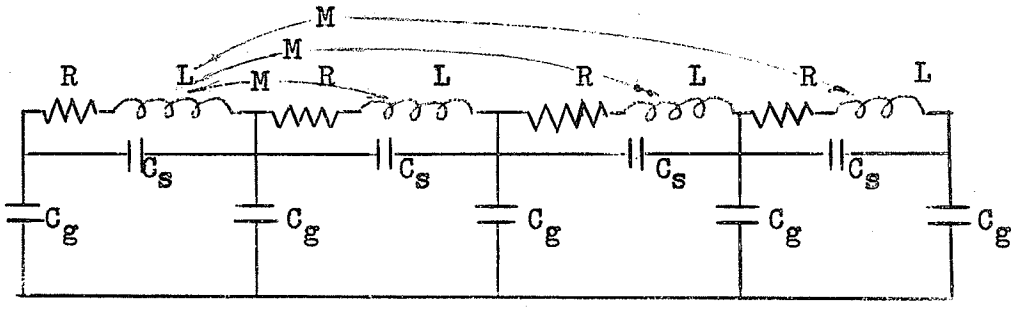

FIGURE A-1_c

LOSSY COIL

C_g = ground capacitance per unit length

C_s = layer capacitance per unit length

L = inductance per unit length

M = mutual inductance per unit length

EQUIVALENT CIRCUITS FOR COIL

The construction and solution of these equivalent circuits involve a considerable amount of work. The coil parameters would have to be measured accurately. The self-inductance and mutual inductances of any air core coil may be obtained from tables. Also, it can be shown that for each linear iron core coil there exists an equivalent air core coil such that the mutual linkages are the same in both coils (reference 1). These circuits can then be solved either numerically or by a network analyzer. The former method leads to more accurate values of the natural frequencies; the latter is more rapid and lends itself well to investigating the effect of changes in circuit constants.

An equivalent circuit was not produced for these coils because of the irregularities existing between the coils and between layers of any coil. Thus, the destruction of one coil to obtain values for an equivalent circuit would not necessarily yield suitable results for another coil. These equivalent circuit representations have been included to assist in the understanding of the coil behaviour and to show that it is analogous to a transmission line.

A - IV NATURAL FREQUENCY RESPONSE OF THE COILS

The circuit of figure A-1$_c$would have a transient response very similar to that for the actual coil. If the mutual terms were neglected and a sufficient number of sections were considered the network response would not change significantly. As the number of sections increased, this network would approach a lossy transmission line. The differential equations resulting from an elementary section of such a transmission line are:

$$\frac{\partial e_{x,t}}{\partial t} = R_1 + L \frac{\partial i_{x,t}}{\partial t} + \frac{1}{C}\int i_{x,t}\, dt$$

and $$\frac{\partial i_{x,t}}{\partial x} = C \frac{\partial e_{x,t}}{\partial t}$$

If the voltage and current are assumed to be complex exponential functions of time, then the equations reduce to:

$$\frac{\partial e_{x,t}}{\partial x} = (R + j\omega L)i_1 + \frac{i_2}{j\omega C} = \frac{(R + j\omega L)i}{1 + (R + j\omega L)j\omega C} = Zi$$

$$\frac{\partial i_{x,t}}{\partial x} = j\omega C\, e_{x,t} = Ye$$

Combining these equations would result in:

$$\frac{\partial^2 e}{\partial x^2} = ZY\, e_{x,t}$$

The solution to this equation is of the form:

$$e_{x,t} = E\, e^{\sqrt{ZY}\, x}\, e^{j\omega t}$$

It is desired to reduce this expression to:

$$e_{x,t} = E\, e^{-\alpha x}\, e^{j\beta x}\, e^{j\omega t}$$

now $$\sqrt{ZY} = \sqrt{\frac{(R + j\omega L)\, j\omega L}{1 + (R + j\omega L)\, j\omega C}} = \sqrt{\frac{a}{A} + j\frac{b}{A}} = \alpha + j\beta$$

Squaring both sides $\frac{a}{A} + j\frac{b}{A} = \alpha^2 - \beta^2 - 2j\alpha\beta$

Equating real and imaginary components yields:

$$\alpha = \frac{b}{2A\beta} \qquad \text{....A-16}$$

$$\beta = \sqrt{-\frac{a}{2A} - \frac{1}{2}\sqrt{\left[\frac{a}{A}\right]^2 - \left[\frac{b}{A}\right]^2}} \qquad \text{....A-17}$$

where-

$$a = \omega^2 LC_2\left[1 - \omega^2 LC_1\right] - \omega^2 R^2 C_1 C_2$$

$$b = RC_2\left[1 - \omega^2 LC_1\right] - \omega^3 RLC_1 C_2$$

$$A = (1 - \omega^2 LC_1)^2 - \omega^2 R^2 C_1$$

As a result, the solution of the differential equation may be written in the form:

$$e_{x,t} = E\, e^{-\alpha x}\, e^{j\beta x}\, e^{j\omega t}$$

That is, the voltage is an exponential function of time and position and is damped as it progresses along the coil.

When R = 0 the results reduce to:

$$\alpha = 0 \qquad \text{and} \qquad \beta = \sqrt{\frac{\omega^2 LC_2}{1-\omega^2 LC_1}}$$

Examining equation A-17 indicates that β will become infinitely large when

$$1 - \omega^2 LC = 0$$

$$\text{or } \omega = 1/\sqrt{LC_1}$$

This frequency is called the critical frequency since standing waves will not be produced above this frequency.

The space wave densities, β , are limited to specific values that satisfy the boundary conditions. Since the coil can be considered as a short-circuited transmission line, the space functions have the wavelengths given by:

$\lambda = c/m$ where $m = \frac{1}{4} \times 2, 4, 6 \ldots\ldots\ldots$ even indices

c = electrical length of coil winding.

The wave density would then be given as:

$$\beta = \frac{2\pi m}{c} \qquad \ldots\ldots \text{A-18}$$

Substituting these values into equation A-17 and solving for various values of m will yield the various natural frequencies of the coil winding.

If the coil develops a permanent failure, shorting a portion of the winding, the natural frequencies will be altered accordingly. This shift results due to changes in c and β. However, a further effect becomes prominent. The coil acts as a transformer with the secondary short-circuited. Therefore, as the failure increases, the effective secondary increases, and more current is required at the input. Since failures reflect back into the main winding as an impedance reduction, it appears that measurement of this input current would provide a means of detecting coil failures.

A - V TRAVELLING WAVES IN COILS

As mentioned previously, the coil may be considered as a short-circuited lossy transmission line subject to standing or travelling waves. This section will consider the travelling wave solution.

In general the applied wave across the coil will not necessarily be sinusoidal and, in this case, will consist of a specified impulse wave. However, any wave form can be represented by a sum of sinusoidal oscillations by the Fourier theorem. The sinusoidal components will travel with various velocities depending on the frequency. If the frequency is very low, then the veolcity will approach the speed of light. As the critical frequency is approached, the velocity decreases to zero.

The velocity, v, is given by:

$$v = \omega/\beta$$

where β is defined in equation A-17.

As the voltage wave travels along the transmission line its shape is altered since the velocity of the various frequencies differ. The wave front may be flattened considerably since the frequencies above the critical frequency are not transmitted. It should not be forgotten that each of the frequencies propagated are attenuated by the constant, α. The coil response would be found by considering the effect on all the components of the input wave, especially those approaching the critical frequency. Any failure in this case would alter the velocities of these components.

No matter which of the solutions to the differential equations is considered, the same conclusions may be arrived at. The standing wave approach is more useful as it enables a direct comparison with artificial transmission line circuits. Moreover, the natural frequencies calculated from these circuits would yield information as to the internal voltage distribution of the coil and may be interpreted directly for fault detection.

APPENDIX "B"

RECORDING AND DEVELOPING OF OSCILLOGRAMS

The Tektronix type 533 oscilloscope was used to display the desired waveforms, and the oscillograms of these waveforms were recorded from this display by a Dumont Oscillograph Record Camera type 299.

It was found that an aperture opening slightly greater than f4 and an exposure time of approximately 0.7 seconds was best suited for recurrent oscillographic work. When a time base speed of 20 microseconds/cm. and a vertical deflection of 10 volts/cm. were used, the best results occurred when the intensity was set at a point of medium intensity. The intensity had to be adjusted slightly for other oscilloscope settings.

The film was developed by an Eastman D-76 developer modified by addition of borax. The developing time ranged from 12 to 15 minutes.

It is noted that in an effort to conserve film, some of the photographs were taken too close to one another and, as a result, some prints included extraneous material which had to be retouched.

APPENDIX "C"

ADDITIONAL OSCILLOGRAMS FOR VOLTAGE OSCILLOGRAM FAULT DETECTION METHOD

The coils used for these tests are illustrated in figure 3-4, page 15, and a detailed illustration of the winding is shown in figure 3-5, page 16. The tapped turns for coils (1) and (2) are listed on page 14.

Tables C-1 and C-2 list all the tap combinations tested for coils (1) and (2) with their respective number of turns and percentage of winding affected.

Table C-3 lists the page numbers of the illustrations for simulated failures shown in Chapter V and this appendix, their tap combinations, and their size expressed as a percentage of the total winding.

TABLE C-1

VARIOUS TAP COMBINATIONS FOR COIL (1) WITH THE NUMBER OF TURNS AFFECTED AND PERCENT OF WINDING INVOLVED

Tap Combination	No. of Turns	Percent of Wdg affected
1-2	211	9.6
1-3	402	20.0
1-4	624	21.8
1-5	722	34.4
1-7	610	28.0
1-8	827	39.9
1-9	1097	52.3
1-10	893	42.5
1-11	1297	58.9
2-3	209	9.5
2-4	422	19.0
2-5	620	29.5
2-7	426	20.3
2-11	1074	51.2
2-9	895	42.6
3-4	217	9.8
3-5	425	20.2
3-11	874	41.5
5-4	198	9.0
5-7	194	8.8
7-9	469	22.3
7-8	203	9.5
8-9	270	12.8
8-11	449	20.6
9-10	204	9.7
9-11	179	8.5
10-11	383	18.2

TABLE C-2

VARIOUS TAP COMBINATIONS FOR COIL (2) WITH THE NUMBER OF TURNS AFFECTED AND PERCENTAGE OF WINDING INVOLVED

Tap Combination	No. of Turns	Percent of Wdg affected
1-2	315	7.5
2-3	8	.19
3-4	324	7.72
5-6	322	7.68
6-7	7	.16
7-8	338	8.05
7-9	672	16.
8-9	334	7.95
8-2	1102	26.5
8-5	667	15.9
2-G	582	13.9
4-G	914	21.8
5-G	917	21.9
6-G	1239	29.5
7-G	1246	29.7
8-G	1584	38.7
9-G	1918	45.6

TABLE C-3

ILLUSTRATIONS FOR SIMULATED FAILURES ALONG WITH THEIR SIZE AND TAP COMBINATIONS

Figure No.	Tap Combinations	Percent of Wdg. Affected	Page No.
	Coil (1) - 2200-turn coil		
1½ by 40 applied impulse			
5-8	1-2, 3, 4, 5	9.6, 20.0, 28.0, 34.4	34
5-9	1-7, 8, 9, 10	29.9, 39.4, 42.5, 52.3	34
5-10	2-3, 7, 11	9.5, 20.3, 51.2	37
C-1	3-5, 11	20.0, 41.5	126
C-2	5-7, 3	9.2, 20.3	126
C-3	7-8, 9	9.5, 22.3	126
C-4	8-9	12.8	126
C-5	9-10, 11	9.7, 8.5	127
C-6	10-11	18.2	127
1½ by 200 applied impulse			
5-11	1-2, 3, 4, 5	9.6, 20.0, 28.0, 34.4	37
5-12	1-7, 8, 10	29.9, 39.4, 52.3	37
5-13	5-7	8.8	37
C-7	3-4, 5	9.85, 20.2	127
C-8	2-3, 4, 5	9.6, 12.1, 29.4	127
C-9	4-5	9.0	128
C-10	7-8	9.5	128
C-11	9-8	12.2	128
C-12	9-10	9.7	128
C-13	10-11	18.2	129
	Coil (2) - 4200-turn coil		
1½ by 40 applied impulse			
5-14	2-3	0.19	39
5-15	5-6; 7-8	7.68, 8.05	39
5-16	8-9	7.95	39
5-17	7-9; 8-2	16.5, 26.5	39
C-14	3-6	15.2	129
C-15	5-6	7.68	129
C-16	7-9	16.0	130

TABLE C-3
(Continued)

Figure No.	Tap Combinations	Percent of Wdg. Affected	Page No.
1½ by 300 applied impulse			
5-18	2-3	0.19	41
5-19	1-2	7.5	41
C-17	7-8	8.05	130
3 by 350 applied impulse			
5-20	2-3	0.19	41
5-21	1-2	7.5	41
C-18	8-9	7.95	130
	Coil (3) - 2200-turn coil		
1½ by 200 applied impulse			
5-22	3-turn failure	0.13	42
5-23	7-turn failure	.38	42
5-24	15-turn failure	.68	42
5-25	25-turn failure	1.15	42
	Coil (4) - High Voltage Tests Results		
5-26	1½ by 40 impulse	untested coil	44
5-27	1½ by 40 impulse	tested coil	44
5-28	1½ by 200 impulse	untested coil	44
5-29	1½ by 200 impulse	tested coil	44

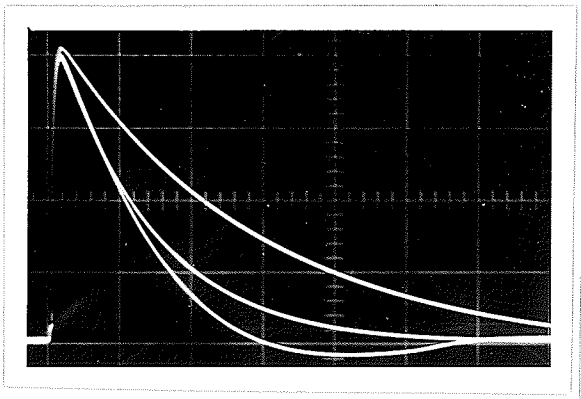

FIGURE C-1

$1\frac{1}{2}$ by 40 impulse for no failure 20.2, and 41.5 percent failures respectively

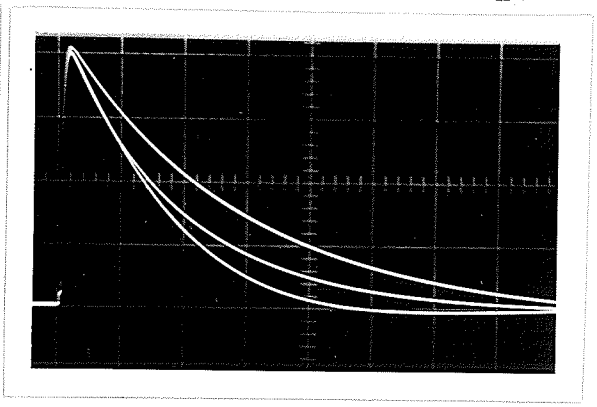

FIGURE C-2

$1\frac{1}{2}$ by 40 impulse for no failure 9.25, and 20.3 percent failures respectively

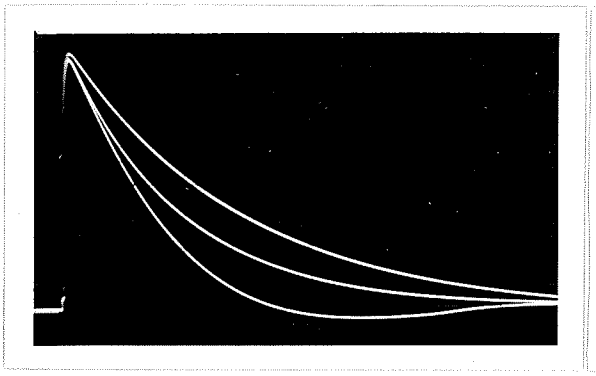

FIGURE C-3

$1\frac{1}{2}$ by 40 impulse for no failure 9.5, and 22.3 percent failures respectively

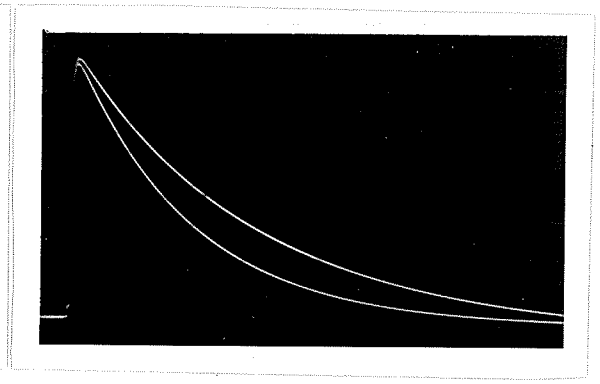

FIGURE C-4

$1\frac{1}{2}$ by 40 impulse for no failure and 12.8 percent failures respectively

DISTORTIONS IN OUTPUT VOLTAGE WAVEFORM FOR FAILURES

SIMULATED ON A 2200-TURN COIL

All oscillograms have a vert. defl. of 100^{V}/cm. and a sweep speed of 20 usec./cm.

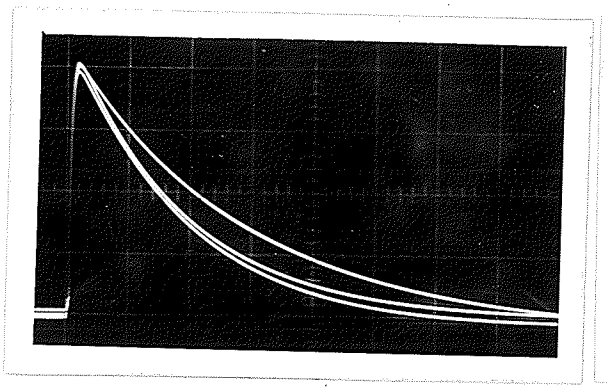

FIGURE C-5

$1\frac{1}{2}$ by 40 impulse for no failure 9.7, and 8.5 percent failures respectively

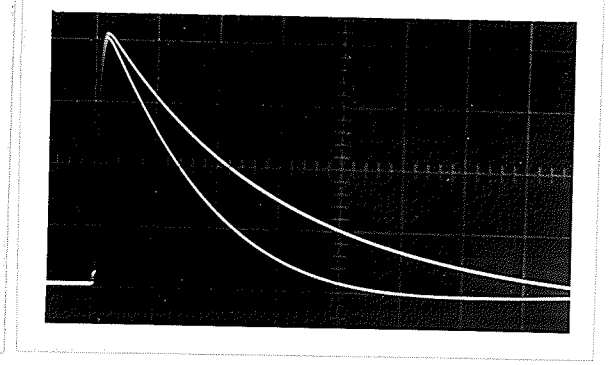

FIGURE C-6

$1\frac{1}{2}$ by 40 impulse for no failure and 18.2 percent failures respectively

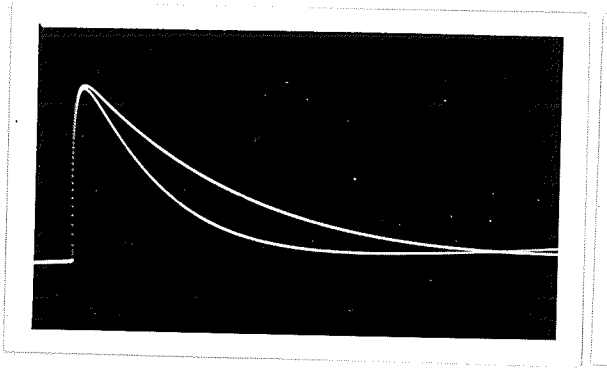

FIGURE C-7

$1\frac{1}{2}$ by 200 impulse for no failure 9.85, and 20.2 percent failures respectively

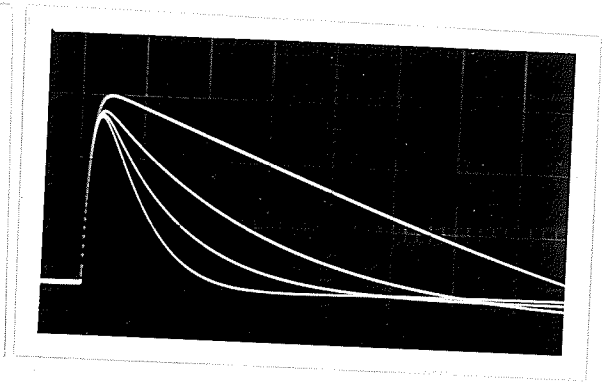

FIGURE C-8

$1\frac{1}{2}$ by 200 impulse for no failure 9.6, 12.1, and 29.4 percent failures respectively

DISTORTIONS IN OUTPUT VOLTAGE WAVEFORM FOR FAILURES SIMULATED ON A 2200-TURN COIL

All oscillograms have a vert. defl. of 100 V/cm. and a sweep speed of 50 usec./cm.

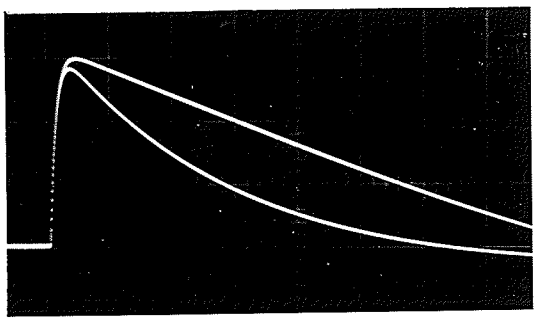

FIGURE C-9

$1\frac{1}{2}$ by 200 impulse for no failure and 9.0 percent failures respectively

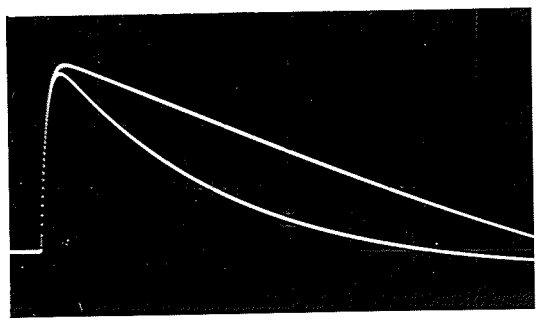

FIGURE C-10

$1\frac{1}{2}$ by 200 impulse for no failure and 9.5 percent failures respectively

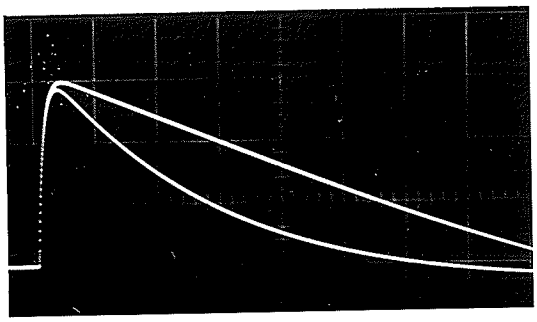

FIGURE C-11

$1\frac{1}{2}$ by 200 impulse for no failure and 12.2 percent failures respectively

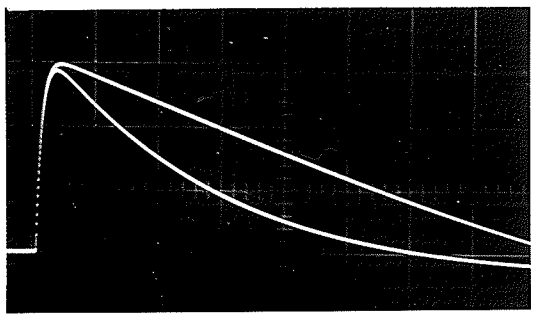

FIGURE C-12

$1\frac{1}{2}$ by 200 impulse for no failure and 9.7 percent failures respectively

DISTORTIONS IN OUTPUT VOLTAGE WAVEFORM FOR FAILURES

SIMULATED ON A 2200-TURN COIL

All oscillograms have a vert. defl. of 100^{v}/cm. and a sweep speed of 50 usec./cm.

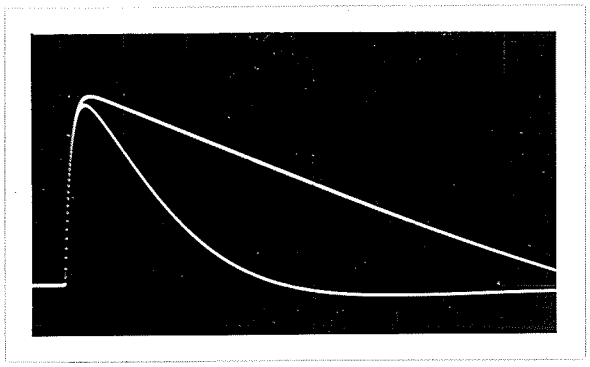

FIGURE C-13

$1\frac{1}{2}$ by 200 impulse for no failure
and 18.2 percent
failures respectively

DISTORTION IN OUTPUT VOLTAGE WAVEFORMS FOR FAILURES

SIMULATED ON A 2200-TURN COIL

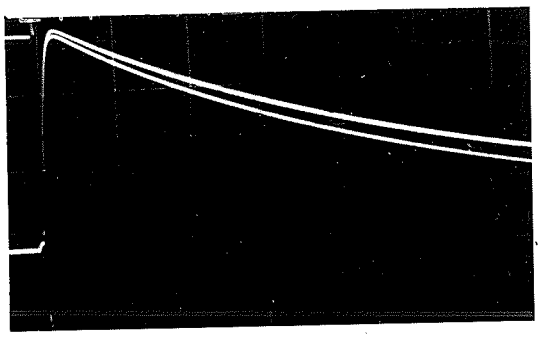

FIGURE C-14

$1\frac{1}{2}$ by 40 impulse for no failure
and 15.2 percent
failures respectively

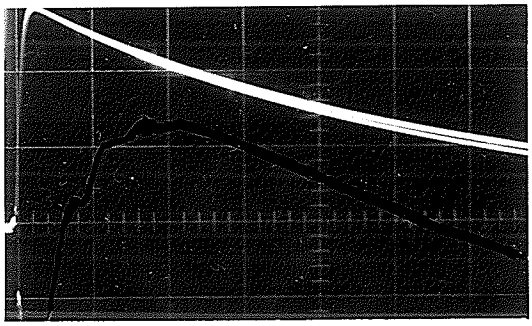

FIGURE C-15

$1\frac{1}{2}$ by 40 impulse for no failure
and 7.68 percent
failures respectively

DISTORTION IN OUTPUT VOLTAGE WAVEFORMS FOR FAILURES

SIMULATED ON A 4200-TURN COIL

All oscillograms have a vert. defl. of 100 V/cm. Figure C-13 has a sweep speed of 50 usec./cm. and Figures C-14 and C-15 have a sweep speed of 10 usec./cm.

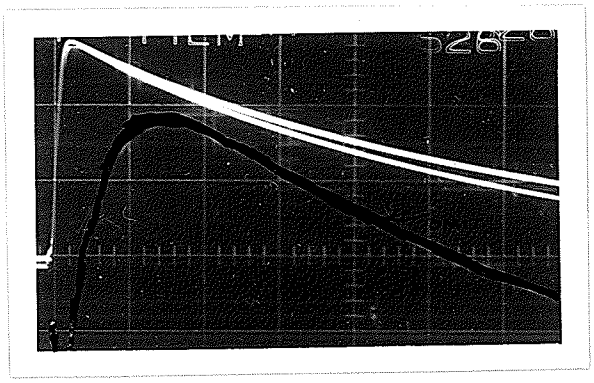

FIGURE C-16

$1\frac{1}{2}$ by 40 impulse for no failure
and 16 percent
failures respectively

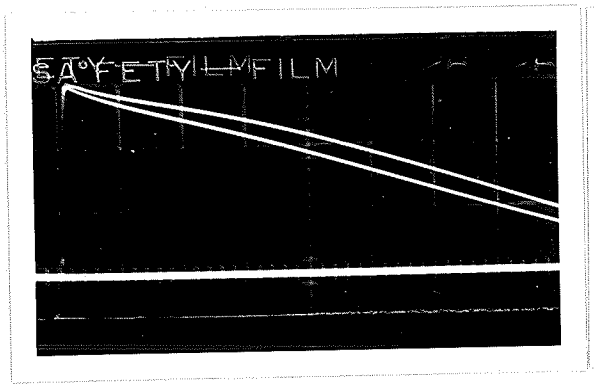

FIGURE C-17

$1\frac{1}{2}$ by 300 impulse for no failure
and 8.05 percent
failures respectively

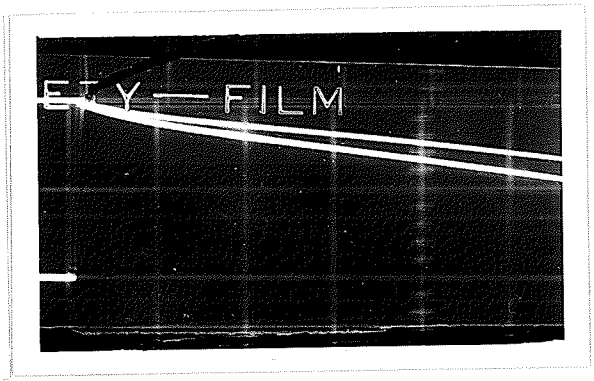

FIGURE C-18

3 by 350 impulse for no failure
and 7.95 percent
failures respectively

DISTORTIONS IN OUTPUT VOLTAGE WAVEFORM FOR FAILURES

SIMULATED ON A 4200-TURN COIL

All oscillograms have a 100^{V}/cm. vert. defl. Figures C-16 and C-17 have a sweep speed of 10 usec./cm. and figures C-18 and C-19 have a sweep speed of 50 usec./cm.

APPENDIX "D"

ADDITIONAL OSCILLOGRAMS FOR CURRENT OSCILLOGRAM FAULT DETECTION METHOD

Table D-1 lists the page numbers of the illustrations for simulated failures shown in Chapter VI and this appendix, their tap combinations, wherever possible, and their size expressed as a percentage of the total winding.

The waveforms in figures D-1 to D-5 illustrate the results for tests performed on coil (1); those in figures D-7 to D-10 illustrate the results for tests performed on coil (2); and those in the remaining figures illustrate the results for tests performed on coil (3). The armature core was contained in the coil shell for all tests, and a current shunt of 150 ohms was used unless otherwise specified.

TABLE D-1

ILLUSTRATIONS FOR SIMULATED FAILURES ALONG WITH THEIR SIZE AND TAP COMBINATIONS

Figure No.	Tap Combinations	Percent of Wdg. Affected	Page No.
	Coil (1) - 2200-turn coil		
$1\frac{1}{2}$ by 40 applied impulse			
6-1	3-4, 5	9.85, 20.2	47
6-2	1-2, 3, 7	9.6, 20.8, 28.0	47
6-3	7-8	9.5	47
6-4	10-11	18.2	47
D-1	5-7	9.25	135
D-1	4-5	9.0	135
D-3	2-3; 3-4	9.5, 19.1	135
D-4	8-9	12.8	135
$1\frac{1}{2}$ by 200 applied impulse			
6-5	1-2, 3	9.0, 20.0	49
6-6	2-3, 4	9.5, 19.0	49
6-7	7-8	9.25	49
6-8	4-5	9.0	49
D-5	3-4	9.85	136
D-6	10-11	28.2	136
	Coil (2) - 4200-turn coil		
$1\frac{1}{2}$ by 40 applied impulse			
6-9	6-7	0.16	51
6-10	1-2	7.5	51
6-11	1-2	7.5	51
6-12	6-7	0.16	51
6-13	6-7	0.16	53
D-7	3-4	7.72	137
D-8	7-9	16.0	137
D-9	1-2	7.5	137

TABLE D-1
(Continued)

Figure No.	Tap Combinations	Percent of Wdg. Affected	Page No.
$1\frac{1}{2}$ by 300 applied impulse			
6-14	6-7	0.16	53
6-15	5-8	16.0	53
3 by 350 applied impulse			
6-16	4-8	16.0	53
D-10	7-8	8.05	137

Figure No.	Fault	Applied Impulse	Percent of Wdg. Affected	Page No.
		Coil (3) - 2200-turn coil		
6-17	1-turn	$1\frac{1}{2}$ by 40	.045	55
6-18	1-turn	$1\frac{1}{2}$ by 200	.045	55
6-19	5-turn	$1\frac{1}{2}$ by 40	.23	55
6-20	5-turn	$1\frac{1}{2}$ by 200	.23	55
6-21	2-turn	$1\frac{1}{2}$ by 40	.09	56
6-22	2-turn	$1\frac{1}{2}$ by 40	.09	56
6-23	1-turn	$1\frac{1}{2}$ by 200	.045	56
6-24	2-turn	$1\frac{1}{2}$ by 200	.09	56
D-11	3-turn	$1\frac{1}{2}$ by 40	.13	138
D-12	3-turn	$1\frac{1}{2}$ by 200	.13	138
D-13	15-turn	$1\frac{1}{2}$ by 40	.69	138
D-14	7-turn	$1\frac{1}{2}$ by 40	.32	138
D-15	7-turn	$1\frac{1}{2}$ by 200	.32	139
D-16	15-turn	$1\frac{1}{2}$ by 200	.69	139
D-17	1-turn	$1\frac{1}{2}$ by 40	.045	139
D-18	7-turn	$1\frac{1}{2}$ by 40	.32	139
		Detection by Charging Current Pulse		
6-25	1-turn	$1\frac{1}{2}$ by 40	.045	59
6-26	7-turn	$1\frac{1}{2}$ by 200	.32	59
6-27	1-turn	$1\frac{1}{2}$ by 40	.045	59
6-28	7-turn	$1\frac{1}{2}$ by 200	.32	59

TABLE D-1
(Continued)

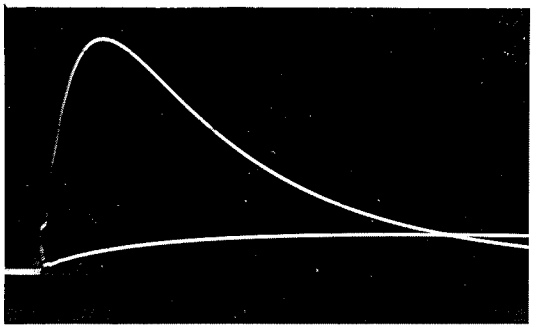

FIGURE D-1

$1\frac{1}{2}$ by 40 applied impulse
lower - no failure
upper - failure of 9.25% of wdg.

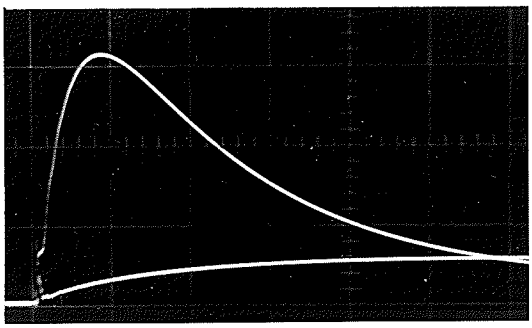

FIGURE D-2

$1\frac{1}{2}$ by 40 applied impulse
lower - no failure
upper - failure of 9% of wdg.

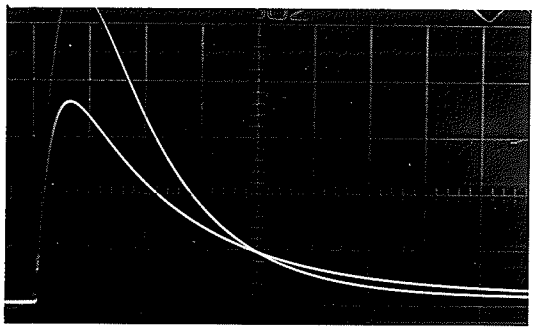

FIGURE D-3

$1\frac{1}{2}$ by 40 applied impulse
lower - no failure
center - failure of 9.5% of wdg.
upper - failure of 19.1% of wdg.

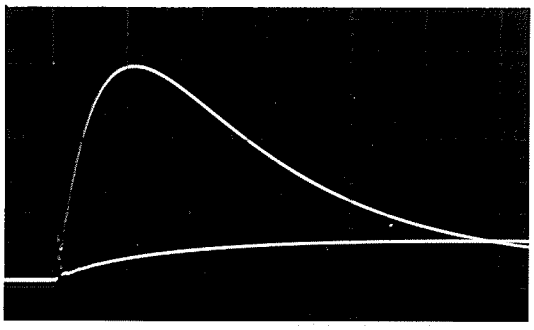

FIGURE D-4

$1\frac{1}{2}$ by 40 applied impulse
lower - no failure
upper - failure of 12.8% of wdg.

DISTORTIONS IN CURRENT IMPULSE WAVEFORM FOR FAILURES

SIMULATED ON A 2200-TURN COIL

All oscillograms have a vert. defl. of 10^{v}/cm. and a sweep speed of 20 usec./cm.

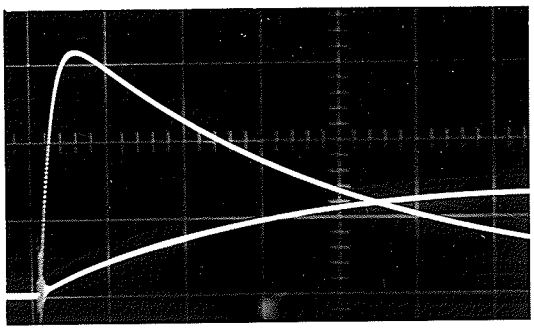

FIGURE D-5

1½ by 200 applied impulse
lower - no failure
upper - failure of 9.85% of wdg.

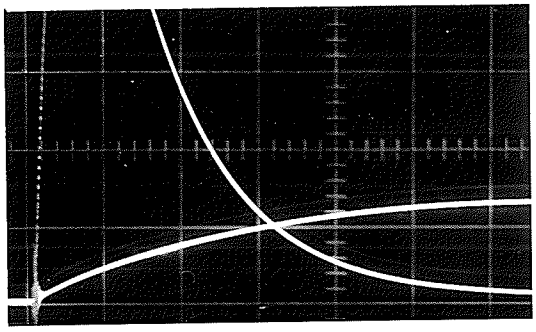

FIGURE D-6

1½ by 200 applied impulse
lower - no failure
upper - failure of 28.2% of wdg.

DISTORTION IN CURRENT IMPULSE WAVEFORM FOR FAILURES

SIMULATED ON A 2200-TURN COIL

All oscillograms have a vert. defl. of 10^{V}/cm. and a sweep speed of 50 usec./cm.

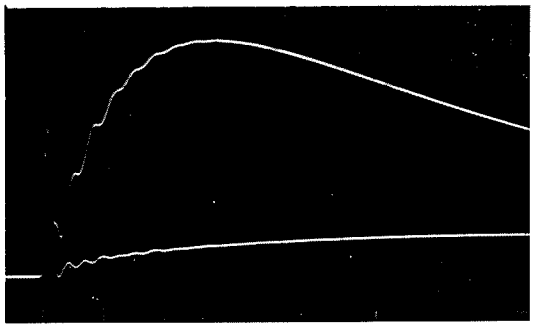

FIGURE D-7

$1\frac{1}{2}$ by 40 applied impulse
lower - no failure
upper - failure of 7.72% of wdg.

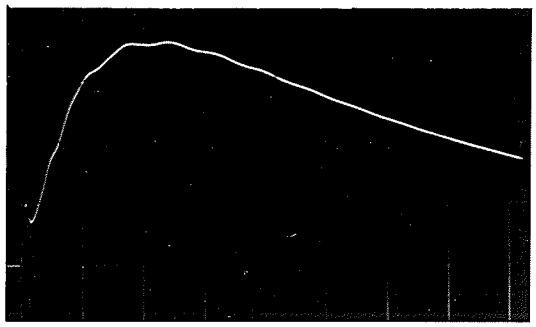

FIGURE D-8

$1\frac{1}{2}$ by 40 applied impulse
lower - no failure
upper - failure of 16% of wdg.

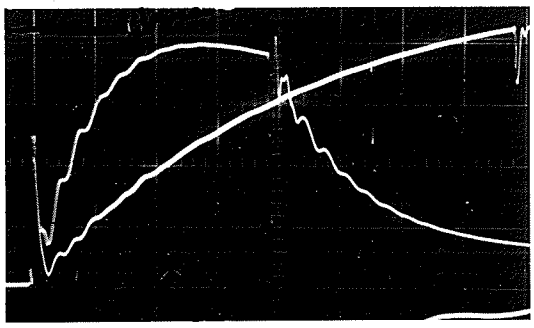

FIGURE D-9

$1\frac{1}{2}$ by 40 chopped impulse
lower - no failure
upper - failure of 7.5% of wdg.

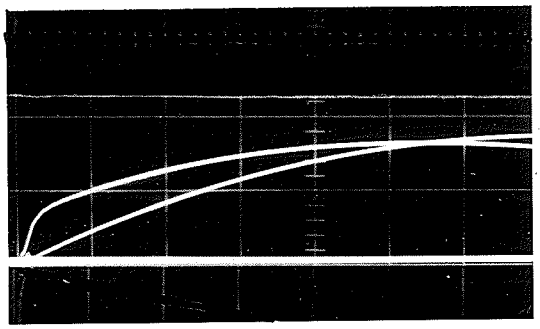

FIGURE D-10

3 by 350 current impulse
lower - no failure
upper - failure of 8.05% of wdg.

DISTORTION IN CURRENT IMPULSE WAVEFORM FOR FAILURES

SIMULATED ON 4200-TURN COIL

All oscillograms have a vert. defl. of 5 V/cm. Figures D-7, D-8 and D-9 have a sweep speed of 10 usec./cm. Figure D-10 has a sweep speed of 50 usec./cm. Figures D-8 and D-10 have a vert. defl. of 10 V/cm.

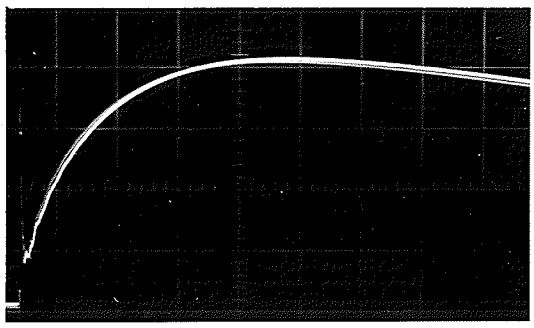

FIGURE D-11

$1\frac{1}{2}$ by 40 applied impulse
lower - no failure
upper - 3-turn wdg. failure
150 ohms shunt resistor

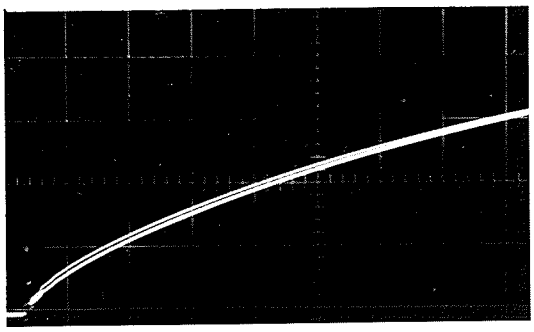

FIGURE D-12

$1\frac{1}{2}$ by 200 applied impulse
lower - no failure
upper - 3-turn wdg. failure
15 ohms shunt resistor

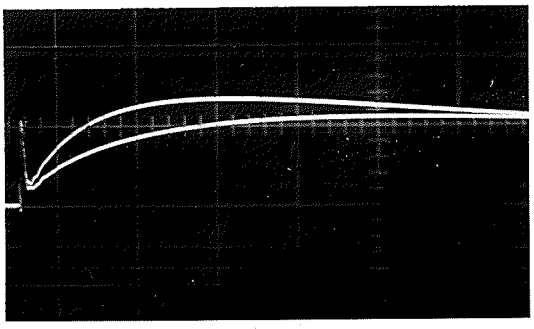

FIGURE D-13

$1\frac{1}{2}$ by 40 applied impulse
lower - no failure
upper - 15-turn wdg. failure
15 ohms shunt resistor

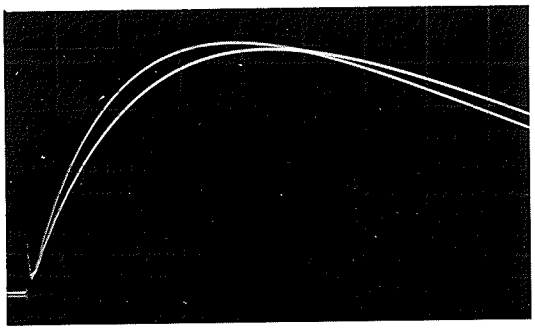

FIGURE D-14

$1\frac{1}{2}$ by 40 applied impulse
lower - no failure
upper - 7-turn wdg. failure
15 ohms shunt resistor

DISTORTION IN CURRENT IMPULSE WAVEFORM FOR FAILURES

SIMULATED ON 2200-TURN COIL

All oscillograms have a sweep speed of 20 usec./cm. Figures D-11 and D-14 have a vert./defl. of 1^{V}/cm. and Figures D-12 and D-13 have a vert. defl. of 5^{V}/cm.

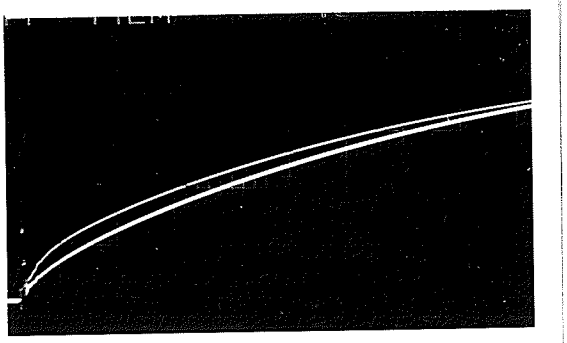

FIGURE D-15

1½ by 200 applied impulse
lower - no failure
upper - 7-turn wdg. failure
15 ohms shunt resistor

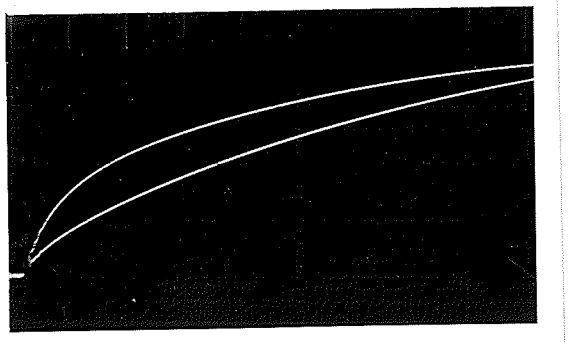

FIGURE D-16

1½ by 200 applied impulse
lower - no failure
upper - 15-turn wdg. failure
15 ohms shunt resistor

FIGURE D-17

1½ by 40 applied impulse
lower - no failure
upper - 1-turn wdg. failure
shunt - 15 ohm resistor and
.25 uf. capacitor

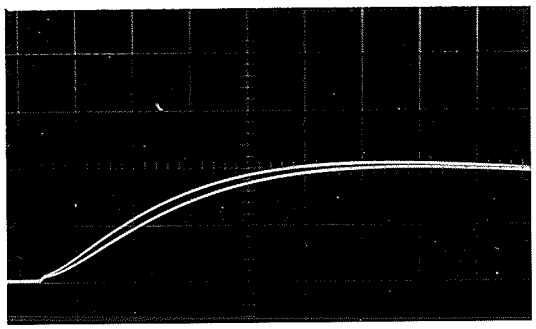

FIGURE D-18

1½ by 40 applied impulse
lower - no failure
upper - 7-turn wdg. failure
shunt - 15 ohm resistor and
.25 uf. capacitor

DISTORTION IN CURRENT IMPULSE WAVEFORM FOR FAILURES

SIMULATED ON A 2200-TURN COIL

All oscillograms have a sweep speed of 20 usec./cm. Figures D-15, D-16 and D-17 have a vert. defl. of 5^{V}/cm. and Figure D-18 has a vert. defl. of 2^{V}/cm.

APPENDIX "E"

ADDITIONAL OSCILLOGRAMS FOR TRANSMITTED IMPULSE DETECTION METHOD

Table E-1 lists the page numbers for the illustrations of the simulated failures shown in Chapter VI and this appendix, their size expressed as a percentage of the total winding, and the type of impulse used for the test. The notation N and C are placed after the applied impulse to denote a normal or chopped impulse respectively.

Figures E-1 and E-2 illustrate the results for failures simulated on a 4200-turn coil with a 150 ohm resistance in the coil circuit and the armature core contained in the coil shell. Figure E-3 illustrates the result for a 7.9% failure when the armature core was removed from the coil shell.

The remaining illustrations represent the results for simulated failures performed on a 2200-turn coil with no resistance in the coil circuit and the armature core contained in the coil shell.

TABLE E-1

ILLUSTRATIONS FOR SIMULATED FAILURES ALONG

WITH THEIR SIZE AND APPLIED IMPULSE

Figure No.	Applied Impulse	Coil	Percent of Wdg. Affected	Page No.
	Coil excited through Terminal (1)			
7-1	1½ by 40N	4200	0.16	63
7-2	1½ by 40N	4200	0.195	63
7-3	1½ by 40N	4200	7.72	63
7-4	1½ by 40N	4200	.09	63
7-5	1½ by 40N	4200	.16	66
7-6	1½ by 40N	4200	7.72	66
7-7	1½ by 40N	2200	.045	66
7-8	1½ by 40C	2200	.045	66
7-9	1½ by 200N	2200	.045	67
7-10	1½ by 200C	2200	.045	67
7-11	Comparison of chopped 1½ by 40 and 1½ by 200			67
7-12	Results of chopped 1½ by 40 and 1½ by 200			67
E-1	1½ by 40N	4200	7.67	143
E-2	1½ by 40N	4200	7.9	143
E-3	1½ by 40N	4200	7.9	143
E-4	1½ by 40C	2200	.045	143
E-5	1½ by 40C	2200	.09	144
E-6	1½ by 200N	2200	.09	144
E-7	1½ by 200N	2200	.18	144
E-8	1½ by 200N	2200	.32	144
	Coil excited through Terminal (2)			
7-13	1½ by 40N	2200	.09	69
7-14	1½ by 40C	2200	.09	69
7-15	1½ by 200N	2200	.09	69
7-16	1½ by 200C	2200	.09	69
7-17	1½ by 15N	2200	.09	70
7-18	1½ by 200N	2200	.045	70
7-19	1½ by 200N	2200	.20	70
7-20	1½ by 200N	2200	.32	70
E-9	1½ by 40 N&C	2200	.00	145
E-10	1½ by 40 N&C	2200	.09	145
E-11	1½ by 40 N&C	2200	.36	145
E-12	1½ by 40N	2200	.045	145
E-13	1½ by 40C	2200	.045	146
E-14	1½ by 200N	2200	.18	146

TABLE E-1
(Continued)

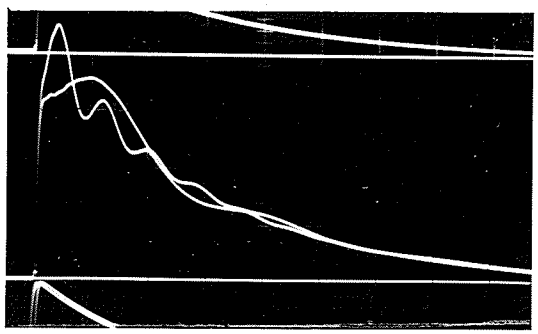

FIGURE E-1

failure involving 7.67 percent
of the total winding
armature core contained in
coil shell

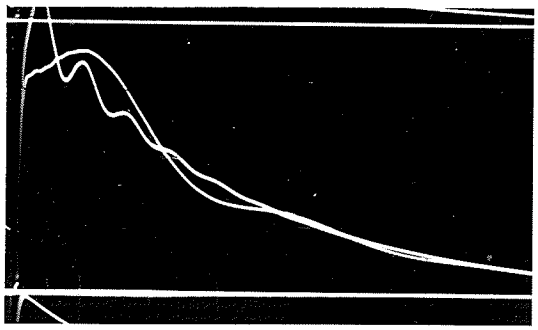

FIGURE E-2

failure involving 7.9 percent
of the total winding
armature core contained in
coil shell

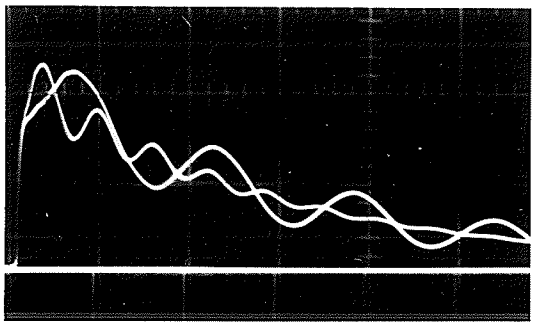

FIGURE E-3

failure involving 7.9 percent
of the total winding
armature core removed from
coil shell

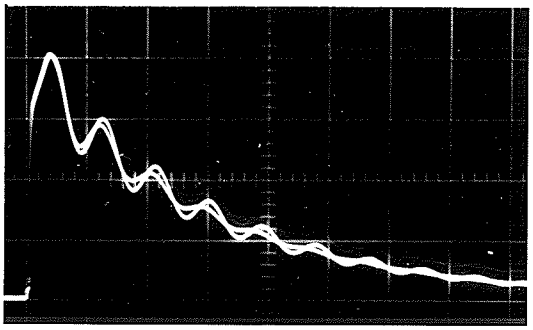

FIGURE E-4

failure of 1 turn in 2200 coil
chopped input impulse
armature core removed from
coil shell

FAULTED AND UNFAULTED WAVEFORMS FOR A $1\frac{1}{2}$ BY 40 IMPULSE

APPLIED BETWEEN TERMINAL (1) AND THE COIL SHELL

The waveform with the largest amplitude at 20 usec. represents the unfaulted waveform. All oscillograms have a vert. defl. of 100 /cm. and a sweep speed of 20 usec./cm. A 150 ohm resistor was connected between the coil shell and the low potential terminal of generator.

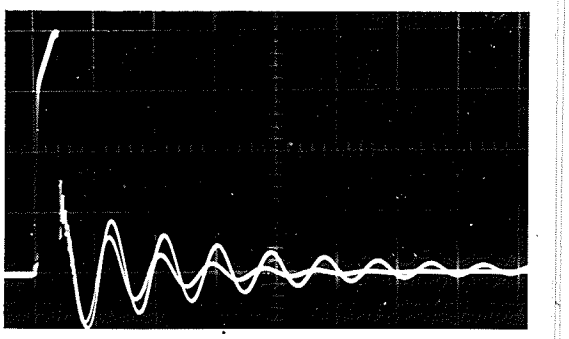

FIGURE E-5

chopped $1\frac{1}{2}$ by 40 impulse
failure of 2 turns in 2200

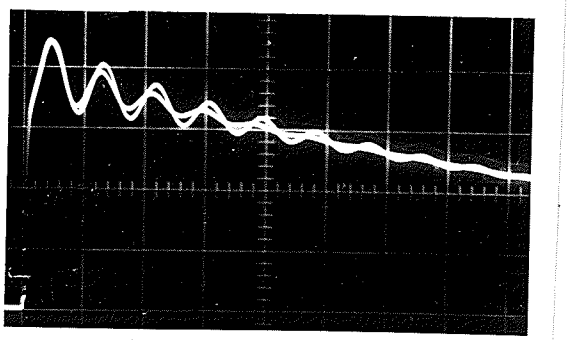

FIGURE E-6

$1\frac{1}{2}$ by 200 input impulse
failure of 2 turns in 2200

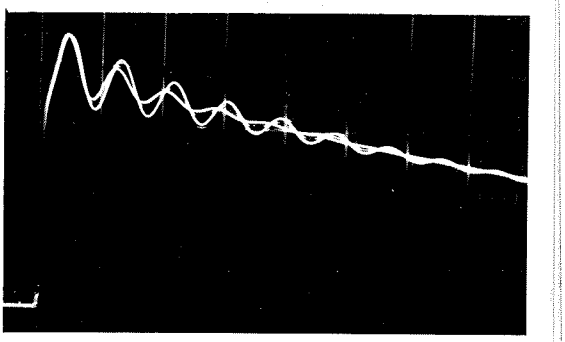

FIGURE E-7

$1\frac{1}{2}$ by 200 input impulse
failure of 4 turns in 2200

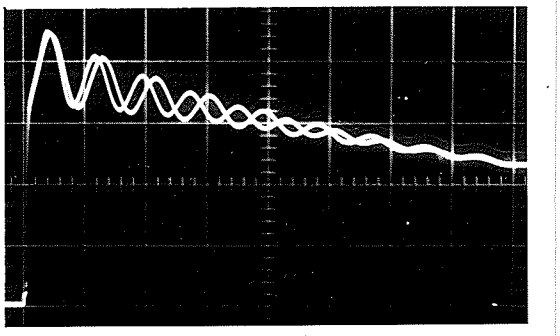

FIGURE E-8

$1\frac{1}{2}$ by 200 input impulse
failure of 7 turns in 2200

FAULTED AND UNFAULTED WAVEFORMS FOR AN IMPULSE APPLIED

BETWEEN TERMINAL (1) AND THE COIL SHELL

The waveform with the largest amplitude at 20 usec. represents the unfaulted waveform. All oscillograms have a vert. defl. of 100V/cm. and a sweep speed of 20 usec./cm. Armature core was contained in coil shell.

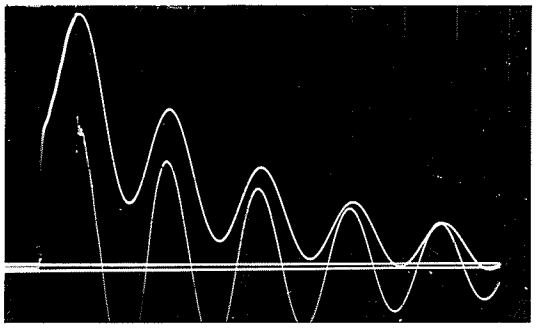

FIGURE E-9

chopped and unchopped input
$1\frac{1}{2}$ by 40 impulses for
no failure

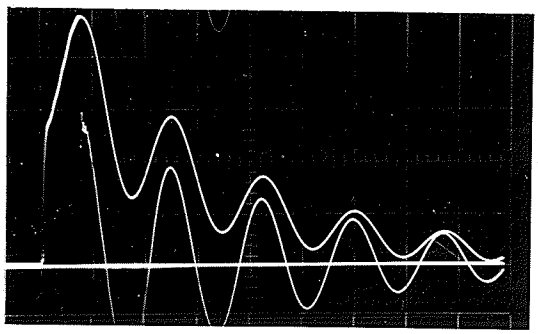

FIGURE E-10

chopped and unchopped input
$1\frac{1}{2}$ by 40 impulses for a
loosely coupled two-turn failure

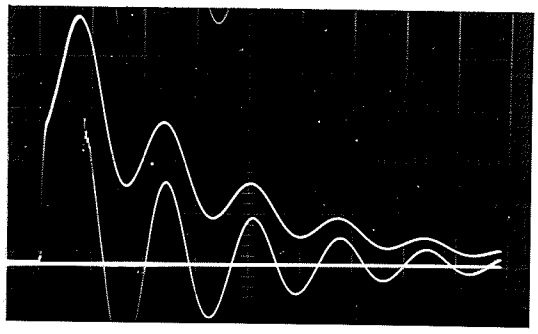

FIGURE E-11

chopped and unchopped input
$1\frac{1}{2}$ by 40 impulses for an
eight-turn failure

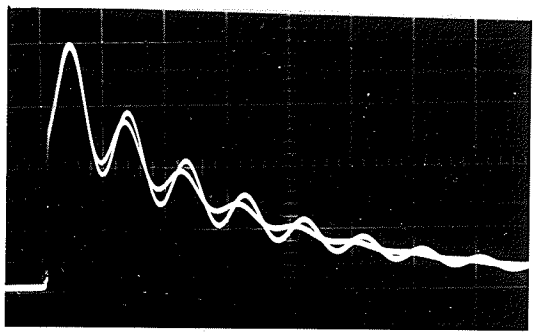

FIGURE E-12

$1\frac{1}{2}$ by 40 applied impulse
1-turn failure

FAULTED AND UNFAULTED WAVEFORMS FOR AN IMPULSE APPLIED

BETWEEN TERMINAL (2) AND THE COIL SHELL

The waveform with the largest amplitude at 20 usec. represents the unfaulted waveform. All oscillograms have a vert. defl. of 100^{v}/cm. and a sweep speed of 20 usec./cm.

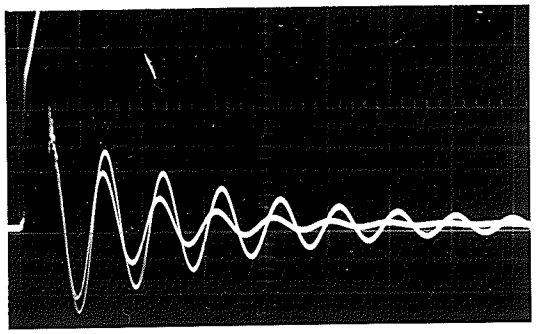

FIGURE E-13

1½ by 40 chopped impulse
1-turn failure

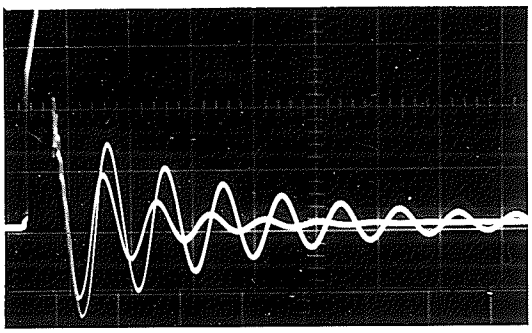

FIGURE E-14

1½ by 200 chopped impulse
4-turn failure

FAULTED AND UNFAULTED WAVEFORMS FOR AN IMPULSE APPLIED

BETWEEN TERMINAL (2) AND THE COIL SHELL

Both oscillograms have a vert. defl. of 100 /cm. and a sweep speed of 20 usec./cm. The waveform with the larger oscillations represents the unfaulted waveform.